Characterizing ParA2, an essential protein for *Vibrio cholerae* chromosome segregation

A dissertation

submitted by

Monica Ping-Ting Hui

in partial fulfillment of the requirements
for the degree of

Doctor of Philosophy

in

Molecular Microbiology

TUFTS UNIVERSITY

Sackler School of Graduate Biomedical Sciences

May, 2011

ADVISER:

Matthew K. Waldor

ABSTRACT

Partitioning, or *par*, loci were initially identified on low copy plasmids as elements essential for plasmid segregation and inheritance. However, it is now apparent that many bacterial chromosomes harbor *par* loci as well. The role of chromosomal *par* loci remains incompletely understood, but their homology to plasmid *par* loci has led to speculation that chromosomal *par* loci may play a key role in mediating chromosome segregation.

The genome of *Vibrio cholerae*, the causative agent of cholera, is divided between two chromosomes, each of which encodes its own *par* locus. Prior studies have shown that the *parAB2* locus is essential for the proper segregation of chromosome II. In order to begin to elucidate the molecular mechanisms by which *parAB2* mediates *V. cholerae* chromosome II segregation, I focused on ParA2, the protein thought to drive the partitioning process. *In vitro*, I found that ParA2 shares biochemical characteristics with other members of the ParA family of partitioning proteins. However, unlike most ParA family proteins, which polymerize in the presence of ATP, ParA2 only formed higher ordered filamentous structures on DNA. Three-dimensional reconstructions of these filaments revealed that ParA2 binds DNA to form unusual left-handed nucleoprotein filaments that are bipolar and symmetric. These filaments do not distort the DNA helix bound in the interior. Subsequent *in vivo* studies using ParA2 fluorescent protein fusions showed that this partitioning protein is dynamic and nucleoid associated. Strikingly, ParA2 is often found between a ParB2-*parS2* centromere complex and the cell pole towards which that complex is moving. Together, my findings suggest that ParA2 forms bipolar filaments over the nucleoid and utilizes a pulling mechanism to mediate partitioning of chromosome II.

ACKNOWLEDGEMENTS

First and foremost, I would like to acknowledge Matthew K. Waldor for being a truly fantastic adviser. Not only did he enable me grow as a scientist during my time in his lab, but I would have had a much tougher time completing my thesis if not for his continual optimism, enthusiasm for science, and encouragement. I would like to extend a thank you to past and present members of the Waldor lab for creating a wonderfully supportive and fun environment in which a student can learn. Special thanks go to Sarah McLeod, for patiently teaching me the basics of biochemistry; Yoshiharu Yamaichi, for the many discussions and technical help over the years; and Harvey Kimsey, for biochemistry consultations. I would also like to thank my committee members for their time and suggestions in guiding my work.

My journey through graduate school would not have started without my past mentors, who fostered and nurtured my love for bacterial molecular mechanisms, and for that I am infinitely grateful: John Helmann, Charlie Moore, Ding Jin, and Yanning Zhou. And last, but not least, a big thank you goes to my Tufts classmates, friends, and family, all of whom have provided invaluable support and encouragement throughout the years.

TABLE OF CONTENTS

LIST OF FIGURES

Chapter One

Chapter Two

Chapter Three

Appendix A

Appendix B

LIST OF TABLES

Chapter One

Chapter Three

Characterizing ParA2, an essential protein for *Vibrio cholerae* chromosome segregation

CHAPTER ONE

Introduction

Essential to all life—prokaryotic and eukaryotic cells alike—is the maintenance of genomic integrity. Survival of the population and species is wholly dependent on the ability of parental cells to successfully pass along a complete, intact, and functional genome to successive generations. For bacteria, proper chromosomal inheritance relies on many processes. Replication provides the copies of the genome ultimately inherited by each daughter cell. Cellular stress responses such as the SOS response and the mismatch repair system serve as ways to ensure the fidelity of the genomic template. For circular chromosomes, dimers and catenanes are resolved with the aid of enzymes like FtsK, XerCD and Topoisomerase IV to provide two physically unlinked copies of the DNA. And finally, it is essential that the bacteria segregate and position the duplicated chromosome(s) in such a manner that each daughter cell receives one complete copy of the DNA by the time the division septum forms.

Chromosome partitioning involves ordered DNA movement

Segregation is not a haphazard process. The average bacterial genome is 4 Mbp in size and roughly equivalent to 1.3 mm in contour length (195). Yet, despite being approximately 1,000 times longer than the average bacterial cell, the chromosome is condensed into a space smaller than 0.6 - 0.7 μm^3 (108). To achieve this feat, bacteria utilize an arsenal of nucleoid associated proteins such as HU, H-NS, and the SMC/MukB complexes to compact the chromosomal DNA into a highly organized structure (36, 129, 175, 186, 201, 204).

Through FROS, a fluorescent reporter-operator system that allows tracking of specific loci within the cell, and fluorescence in situ hybridization (FISH), it was observed

that specific genetic loci consistently occupy specific sub-cellular addresses across a wide range of species (57, 59, 73, 98, 112, 124, 146, 148, 150, 173, 187, 194, 203, 210). In *Bacillus subtilis* and *Escherichia coli*, the origin (*ori*) region localizes as two foci at opposing polar edges of the nucleoid at the cell quarters and the terminus (*ter*) region localizes at the mid-cell (73, 112, 124, 148, 194, 210). The presence of multiple *ori* foci represent cells in which replication has initiated, giving rise to two *ori* regions located at the mid-cell regions of the future daughter cells, but has not yet been completed to yield duplicated *ter* regions (73). Cell division in *E. coli* yields newborn cells with the *ori* and *ter* located near the mid-cell (206). In *Caulobacter crescentus*, which initiates replication only once per cell cycle, the *ori* and *ter* are separated to positions at the bipolar regions of the nucleoid (98, 203).

Furthermore, in each of these three cases, the intervening regions between *ori* and *ter* are arranged between the *ori* and *ter* foci in an order that corresponds to their position on the chromosomal map, strongly indicating that linear arrangement of chromosomes is a feature conserved in bacteria. The *B. subtilis* and *C. crescentus* chromosomes are organized linearly along the longer cell axis, while the *E. coli* chromosome is arranged with the left and right arms of the chromosome in opposite halves of the cell (147, 194, 203, 205). Subsequent timelapse studies show that this order is maintained as segregation proceeds along the chromosome, progressing from the proximal *ori* region to *ter* to yield daughter cells with the same chromosomal arrangement (146, 194, 203). Therefore, one aspect of partitioning involves carefully orchestrated DNA movement with respect to the sub-cellular locale.

A second aspect of partitioning involves careful timing of segregation with respect to cell division. Proper positioning of the chromosome is meaningless if the division septum forms before segregation completes, resulting in guillotined chromosomes. Therefore,

bacteria have evolved methods ensure the division septum forms at the correct time. For the most part, these strategies involve the sensing of chromosome sub-cellular positioning. In *E. coli* and *B. subtilis*, timing of septation is regulated, in part, through the combined efforts of the Min system and nucleoid occlusion. In the Min system, the septal inhibitor MinC localizes to the cell poles through an oscillatory system to ensure FtsZ ring assembles away from the poles at the mid-cell (132). In nucleoid occlusion, SlmA and Noc from *E. coli* and *B. subtilis*, respectively, bind DNA to inhibit FtsZ ring formation over the nucleoid (16, 214). This ensures septal constriction only occurs in the cytoplasmic regions between separated nucleoids at the mid-cell. Interestingly, Noc binding sites have been found to be scattered throughout the *B. subtilis* chromosome, but conspicuously absent around the *ter* region (217). The placement of Noc binding sites near the *ter* region leads to a delay in cell division and cell elongation—again, suggestive of a temporal link between segregation and cell division via nucleoid occlusion. In *C. crescentus*, timing of septation is directly linked to the chromosome partitioning proteins and their interaction with a protein called MipZ (discussed below). FtsZ ring formation only occurs in areas of low MipZ concentration, coinciding with the mid-cell when segregation has just completed (196). Interference in chromosomal partitioning results in cell cycle arrest, filamentation, aberrant septation, and anucleate cell formation (136, 137). Finally, in cases where the chromosome becomes entrapped by the septal ring due to a delay in segregation or due to mislocalization of the FtsZ ring, the DNA translocase, FtsK, localizes to the septal ring and pumps the chromosome into the appropriate cell compartment before division is completed (130, 183).

What is remarkable is the fact that this coordinated movement of the chromosome over space and time is extraordinarily consistent. Errors in segregation are rare, occurring as

low as 1 in every 10,000 cell division events (88, 93). The mechanisms behind chromosomal partitioning must therefore be robust and highly reliable. How, then, do bacteria mediate segregation of their chromosomes?

Models for chromosome partitioning

In 1963, Jacob, Brenner, and Cuzin postulated that partitioning could involve chromosomal attachment to the membrane at the mid-cell. Cell elongation and zonal membrane growth would result in gradual separation of the duplicated replicons (94). However, in conflict with the key premise of this model, membrane growth is dispersed in the cell envelope, and the model was re-evaluated once fluorescence microscopy revealed that chromosomal movement is rapid and directed, occurring at a rate that eclipses cell elongation (57, 74, 75, 209). These observations quickly led to the idea of a motor protein acting as an active partitioning force, and a number of proteins have been hypothesized to serve in this capacity—including two powerful DNA threading machines, DNA and RNA polymerase (46, 118). The mechanisms are diagrammed in **Fig. 1-1**.

In the extrusion-capture model for chromosome partitioning proposed by Lemon and Grossman, the force for chromosomal movement is provided by DNA polymerase (116). Fluorescence tagging of the replisome in *B. subtilis* revealed that DNA polymerase localizes to discrete positions corresponding to the mid- or quarter-cell positions (117). This suggested that the replisome does not move along the DNA, but remains stationary while DNA is threaded through during replication. Taking advantage of the replication arrest that occurs when *B. subtilis* enters the stringent response, Lemon and Grossman reasoned that if

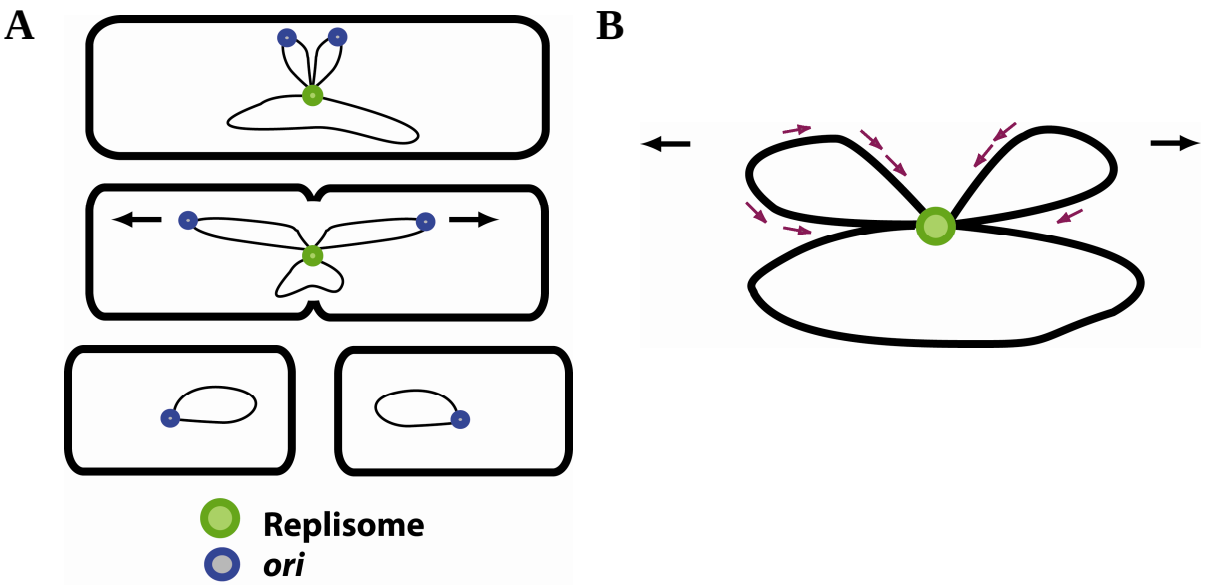

Fig. 1-1. The power of DNA threading machines. (A) The extrusion-capture model for DNA partitioning. As replication proceeds, polymerization of DNA is spooled outward in a bipolar fashion. The *ori* is captured by a putative anchor protein and DNA condensing proteins help with bulk chromosome separation. **(B)** Harnessing RNA polymerase activity. As replication proceeds, movement of the DNA is propelled by concomitant transcription along the newly synthesized chromosome. Purple arrows indicated direction of transcription; black arrows indicate the direction of resulting chromosome movement. The bias in gene orientation leads to bipolar movement of the sister replicons.

Adapted from Dworkin and Losick (46).

the latter hypothesis were true, the DNA pause site marked by FROS should co-localize with the replisome upon arrest. When the cells exit the stringent response and replication resumes, duplication of this site would result in the replisome flanked by two foci. This is precisely what they observed (118). From their observations, the extrusion-capture model was born. DNA polymerase initiates replication at the mid-cell where the chromosomal *ori* is located. As DNA is replicated, the two copies are spooled outward from mid-cell towards opposite poles after passing through the replisome. The *ori* regions are then captured by a membrane anchor protein and DNA condensing proteins aid the movement of the DNA bulk from the replisome (116).

The case for RNA polymerase serving as the force for partitioning arose upon the observation that RNA polymerase can translocate DNA with incredible force in single molecule tracking experiments *in vitro* (68). Since a majority of transcribed genes are oriented away from the *ori*, the combined movement of RNA polymerase along these genes during transcription could result in bulk chromosome separation (46). To test this theory, Dworkin and Losick used FROS to examine replication synchronized *B. subtilis* cells for the ability of recently replicated loci near the *ori* to migrate apart from each other in wild type cells compared to cells treated with the transcriptional inhibitor, streptolydigin (46). In treated cells, separation of loci was minimal compared to non-treated cells as expected from their hypothesis. Essential to this model is the anchoring of RNA polymerase, and there is evidence of RNA polymerase assembling into transcription factories which could be anchored in some manner (29).

However, it is unlikely that either of these two polymerases serve as the sole active partitioning force. First, DNA is a highly flexible polymer, and its short persistence length

and low rigidity is simply not enough for DNA to be pushed the entire distance from the mid-cell to the quarter-cell positions without bending (46). Second, while DNA polymerase remains stationary in *B. subtilis* during replication, the replisome in *C. crescentus* is not fixed and migrates along the DNA from the pole to the mid-cell (99, 107, 117). Similarly, in *E. coli*, the replisome assembles at the *ori* located at the mid-cell and tracks along the DNA during replication (166). Third, the starting position of segregation is not dictated by the *ori*. Segregation continues to initiate at the native *ori* proximal regions despite relocating the *ori* sequence elsewhere on the chromosome (15, 72, 199). This does not automatically preclude DNA and RNA polymerase from having a role in partitioning, though. The spooling of DNA through the replisome can work to separate the origin-proximal regions which are, in turn, acted upon by a partitioning machinery. Furthermore, increase in transcription has been shown to correlate with increased nucleoid condensation, and nucleoid condensation has been shown to be required for successful partitioning (28, 76, 98, 190). Therefore, DNA and RNA polymerases may very well have auxiliary roles in segregation.

This returns us back to the original question: what provides the active mechanism that bacteria rely on to partition their DNA? In the age of genome sequencing, data mining and homology searches revealed the presence of genetic loci homologous to genetic cassettes responsible for low copy plasmid partitioning on nearly 70% of the sequenced bacterial genomes (notable exceptions include *E. coli* and *Haemophilus influenzae*) (82, 131). In some respects, low copy plasmids and the bacterial chromosome face the same challenges. Both are replicons present in low copy, and thus need to segregate sister replicons with high fidelity. This suggested that the mechanisms responsible for plasmid partitioning may also work to mediate chromosome partitioning as well.

Anatomy of a *par* locus

Most of what is understood about *par* loci and the proteins they encode come from studies on low copy plasmids. Initially discovered in *E. coli* on the conjugative factor F and the P1 prophage, these genetic elements were identified as self-contained units required for equipartitioning of plasmids (7, 8, 152). Since then, Par systems have been found on an increasing number of plasmids from both Gram-negative and Gram-positive hosts (70, 131).

The minimal *par* locus encodes three elements that work together to carry out partitioning: an NTPase, a site-specific DNA binding or adaptor protein, and a *cis*-acting DNA site often referred to as a centromere-like site. This centromere-like site typically consists of a varying number of direct or indirect repeats, and is the site which the adaptor recognizes and binds to form a large nucleoprotein complex (1, 35, 39, 42, 50, 85, 110, 133, 167, 171, 172, 207). The nucleoprotein complex, in turn, is recognized by the NTPase (10, 21, 96, 140, 145, 161, 185, 191). In a number of partitioning systems, the NTPase has been shown to form polymers or filaments in a nucleotide dependent manner (11, 20, 45, 52, 96, 126, 139). For this reason, many models for Par-mediated partitioning consider the NTPase as the motor protein driving the segregation process, forming cytomotive filaments that interact with their cognate nucleoprotein complex to effect partitioning (11, 52, 66, 67, 111, 121, 126, 139, 161).

Par systems are classified into one of three major categories based on the nature of the NTPase they encode. The Type I Par systems utilize an ATPase containing a deviant Walker box ATP binding motif called ParA, the Type II Par systems have an ATPase that shares structural homology with eukaryotic F-actin called ParM, and the Type III Par systems encode a tubulin-like GTPase called TubZ (19, 70, 106, 111, 145, 155, 200). Despite the

lack of conserved structural homology between the three classes, these systems are functionally homologous and share a similar genetic organization as shown in **Fig. 1-2**. Deletion of a *par* locus from its cognate replicon results in plasmid instability and loss (7, 44, 50, 69, 82, 151, 152, 193). It appears evolution has derived more than one solution to ensure proper plasmid partitioning.

Type I systems

Type I systems are the most common active partitioning systems found on low copy plasmids. The *par* loci in this category encode ATPases with a deviant Walker box motif called ParA (70, 106). The centromere-binding or adaptor protein is called ParB, and binds to the centromere-like site, *parS* (39, 42, 133, 167, 207). Type I systems are further sub-categorized into two classes based on ParA sequence and locus organization. Type Ia ParA proteins have an additional N-terminal domain while Type Ib ParA proteins do not (51, 70). This N-terminal domain allows for autoregulation of the *par* operon by Type Ia ParA proteins, while Type Ib systems rely on ParB for autoregulation (40, 165). Prototypical members of the Type Ia systems include ParABS of the P1 prophage and SopABC of the plasmid F. Members of the Type Ib systems include ParABC from pB171 and δ/ω from pSM19035. Curiously, all Type Ia *par* loci are found on plasmids from Gram-negative bacteria while Type Ib *par* loci are found on plasmids from both Gram-positive and Gram-negative hosts.

The search for the mechanism by which the Type I systems mediate partitioning has spanned multiple decades and resulted in detailed studies of a number of Type I systems. The obstacle to building a single model for ParA mediated partitioning is finding consensus

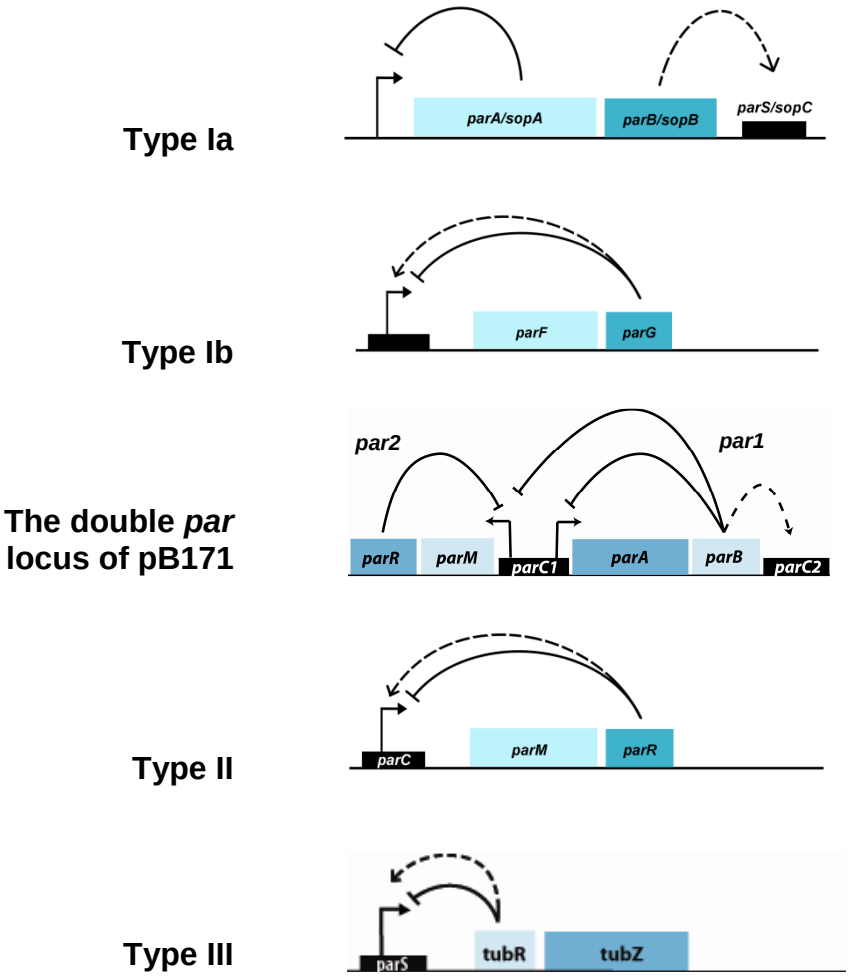

Fig. 1-2. Organization of *par* loci. The dotted lines denote centromere binding and the solid lines denote repression of the *par* operon. The organization of pB171 is included to demonstrate its unusual double *par* composition of a Type 1b and a Type II locus arranged in tandem.

Adapted from Ebersbach and Gerdes 2005 (51).

among the microscopy, biochemical, and cytological data across the many partitioning systems studied. The best understood Type I systems and the accompanying models partitioning are discussed below.

***Type 1a* par *loci: SopABC of the plasmid F*.** The F partitioning system is known as *sopABC*, short for system of partitioning. SopA is the ATPase and SopB is the adaptor protein which binds *sopC*, a site consisting of a series of twelve 43-mer repeats (85, 110, 141, 142, 207, 208). The intracellular levels of all three elements must be carefully regulated as imbalances in the levels of SopA and SopB result in plasmid loss (1, 109, 119, 153). Likewise, excess copies of *sopC* in the cell result in plasmid destabilization (23).

The F plasmid localizes near the mid-cell and rapidly migrates toward the quarter-cell positions prior to cell division. These sites correspond to the mid-cell positions of future daughter cells post-septation (73, 81, 149, 189). SopB co-localizes with the F plasmid whereas SopA forms an oscillating focus that moves over the nucleoid in a helical manner dependent on SopA ATPase activity and SopB (2, 81, 89, 126). Why loss of SopA oscillation contributes to plasmid loss is unclear. However, these oscillations appear to give directionality to F plasmid movement, as microscopy timelapses show that the plasmid often "chases" after the SopA focus over the course of repeated oscillations (2, 81). Curiously, the segregation pattern is not symmetrical, as would be assumed by the plasmid's affinity for the mid- and quarter-cell positions. During separation, one plasmid remains at one quarter-position while the duplicated plasmid follows SopA to the other quarter-position (81).

Complementing biochemical analyses of the individual SopABC components have allowed for a closer look into the molecular foundations of the F partitioning system,

particularly into the structure of the SopB-*sopC* complex. Binding of SopB to *sopC* leads to the formation of an extensive nucleoprotein complex where SopB makes specific and non-specific DNA contacts along the surrounding DNA, rendering it transcriptionally silent (133, 180). Contacts are also made between F plasmids *in trans* via SopB (180).

Initially, topological assays showed that binding was accompanied by changes in F plasmid supercoiling, leading to the hypothesis that changes in supercoiling may be a result of DNA wrapping around a SopB complex (18). It is now understood that SopB spreading on DNA blocks a number of cellular proteins other than RNA polymerase from accessing the DNA (133). Since wild type plasmids are less negatively supercoiled compared to *sopB* mutants, SopB likely blocks gyrase from introducing negative supercoils into the F plasmid rather than SopB forming a complex with the DNA wrapped around it (22, 133). Consistent with this view, crystal structures of SopB bound to DNA shows association in a linear fashion along the DNA (180).

The third element of the Sop system, SopA, has intrinsic ATPase activity that is weakly stimulated by SopB and DNA separately, synergistically stimulated when both SopB and DNA are present, and synergistically stimulated to a higher degree if the DNA includes *sopC* (3, 20, 208). Mutations in the ATP-binding site result in increased rates of plasmid loss. This has been attributed to the inability of SopA to effectively interact with the SopB-*sopC* complex to promote separation of plasmid pairs (119, 125). Upon binding ATP, SopA forms bundled, fibrous structures readily observable by EM (20). Polymerization is highly sensitive to concentrations of DNA. At high concentrations of DNA, SopA depolymerizes, but the polymers can be stabilized by the addition of SopB and DNA containing *sopC* (20). SopA also has the ability to bind DNA non-specifically in its ATP-bound form. This *in vitro*

activity translates into its ability to associate with the cell nucleoid *in vivo* and is essential for partitioning (20, 31).

No consensus has been reached as to how partitioning of the F plasmid is carried out. **Table 1-1** outlines a number of models that have been proposed based on microscopy or biochemistry. The first model focuses on the helical oscillations of SopA within the cell, where SopA polymerization forms a helical track along which the plasmid segregates (81). While this takes into account the oscillatory nature of SopA guiding the movement of SopB-*sopC*, it does not explain why SopA would preferentially nucleate at the quarter positions and why F would remain at the quarter positions. A hitherto unidentified host factor would have to be responsible for positioning. The second model is based on *in vitro* observations of radial aster formation of SopA from a SopB-*sopC* center (126). This model gives an explanation for how plasmids localize to the quarter positions of the cell; however, it is difficult to see how aster formation translates to SopA oscillation *in vivo* and attempts to see this organized structure by EM has failed (20). Finally, the last model invokes the notion of SopA sequestration as a means for regulating partitioning. Productive filament formation of SopA for active partitioning occurs only when SopB binds *sopC* and spreads along the DNA to occlude SopA from binding to the DNA (20, 180). This is the only model thus far to account for the non-specific DNA binding properties of SopA and the free forming SopA filaments, but also fails to address the role for SopA oscillations.

It is possible that SopABC mediated partitioning uses a combination of these models. For example, partitioning can be held in check by DNA sequestration of SopA until SopB-mediated DNA occlusion allows SopA to form the helical track observed by Hatano et al. and Adachi et al. (2, 81). However, more studies are needed before what is known about the

Table 1-1. Models of SopABC function.

System	Model	
SopA as a helical track (81) Plasmid: F	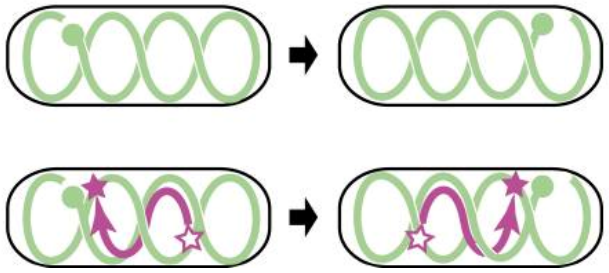 * magenta arrows denote plasmid movement	1. SopA polymerizes at one polar edge of the nucleoid (grey circle) to form a helical track. 2. A SopB-*sopC* complex (star) interacts with one end of the track to trigger depolymerization of the filament to move the plasmid along the SopA path to the nucleation site. 3. As the SopABC complex is disrupted by a high concentration of SopA at the nucleation site, a second nucleation event at the opposite end of the pole gives rise to a SopA track of opposite polarity. 4. The process repeats with the other SopB-*sopC* complex to move the second plasmid in the opposite direction.
Spindle formation of SopA (126) Plasmid: F	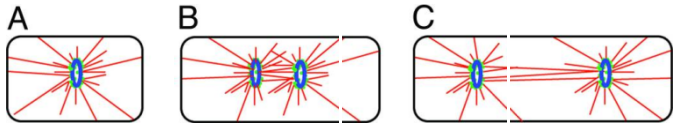	1. SopB-*sopC* nucleates polymerization of SopA radially outward from each sister plasmid and the force of SopA 2. Polymers extending from the segrosome to the cell poles fix the F plasmid to the quarter positions in the cell. Blue = plasmid; Green = SopB; Red = SopA filaments
Sequestration of SopA (20) Plasmid: F	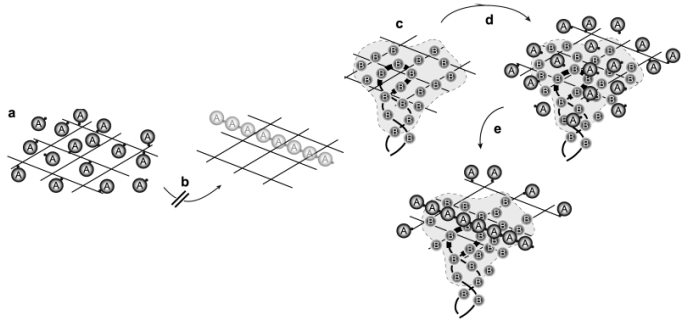	1. SopA polymerization is prevented by non-specifically coating the nucleoid DNA (A is preferred while B is blocked). 2. Initiation of partitioning is cued when SopB binds the *sopC* region (C), preventing SopA from binding (D). 3. The increase in the amount of free SopA in a local "nucleoid free" region allows for polymerization of SopA and segregation of the sister plasmids (E). Large, dark grey circles = SopA Small light grey circles = SopB

biochemistry of SopABC is reconciled with the microscopy studies, and a single model is proposed to encompass all observations reported to date.

Type 1a* par *loci: ParABS of the P1 prophage. In some respects, the partitioning of the P1 prophage is very similar to that of the F plasmid. P1 plasmids can be found at the mid- and quarter-cell positions (56, 80, 123, 181). Again, partitioning depends on the weak intrinsic ATPase activity of ParA that is stimulated by ParB or DNA and is synergistically stimulated by ParB and DNA (40, 41, 62). ParB binds to *parS* to form a large nucleoprotein complex that renders nearby DNA inaccessible to cellular proteins (53, 171, 176).

However, a closer look at P1, ParB, and ParA intracellular localization reveals distinct differences from the SopABC system. Instead of directed movement, P1 movement is much more dynamic in the cell, with plasmids undergoing continual movement and experiencing random joining and splitting events (181). ParA localizes to the nucleoid region as a diffuse cloud (80, 181). Hatano and Niki report that within this cloud, ParA foci can be seen corresponding to the quarter-cell positions, co-localizing with P1. These foci blink over the course of the cell cycle, rather than oscillate in a helical pattern as observed for SopA (80, 81). The appearance of ParA foci is dependent on ATP hydrolysis and ParB-*parS*, and always appear prior to P1 co-localizing with the focus. This has lead to the hypothesis that these ParA foci serve as markers for P1 plasmids to migrate towards (80). Intriguingly, no hint of filamentous structure has been reported *in vivo*. There is one report of capturing ParA filaments *in vitro*, but these

filaments are likely an experimental artifact and recent work suggests that ParA may not even form filaments at all (45, 202).

A majority of what we do know about the ParABS system comes from studies on the ParB-*parS* complex and the interplay between ParA, ParB-*parS*, and an additional host encoded factor, IHF. ParABS is the first partitioning system where a role for a host encoded protein has been identified (64). The P1 *parS* site is comprised of one 20 bp inverted sequence with an IHF binding site (39, 65). IHF is a DNA bending protein, and its binding to the *parS* region induces a sharp bend in the DNA that allows for loading of one ParB dimer onto supercoiled DNA and subsequent binding of additional ParB dimers to form a complex of DNA wrapped around a ParB protein core (24, 63, 65, 179). This is in contrast to SopB-*sopC*, where SopB binding occurs in linear fashion on *sopC*, and likely reflects the different organization of *parS* and *sopC* (22, 78, 133, 180). The *parS* site is comprised of one 20 bp inverted repeat, while *sopC* is comprised of a series of repeats arranged in tandem. ParB spreading is not essential for proper partitioning, but the ParB-*parS* complex is required for effective plasmid pairing (53, 83, 172). ParA can interact with this complex if the ratio of ParA:ParBS is low. Higher ratios result in complete complex destabilization (21, 61). This observation has lead to the hypothesis that one role of ParA is to promote unpairing of the sister plasmids when the time to segregate arrives.

Much less is known about the ParA protein and its role in P1 partitioning, but this is rapidly being remedied. For years, the body of research focused on the role of ParA as a repressor in its ADP bound state (21, 37, 38, 45, 61). ParA in its ATP-bound state is known to be critical for plasmid stability and hypothesized to play a role in the

partitioning mechanism (41). However, other molecular details remained elusive until recently, when Vecchiarelli and colleagues reported on the role of ParA-ATP in partitioning (202). When linear DNA was affixed on one end to a flow cell surface, ParA was found to bind DNA non-specifically in clusters under sub-saturating conditions in its ATP-bound state rather than polymerize along the DNA in continuous fashion. Only under saturating conditions does ParA fully coat DNA.

Using circular dichroism and by analyzing ParA-DNA binding kinetics, ParA was observed to dimerize and undergo two conformational changes only upon the binding of ATP. Based on their results, the diffusion-ratchet model was proposed for ParA-mediated segregation as outlined in **Fig. 1-3** (91, 202). ParA binds to ATP and dimerizes to form $ParA_2$:ATP_2. Over time, $ParA_2$:ATP_2 slowly adopts a conformation that can only be assumed upon the binding of ATP: $ParA^*_2$:ATP_2. $ParA^*_2$:ATP_2 is the state that is competent for binding the nucleoid DNA. When $ParA^*_2$:ATP_2 encounters ParB-*parS*, the conformation changes one more time to ParA-ADP, and ParA dissociates from the DNA. Because the rate limiting step in this model is the assumption of a DNA-binding competent state for ParA, this effectively creates a local area around ParB-*parS* that is depleted of $ParA^*_2$:ATP_2. ParB-*parS* migrates towards higher intracellular concentrations of $ParA^{*}_2$:ATP_2, dragging the P1 plasmid in the same direction, typically towards the edges of the nucleoid away from the mid-cell starting location.

Is this the mechanism by which the P1 ParA mediates partitioning? There doesn't appear to be any conflict with the observations recorded for P1 to date. The constant P1 plasmid movements observed by Sengupta et al. is consistent with ParB-*parS* complexes responding to local fluctuations of ParA in the cell (181). Similarly, the diffuse ParA

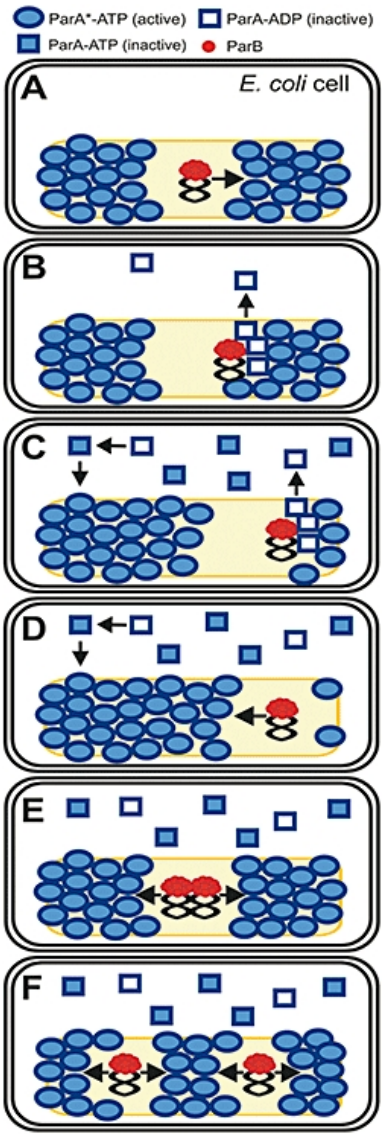

Fig. 1-3. The diffusion-rachet model of P1 partitioning. (A) ParA*-ATP binds to the nucleoid (yellow region) and the ParB-*parS* complex assembles; **(B)** Hydrolysis of ParA*-ATP leads to dissociation of ParA-ADP from the nucleoid. ParB-*parS* moves right towards the region of the cell with the higher concentration of ParA*-ATP since a delay in ParA turnover leaves a void to the left of the complex; **(C)** Continued rounds of hydrolysis and movement results in net migration of the plasmid to one nucleoid edge; **(D)** Reaching the polar edge of the nucleoid, ParB-*parS* responds to the re-distribution of ParA*-ATP on the nucleoid; **(E)** The plasmid replicates; **(F)** Each sister plasmid responds to the nucleoid gradient of Par*-ATP to result in equipartitioning of the plasmid.

From Vecchiarelli et al. *(202)*

localization over the nucleoid punctuated by bright foci at the quarter-cell positions observed by Hatano and Niki could represent ParA binding to the nucleoid with areas of high ParA concentrations, explaining why the P1 plasmids specifically migrate towards these foci (80).

Type 1b* par *loci: the double* par *locus of pB171. For the most part, low copy plasmids harbor only one partitioning system—why carry the metabolic burden of encoding two when one will suffice? An exception is found on the *E. coli* virulence plasmid, pB171, where the *par* locus encodes two *par* loci arranged divergently in tandem as diagrammed in **Fig. 1-2**. The Type Ib locus is called *par2* and the Type II *par* locus is called *par1* (50). Situated between the *par1* and *par2* overlapping the promoter regions and situated downstream of *par2* are two centromere-like sites, *parC1* and *parC2*. Plasmid stability assays indicate both *par* loci encode fully functional partitioning systems and act synergistically to mediate stability. However, the Type Ib locus is more efficient at plasmid stabilization than the Type II locus (50). Furthermore, the repressor of *par2* negatively regulates both *par* loci whereas the repressor of *par1* negatively regulates only its own operon, suggesting *par2* is epistatic to *par1* (167). Together, these data suggest that the Type Ib partition system encoded by *par2* may be the primary means by which pB171 ensures its stability.

Type Ib ParA proteins lack the N-terminal domain traditionally found on the Type Ia ParA proteins. However, this difference does not drastically alter the localization phenotypes of pB171 and the Par proteins compared to their Type Ia counterparts. The plasmid follows the same segregation pattern for all Walker box ParA proteins, localizing at the mid-cell and migrating to the quarter-cell positions after replication (49). ParA is a

nucleoid associated protein that oscillates in a helical pattern dependent on ATP hydrolysis, ParB, and *parC* (49, 50). ParB binds to *parC1* and *parC2* in a cooperative manner, forming higher ordered structures *in cis* as well as *in trans* to mediate plasmid pairing (168). As in the case for P1, IHF has been shown to bind to sites in the *par2* operon, perhaps to bend the region and promote association of ParB-*parC* complexes that are physically separated by the location of the *par2* operon. Like SopA, ParA has been shown to form filaments in an ATP dependent manner and binds DNA in a non-specific fashion (52, 169).

The model for pB171 partitioning diagrammed in **Fig. 1-4** emerged from a combination of fluorescence microscopy studies and mathematical simulations by Ringgaard and colleagues (169). Co-visualization of ParA and pB171 showed that pB171 consistently associates with the trailing edge of ParA movement in the cell. ParA would polymerize outwards until encountering a plasmid, upon which ParA would switch into a disassembly stage and retract. Retraction is related to ParB stimulation of ParA ATP hydrolysis, as ParB mutants defective in productive ParA interactions result in static ParA movement and plasmid partitioning defects. These data strongly hinted at a pulling mechanism of action where ParB hydrolyzes ParA-ATP to ParA-ADP at the ends of the filaments it encounters. Continued interaction with the next ParA-ATP dimer in the filament ultimately results in retraction of ParA and pulling of plasmid DNA towards areas with higher ParA-ATP concentration.

Computer simulations were carried out to determine if a pulling mechanism could produce the plasmid positioning observed in these cells. The results were in full agreement with the observed dynamics with one slight modification. Equipartitioning

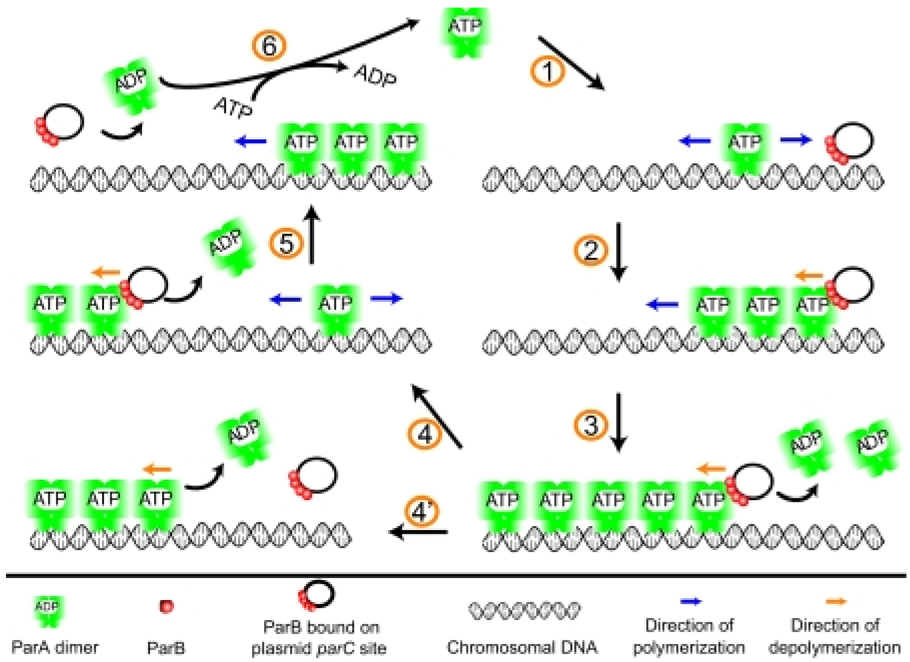

Fig. 1-4. Modeling pB171 partitioning. (1) ParA-ATP forms nucleoprotein filaments on the nucleoid; **(2)** One end of the filament encounters ParB-*parS*; **(3)** ParB-*parS* stimulates ATP hydrolysis, causing ParA-ADP to dissociate from the DNA track and allowing ParB-*parS* to interact with the next ParA-ATP dimer in the filament; **(4)** Rounds of hydrolysis and plasmid movement can be repeated until ParB-*parS* falls off the end of the filament; **(5)** ParA-ATP nucleates to form another filament elsewhere on the nucleoid DNA.; **(6)** The cycle repeats, eventually equipositioning pB171 over the nucleoid region. *From Ringgaard* et al. *2009 (169).*

required that the duration of ParB association with the end of the ParA filament to be proportional to the length of the ParA filament formed. Therefore, the ability of longer ParA filaments to pull pB171 farther distances before the plasmid completely dissociates is due to: 1. a longer filament; and 2. a lower plasmid detachment rate. The reason for this is not known, but one explanation is that longer ParA filaments are comprised of a greater number of protofilaments, mediating a more effective means of contact with ParB-*parC*.

***Type 1b* par *loci: δ and ω from pSM19035*.** The plasmid pSM19035 represents one of the best studied low copy plasmids from a gram-positive host and boasts an unusual organization of its *par* locus. It encodes a Type Ib ATPase known as δ that localizes in the cell in a spiral or helical structure, three separated centromere-like sites known as *parS* comprised of a series of heptad repeats, and ω, the adaptor protein that has been modeled to bind to *parS* in a left-handed helical structure. Unlike the ParA proteins from other systems, δ and ω are not co-transcribed but are co-regulated as *parS* sites overlap the promoters of both genes (44).

Biochemical studies examining the interactions between δ, ω, *parS*, and DNA has led to the conclusion that pSM19035 encodes a partitioning system distinct from the others. This is attributable to the fact that δ does not form free-standing filaments on its own, but requires ω, *parS* and ATP to form nucleoprotein filaments (161). Furthermore, the ω-*parS* complex does not have the destabilizing effects on δ filaments as observed for a number of the other partitioning systems. The interactions between δ and ω-*parS* are extraordinarily sensitive to protein concentrations. Low ratios of ω:δ allows for plasmid

pairing at the centromere-like sites while ratios that favor the ω-*parS* complex results in maximal stimulation of ATPase activity of δ and low frequency of plasmid pairing (161). At high ω:δ, δ polymerizes onto the DNA to form the filaments needed for partitioning. Based on these results, Pratto and colleagues propose a model where δ is recruited to ω-*parS* complexes to promote plasmid pairing. As the local concentration of ω increases as δ brings ω-*parS* complexes together, the ATPase activity of δ is stimulated to result in plasmid separation and nucleoprotein filament assembly on the plasmid DNA towards the next ω-*parS* complex. Movement of the DNA occurs when the nucleating ω-*parS* complex stimulates the ATP activity of the closest δ dimer, the δ dimer dissociates form the DNA, and the ω-*parS* complex is able to interact with the next δ dimer in the filament.

Is there one model to rule them all? In the last twenty years, the combination of improved microscopy techniques and large scale sequencing of bacterial genomes have made *par* loci on low copy plasmids easy to identify and study. This has resulted in a dizzying wealth of accumulated biochemical, structural, and cytological data from multiple partitioning systems.

As we delve deeper into ParA-mediated partitioning of plasmids, however, common properties begin to emerge. There are the fundamental properties of Par proteins—ParA as a ATPase, and ParB as a DNA-binding protein—as well as common roles these proteins carry out in the cell. ParA is a protein whose ATPase activity is synergistically stimulated by their ParB-*parS* counterparts via an ParB N-terminal motif. Plasmids follow a symmetrical localization pattern, moving from the mid-cell to quarter-

cell position. ParB binds *parS* in cooperative fashion, and despite the fact that the complex structure varies from system to system, the role of the ParB-*parS* complex, however, seems to remain the same. The existence of such parallels despite less than 30% shared homology among the plasmid ParA proteins would indicate that while sequence homology is not conserved, surely the molecular basis for partitioning is.

However, one confounding factor is that not all ParA proteins can form filaments in a solely ATP-dependent manner. Early models of ParA-mediated segregation were heavily influenced by the segregational apparatus in eukaryotic cells, where microtubules assemble spindles to push chromosomes apart. It appeared that bacteria may segregate their chromosomes in a similar manner as filamentous structures were reported for several ParA proteins, including SopA, ParB of pB171, and ParF of pTP228 (11, 20, 52). In two of the systems discussed above, however, ParA from P1 and δ from pSM19035 assemble on the DNA itself. Further examination has made it clear that non-specific DNA binding is a common property of all ParA proteins and required for partitioning. The large bundled fibrous structures seen by EM interpreted as ATP-dependent filament formation for a subset of the ParA proteins are likely to be artifacts of staining or grid preparation.

To some extent, the models proposed for ParA-mediated partitioning do overlap. The ParB-*parS* complex stimulates the ATP hydrolysis of ParA and continued interaction with the next available ParA-ATP dimer results in net plasmid movement. In essence, the helical oscillation model for F, the diffusion-ratchet model for P1, and the model for pB171 movement are the same. The distinguishing difference, as pointed out, is whether ParA forms filaments or merely coats the DNA *in vivo* (91).

One last thing to note is that for all of these Type I systems, the models are uniform in proposing a 'pulling' or 'chasing' model. This is in stark contrast to the systems of the Type II variety discussed in the next section, where a pushing model of partitioning reigns. A pulling mechanism of partitioning may be another key feature distinguishing the Walker box Type I systems from their Type II brethren.

Type II systems

Perhaps not as prevalent as the Type I partitioning systems are those of the Type II variety. The *par* loci that fall under classification as a Type II locus typically encode ATPases from the actin superfamily, the first example of a partitioning protein sharing homology with a eukaryotic cytoskeletal counterpart (19, 155, 200). Generally, the ATPase is called ParM, the adaptor or centromere-binding protein is called ParR, and the centromere-like site is called *parC*. Type II systems are exemplified by the ParMRC system found on the plasmid R1, a plasmid that segregates itself based on the principle of dynamic instability.

The ParMRC system from the plasmid R1. The ParMRC system is the most thoroughly characterized active partitioning system from a cytological, structural, and biochemical standpoint. Early studies using immunofluorescence microscopy showed that R1 is often found in one of two states: as one focus representing the plasmid at the cell center or as two foci representing the segregating plasmids en route to the cell poles. In cells with two foci, an axial ParM filament extends from plasmid to plasmid (138). Coupled with the knowledge that ParR promotes plasmid clustering by pairing together

ParR-*parC* complexes, this led to a basic model of R1 segregation where ParM would polymerize to push apart and separate newly replicated sister plasmids (97, 138, 212).

A series of elegant experiments reconstituting the partitioning system *in vitro* by Garner and colleagues allowed for a more detailed picture of R1 partitioning to emerge. By fluorescently tagging ParM, the authors demonstrated that ATP-dependent formation of ParM filaments is bidirectional and unstable, with periods of ParM elongation followed by rapid shortening upon ATP hydrolysis (66). The addition of beads coated with *parC*-ParR complexes allowed for the capture of images demonstrating ParM filament stabilization and polymerization to push the beads apart (67). As a result, the R1 partitioning model in **Fig. 1-5A** was modified to include the inherent instability or dynamic instability of ParM filaments. During cell growth, ParM filaments are in a constant state of flux. ParM binds ATP to polymerize a short length before hydrolysis results in rapid catastrophic disassembly. Filament stabilization only occurs when ParM interacts with a ParR-*parC* complex on each end. Growth of the filament occurs by insertional polymerization to push the sister plasmids apart to opposite poles (66).

Subsequent timelapse microcopy studies have refined the molecular mechanism even further. As stated earlier, R1 localizes as two foci in the polar regions of the cell. Occasionally, cells will produce a third focus that travels between the two foci near the polar regions in a repeated ping-pong-like fashion over the course of a cell cycle as shown in **Fig. 1-5B**. The cause of this motion is due to repeated cycles of ParM-GFP polymerizing and pushing sister plasmids apart from one polar cluster to another. Since the polymers are unstable, they disassemble as soon as the segregating plasmids reach

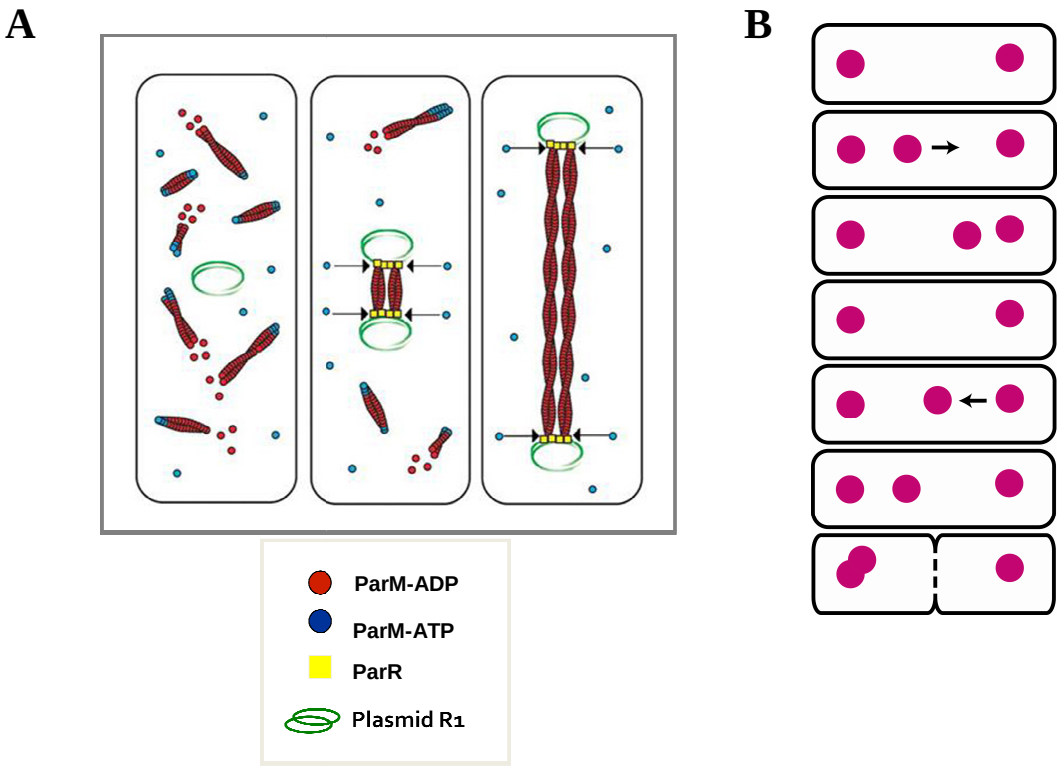

Fig. 1-5. R1 partitioning by means of dynamic instability. (A) Modeling the dynamics of ParMRC function. Left: ParM-ATP assembles into short filaments that undergo periods of polymerizing alternating with periods of catastrophic disassembly triggered by ATP hydrolysis. Middle: Stabilization of filaments occurs when the ends encounter the ParR-*parC* complex. Right: Insertional polymerization pushes sister plasmids towards opposite polar regions of the cell. **(B)** How the ping-pong behavior of R1 ensures plasmid inheritance. Continual movement of R1 from one polar cluster to the other ensures that each pole is occupied by at least one R1 plasmid at any given point in time so that each daughter cell receives one copy by the time the division septum forms.

Adapted from Garner et al. *(66)*

opposite poles. Repeated cycles of ParM mediated pushing thus ensures that each polar region contains at least one copy of R1 (30).

Attention has now shifted to the finer structural aspects of the ParMRC system, namely how the ParM filament tips interact with the ParR-*parC* complexes. Binding of ParR to *parC* yields a complex where the DNA is U-shaped, wrapping around a hollow ParR solenoid to form a superhelical structure just wide enough to accommodate one ParM filament (34, 90, 174, 179). It is likely that ParM polymers interact with the ParR-*parC* complex at the core center, but the manner in which it does is unknown. The interaction can take part in one of two ways: 1. the ends of the ParM filament is threaded through the ParR-*parC* core like thread through a needle; or 2. the ends of the ParM filament interact with ParR through the U-shaped opening, similar to a ball-and-socket joint. Another puzzle is how ParR-*parC* is able to indistinguishably interact with either end of the ParM filament. ParM assembles into a polar filament, making one end distinctly different from the other end, yet a ParR-*parC* complex is able to bind to either end (34, 174, 200).

AlfAB from the plasmid pBET131. For a number of years, ParMRC was considered the prototypical representative of all Type II systems. However, there have been recent hints that despite having ATPases with the common actin-fold motif in common, not all Type II systems utilize the same molecular mechanisms to mediate the segregation of their cognate replicons. AlfAB of pBET131 is one such example.

The stability of pBET131 from *B. subtilis spp. natto* relies on AlfA, the ATPase, and the product of a downstream gene, AlfB, which binds to three tandem repeats

upstream of the *alf* operon and interacts with AlfA (13, 191). Like ParM, AlfA was shown to form dynamic left-handed double-stranded helical filaments capable of polymerizing along length of the cell (13, 159, 160). Unlike ParM, these filaments are stable; they do not appear to undergo the repeated cycles assembly and disassembly associated with dynamic instability as had been observed for ParM. This stability is perhaps a reflection of the difference in filament architecture between ParM and AlfA, where ParM allows for an easier release of ADP while AlfA has a tilted ATP-binding cleft (159, 160). The molecular mechanisms governing pBET131 partitioning remains to be elucidated. It is unclear how one stable filament extending the length of the cell can provide a way to separate replicated plasmids into two separate locales, but what is evident is that there is no longer one paradigm for the Type II systems.

An even larger family than expected. In 2009, Derman and colleagues set out to search the bacterial world for more actin-like proteins with an iterative BLAST approach using the sequence with the least sequence homology to actin—but more homologous than to hsp70—acquired from the previous round of BLAST for the next round of BLAST (43). The net result was the identification of over 35 potential bacterial actin families that share less than 30% sequence homology among them, but still contain the signature motifs associated with actin. One of the proteins, Alp7A show many characteristics common to ParM, including dynamically unstable filament formation, and the ability to grant stability to an otherwise unstable plasmid when cloned with its downstream gene in the operon, *alp7R*, and the 165 bp fragment upstream of the operon start. However, for Alp7A, it appears as if the polymerization nucleates at the plasmids

themselves, as opposed to the plasmids granting stability to a forming filament. Therefore, it is possible that the Type II systems are similar to Type I systems in that motor proteins with shared, albeit low, structural homology are grouped together, but each system has a distinct twist to the molecular mechanism with which it carries out partitioning. This is underscored by the fact that AlfA, Alp7A, and ParM are all members of the actin superfamily, but clearly exhibit mechanistic properties distinct from one another.

Type III systems

Type III partitioning systems represent the newest class of Par proteins discovered to date. A second example of bacterial partitioning proteins sharing homology with eukaryotic cytoskeletal proteins, Type III loci encode a GTPase with the characteristic T4 loop motif commonly found in members of the tubulin superfamily (111, 145). The GTPase is referred to as TubZ, the adaptor protein as TubR, and the centromere-like site as *tubC* (9, 32, 111).

The two best studied examples of the TubZRC partitioning system come from the low copy plasmids pXO1 and pBtoxis from *Bacillus anthracis* and *Bacillus thuringiensis* respectively, where the genetic loci encoding the partitioning systems were originally identified as being essential for plasmid replication (193, 198). However, when homology searches revealed TubZ as a distant relative of tubulin, the hypothesized role of these genetic loci was quickly shifted from promoting replication to that of mediating partitioning instead (17, 32, 111). Subsequent data from microscopy and biochemical studies support view.

The TubZ proteins from pXO1 and pBToxis share only 21% similarity with each other, yet their behaviors *in vivo* and *in vitro* are remarkably similar. TubZ forms linear dynamic polarized filaments that polymerize along the cell membrane, almost stretching from one end of the cell to the other and curving around the cell pole when necessary (4, 111). FRAP and timelapse experiments show these filaments polymerize uni-directionally in a treadmilling fashion, where filament growth occurs at the (+) end and de-polymerization occurs at the (-) end (111).

Two requirements are necessary for dynamic TubZ filament formation: 1. an intracellular concentration exceeding the critical concentration threshold for polymerization; and 2. GTP hydrolysis. TubZ titration studies show TubZ will remain as free monomers below a certain concentration in the cell (4, 111). Introduction of a dominant negative mutant defective in GTP hydrolysis, TubZ-D269A, results in aberrantly long, static filaments—sometimes even branched and irregular in width—that become trapped in division septa since they are no longer able to disassemble from the (-) end (111). *In vitro* studies confirm both properties as being key to TubZ dynamics (5, 32).

TubZ is a right-handed double stranded filament 7 nm in width and forms long bundles consisting of 2-10 protofilaments (5, 9, 32). Curiously, 95% of the monomers in TubZ filaments are bound to GDP rather than GTP, a characteristic of eukaryotic microtubules. This has led Chen and colleagues to hypothesize the existence of a stabilizing GTP cap at the ends of the TubZ filaments (32). However, it has also been shown that hydrolysis of GTP leads to disruption of TubZ-TubZ interactions and filament instability (9). How these two findings can be reconciled is unclear.

Recent crystallographic studies of TubZ and TubR have elucidated the molecular details of TubZRC interactions, resulting in a preliminary model for TubZRC-mediated partitioning. TubR uses an unusual method to bind to DNA. Rather than binding via the canonical helix-turn-helix motif present in its structure, TubR dimerizes to bind a *tubC* site consisting of four 12-bp repeats via a continuous exposed patch of basic residues (145, 193). Four dimers bind in either an overlapping fashion or in a manner resulting in the distortion of the DNA (145, 192). The TubR-*tubC* complex then interacts with the positively charged C-terminal tail on TubZ (9, 145). Based on these and past results, Ni and colleagues propose partitioning occurs according to a tram model for the Type III systems shown in **Fig. 1-6** (145). TubZ-GTP assembles into the linear filament previously observed by microscopy. The TubR-*tubC* complex interacts with the (-) end of the filament, where it is pulled along by continuous interaction with the shrinking end of the filament. As growth still occurs at the (+) end, the plasmid is ultimately transported to the cell pole, where the force of the impact with the cell membrane results release of the plasmid, or "tram", from the TubZ filament. The filament continues to treadmill, and presumably another plasmid attaches to the (-) end via its TubR-*tubC* complex for transport to the opposite pole.

There still remains a number of lingering questions on how these molecular details translate into a functional partitioning system. First, do the plasmids associate with the (-) end of TubZ as would be predicted by the tram model? Second, how is directionality supplied? Or, restated in other words, how does one copy of the replicated plasmid know to move in one direction while the other copy moves in the opposite? The ability of TubZ to assemble with similar dynamics in *E. coli* suggests that there are no

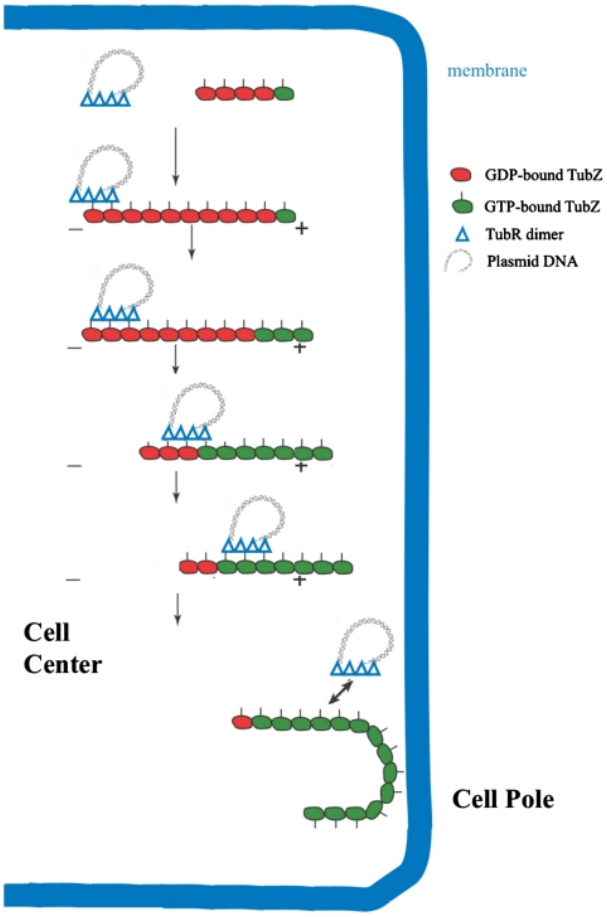

Fig. 1-6. The "Tram" model of TubZ-TubR mediated partitioning. TubR bound to the centromere site interacts with the (-) of the TubZ filament. At the same time, TubZ subunits disassemble from the (-) end and reassemble on the (+) end. Continued interaction between TubR and the (-) end of the TubZ filament ferries the plasmid towards (+) end, when force of hitting the membrane causes TubR-pBtoxis to dissociate and be deposited at the cell pole.

From Ni et al. *2010 (145)*

host specific factors involved in TubZ polymerization (32). Therefore, directionality of TubZ polymerization is likely an inherent property of the filament. Also, there is usually only one filament observed per cell and that filament only translocates in one direction (32). Does segregation of pXO1 and pBtoxis occur in a manner different from the bidirectional segregation pattern observed for the Type I and Type II systems? Answers to all of these questions would greatly benefit from using FROS to track the localization of the plasmids with respect to the TubZ filament and sub-cellular space. It is possible that pXO1 and pBtoxis follows an asymmetrical segregation pattern, where only one copy is ferried to the opposite end of the cell while one copy remains in place. Alternatively, pXO1 and pBtoxis follow a symmetrical segregation pattern, and TubZ ferries the plasmids in a continual ping-pong like fashion to ensure at least one copy in each daughter cell, similar to what was observed to R1.

The role of Par proteins in bacterial chromosome segregation

Of the three types of partitioning systems found in plasmids, only those of the Type Ib variety have ever been found on bacterial chromosomes. As clearly seen in **Fig. 1-7**, phylogenetic analyses show that chromosomal ParA proteins from all three prokaryotic domains cluster as a well-defined group away from their plasmid partitioning ParA homologs (70, 220). This has led to the speculation that there might be a function conserved among the chromosomal ParA proteins that is not conserved in plasmid partitioning (70).

Chromosomal *par* loci differ from their plasmid counterparts in a number of ways. First, chromosomal *par* systems do not appear to be restricted to one *parS* site

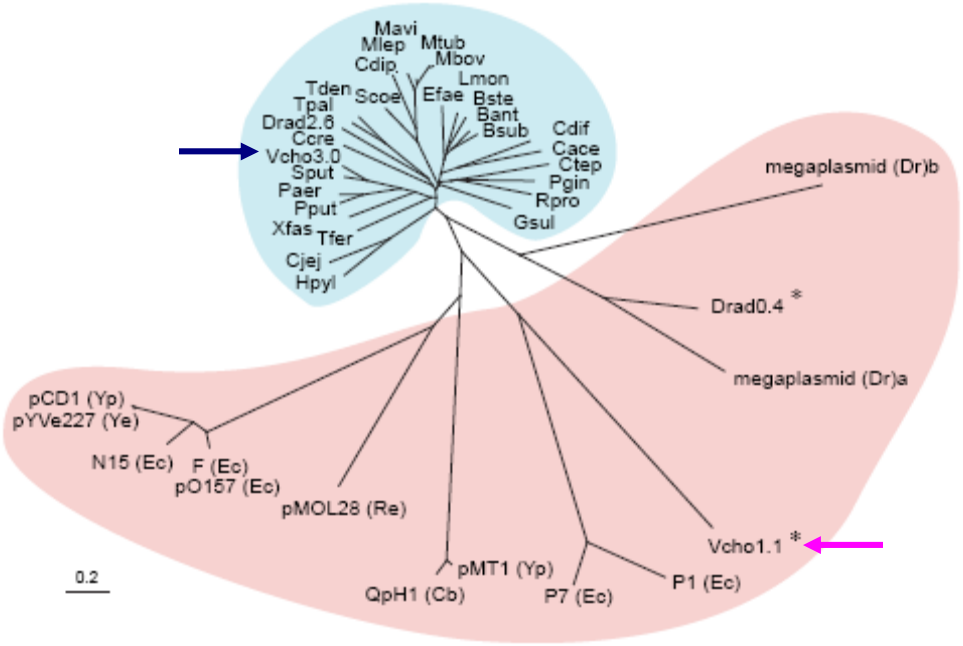

Fig. 1-7. Phylogenetic tree of ParA homologs based on amino acid sequence homology. The chromosomal ParA homologs can be seen to form a tight cluster separate from the plasmid ParA homologs. *V. cholerae* ParA1 (denoted by the blue arrow) forms a clade with the other chromosomal Type I ParA proteins while ParA2 (denoted by the pink arrow) clusters with the plasmid ParA proteins.

Abbreviations:

Vcho = *V. cholerae*; Bsub = *B. subtilis*; Ccre = *C. crescentus*; P1 = plasmid P1; F = F plasmid.

Figure adapted from Yamaichi and Niki 2000 (220).

comprised of a series of tandem repeats. Bioinformatic analyses show most bacterial chromosomes encoding for ParAB homologs contain multiple putative *parS* sites scattered in the origin-proximal region of the corresponding chromosome (131). This finding agrees with experimental findings of multiple functional *parS* sites in *B. subtilis*, *Pseudomonas aeriginosa*, *Helicobacter pylori*, and *Vibrio cholerae* (12, 26, 113, 218). The purpose of having multiple *parS* sites is unknown, since some organisms such as *C. crescentus* only have one and *B. subtilis* is able to support effective partitioning with only one origin-proximal *parS* site (76, 137, 190). Second, *parA*, *parB*, and *parS* mutations do not always result in chromosome loss, as would be predicted from the plasmid *par* studies. In some chromosomal systems, the proteins are essential for cell cycle progression or effective sporulation; in others, deletion of one component results in a mild phenotype (60, 93, 95, 137, 219). Third, recent work show segregation can be directly linked to chromosome replication, indicating that bacteria may have evolved ways to time chromosome partitioning in the larger context of the cell cycle (102, 143). Therefore, it may be that chromosomal *par* systems have functions outside of chromosome segregation. Two of the better studied examples are discussed below.

***ParABS of* Caulobacter crescentus.** Unlike many of the chromosomal *par* loci, the *par* locus in *C. crescentus* is essential (136, 137, 196). Overexpression or depletion of ParB or ParA results in cell filamentation and anucleate cell formation, suggesting that *par*-mediated segregation is intimately linked with the progression of the cell cycle (136, 137). Most of what we understand about ParABS involvement in *C. crescentus* chromosome segregation comes from visualization of the chromosome and the Par

proteins using fluorescence microscopy. These studies have revealed that segregation occurs with exquisite precision with respect to timing and space in a manner coordinated by ParABS localization over the course of the cell cycle as detailed in **Fig. 1-8**.

Localization of the chromosome during cell growth follows a polar, asymmetrical pattern. The chromosome is oriented so that the *ori* (C_{ori}) is anchored at one cell pole and the terminus is at the opposite pole (later to be at the mid-cell as the cell elongates). Upon replication, one copy of the C_{ori} traverses the length of the cell to the opposite pole before septum formation (58). Intracellular localization of ParB mirrors the movement of C_{ori}, confirming *in vitro* data that ParB binds to the *parS* site located near the origin-proximal region (47, 137, 196, 199). This ParB-*parS* complex is the site at which segregation starts: productive partitioning requires the *parS* site and not the C_{ori}. When the C_{ori}-proximal *parS* site is moved elsewhere on the chromosome, segregation does not start until that region is replicated (199).

Plotting GFP-ParB position over time revealed that partitioning is a multi-step process. The first step involves the release of the C_{ori} region from the cell pole. This is then followed by retraction of one copy of the C_{ori} back to the old pole while the second copy begins the early translocation process towards the new pole. The final step is the late translocation step where the segregating chromosome moves rapidly to reach the opposite pole (184). Curiously, ParA is not required to mediate all steps, but only required for the rapid directed movement observed in the final stage of segregation. One explanation is that should ParA encounter both C_{ori} while in such close proximity to each other, both chromosomes would be segregated to the opposite pole.

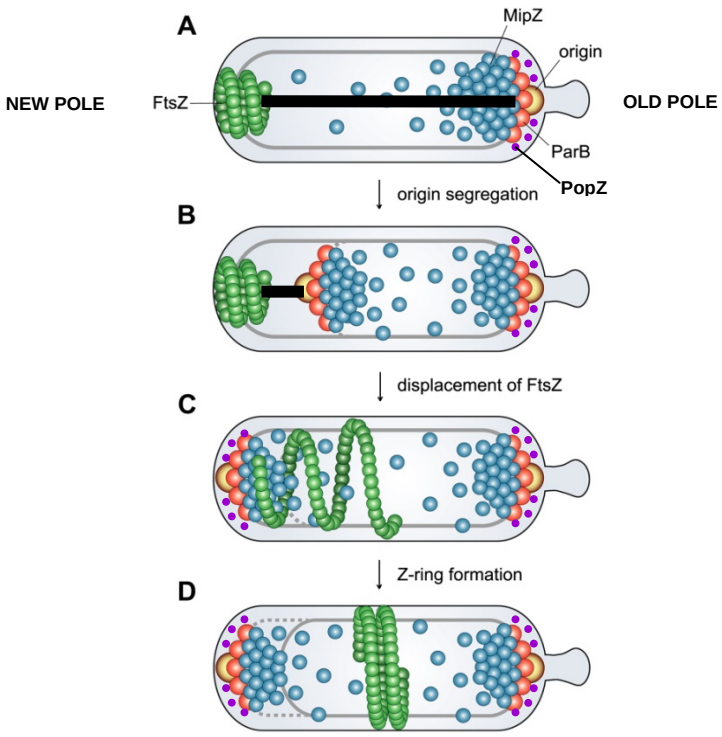

Fig. 1-8. The coordination of proteins involved in *C. crescentus* chromosome segregation. (A) In a newborn cell, FtsZ is located at the new pole at the site of the last cell division and the MipZ-ParB-*parS* complex is anchored to the old pole by PopZ. ParA polymerizes outward from the new pole; **(B)** ParA captures one copy of the C_{ori} complex and depolymerizes to pull it towards the new pole; **(C)** Arrival of the MipZ-ParB-*parS* complex at the new pole displaces FtsZ to the mid-cell where the MipZ concentration is the lowest. Anchoring of the complex is aided by the accumulation of PopZ at the new pole; **(D)** The FtsZ ring forms, and cytokinesis can commence.

Not shown: TipN, which preferentially locates to the new poles to aid proper ParA localization

Adapted from Thanbichler and Shapiro 2006 (196).

ParA localizes as a cloud or haze that grows outward from the opposite pole towards ParB-*parS*. Entry into the last stage of segregation coincides with ParA encountering ParB-*parS*, and the ParA cloud retracts to 'pull' one copy of the chromosome along (162, 177, 184). This cloud is likely to consist of ParA filaments, either associated with the nucleoid or assembled freely in the cytoplasm. Super resolution microscopy revealed the presence of a filamentous ParA structure extending from pole to pole, and ParA filaments have visualized by EM (162). Since biochemical assays have shown ParB serves as a nucleotide exchange factor for ParA by promoting ATP hydrolysis by increasing the turnover rate of ParA, ParB-*parS* may be causing ParA polymer disassembly by stimulating ATP hydrolysis (47, 58). Consistent with this reasoning, surface plasmon resonance experiments show ParB interferes with ParA-DNA binding, and ATP hydrolysis mutants display diffuse intracellular localization (162).

Three questions arise from these observations. First, what prevents ParA from assembling behind the segregating ParB-*parS* complex to pull it in the reverse direction (as seen for pB171)? Preferential localization of a protein called TipN allows *C. crescentus* to distinguish the new pole from the old pole, and co-immunoprecipitation studies show TipN directly interacts with ParA (177). It is possible that TipN serves as a 'sink' for newly dissociated ParA monomers, capturing and sequestering them to prevent reassembly of a second ParA filament that could potentially pull ParB-*parS* back towards its starting point (177). Accordingly, ParA becomes mislocalized in Δ*tipN* mutants, assembling in their normal locale between the new pole and the segregating ParB-*parS* complex as well as behind the segregating ParB-*parS* complex near the mid-cell (162, 177). Second, why is *parABS* essential for FtsZ ring formation? *C. crescentus* does not

have a Min system or nucleoid occlusion to regulate septal ring formation. Instead, an FtsZ inhibitor called MipZ has been found to interact with ParB. As one MipZ-ParB-*parS* complex stays at the old pole and the second complex moves to the opposite pole, FtsZ is unable to form a ring at the old pole or over the segregating chromosome. Only when MipZ-ParB-*parS* reaches the opposite pole does the septal ring form at the location where MipZ concentration is the lowest—at the mid-cell (196). Finally, what is responsible for the polar localization of the chromosome? ParA lends directionality to chromosomal movement, but anchoring of the chromosome involves the actions of a third protein, PopZ. PopZ gradually forms a matrix at the new pole during segregation so that by the time ParB-*parS* arrives, the chromosome can be tethered (25, 48).

Microscopy has afforded us a glimpse into how these proteins coordinate their movement to result in effective partitioning. What remains to be answered is the same question that currently eludes the Type I plasmid partitioning field: what are the molecular mechanisms by which ParA moves the ParB-*parS* complex?

***Soj, Spo0J, and* parS *of* Bacillus subtilis.** Soj (ParA) and Spo0J (ParB) were first identified in relation to the process of sporulation, not partitioning. They are not essential like ParA and ParB are in *C. crescentus*. In fact, there is no phenotype associated with *soj* mutants, and only 1% of the population in a *spo0J* or *soj-spo0J* double mutant background is anucleate (although 1% does represent a 100-fold increase over background levels in wild type cells) (93). Deleting six out of the eight origin-proximal *parS* sites on the chromosome only leads to a minor increase in anucleate cell formation, and only one origin proximal *parS* site is needed to maintain wild type

chromosome organization in the cell (127, 190). Yet, the ability of Soj-Spo0J to confer stability to an otherwise unstable plasmid containing a *B. subtilis parS* site suggests these two proteins can function as a bona fide partitioning system (127, 220). Together, the data indicate that there is some redundancy in the way *B. subtilis* partitions its chromosome.

B. subtilis has two developmental states—one as a vegetatively growing bacterium and one as a spore. In vegetative cells, the DNA is organized into a bi-lobed nucleoid structure with Spo0J located at the polar edges of the nucleoid, coinciding with quarter-cell positioning of the replicated *ori* (27, 71, 122, 128, 210). In sporulating cells, the DNA rearranges into an axial filament extending from pole to pole and Spo0J is found at the polar ends of the DNA (27, 190). Spo0J localization is dependent on both *parS* and Soj, and it has been observed that Spo0J can bind to the *parS* sites and spread along the DNA for a considerable distance (26, 134, 144, 190). Localization of Soj was originally reported as either polar or as patches on the nucleoid (134, 163). However, revisiting Soj localization with Soj-GFP expressed at native levels show Soj as a focus associated with the septum or *ori* regions that co-localizes with Spo0J (143). Similar to the other Type I ParA proteins, Soj is a nucleoid associated protein, whose oscillations are dependent on Spo0J, ATP hydrolysis, and DNA binding (86, 134, 143, 163).

The roles of Soj and Spo0J in chromosome segregation have been difficult to discern, mainly because the phenotypes are so mild. In sporulating cells, Soj and Spo0J have a clear role in mediating chromosome positioning and bulk chromosome segregation. As the chromosome is reorganized into an axial filament during the onset of sporulation, 30% of the chromosomal original proximal region is trapped in the forespore

compartment formed by the asymmetrically placed division septum (213). The amount of DNA and the chromosomal region trapped is dependent on Soj and Spo0J, since *soj* and/or *spo0J* mutants display defects in the amount of DNA as well as the region of the DNA trapped in the forespore (182, 190, 215). Recent work showed this effect is due to the role of Spo0J recruiting the condensin, SMC, to the *ori* to mediate condensation of the chromosomal DNA in the forespore (76, 190). Two additional proteins round out the panoply of proteins involved in chromosome organization at the poles: RacA and DivIVA (182, 215). RacA is a DNA associated protein that is required for reorganization of the nucleoid into the axial filament during sporulation and localizes to the poles to anchor the chromosome (14). This localization is highly dependent on DivIVA, a protein that positions itself at the poles by sensing negative curvature (164, 197). Curiously, *racA* mutants are not greatly impaired in sporulation as would be expected from cells unable to reorganize their DNA to the forespore compartment. One explanation is that the secondary phenotype of *racA* mutants—the formation of a second division site at the opposite pole—gives cells another chance to properly localize their DNA in the other forespore compartment (14). Another explanation is that there is redundancy built into the system. In support of this explanation, *soj-racA* double mutants show a ten-fold reduction in sporulation similar to that of a *divIVA* mutant (216).

In vegetative cells, the role of Soj and Spo0J in partitioning is less clear. Mutants in *soj* and *spo0J* are affected in replication initiation, nucleoid morphology, and *ori* separation (114). It had been previously reported that a high ratio of Soj to Spo0J results in over-initiation of replication, and through careful analysis of a series of Soj mutants, Murray and Errington were able to demonstrate Soj is a regulator of replication initiation

through direct interaction with the initiator DnaA (115, 143, 154). Therefore, the interaction between Soj and DnaA represents a potential link between chromosome segregation and DNA replication. However, microscopy has not offered a clue as to what the partitioning mechanism might be.

Unfortunately, *in vitro* studies of these proteins have yielded little further insight into the mechanism by which Soj-Spo0J may mediate partitioning of the *B. subtilis* chromosome during vegetative growth and/or sporulation. Crystallization of the closely related homolog from *Thermus thermophilus*, Soj_{Tth}, has been accomplished (120). Soj_{Tth} dimerizes upon binding ATP, allowing it to non-specifically bind DNA and form long nucleoprotein filaments readily viewed by EM (86, 120). Encountering Spo0J-*parS* increases the rate of ATP hydrolysis by $Soj_{Tth,}$ and this likely results in de-polymerization of the nucleoprotein filament since ADP-bound Soj_{Tth} is incapable of binding DNA. Extrapolation from these studies has led to the proposal of the treadmilling model of chromosomal segregation in **Fig. 1-9** (121). The basic steps are similar to the model outlined for δ/ω of pSM19035: a) Soj-ATP assembles on the DNA; b) Spo0J-*parS* interacts with one end to hydrolyze the Soj-ATP dimer; c) hydrolysis leads to dissociation of Soj-ADP from the DNA; and d) Spo0J-*parS* is then free to interact with the next Soj-ATP dimer in the filament. Repeated cycles would result in net movement of the chromosome. However, it still remains to be seen if Soj-Spo0J mediates partitioning in the classical cytomotive filament manner we expect.

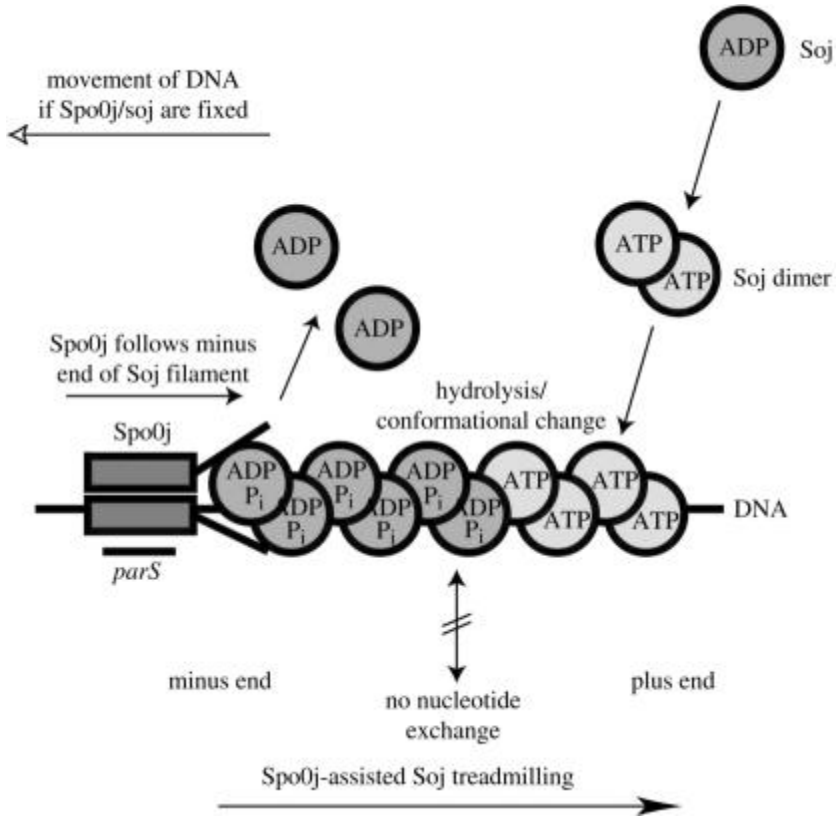

Fig. 1-9. Treadmilling model for Soj-Spo0J. The basic steps of the model are outlined in the text. Critical to this model is the existence of an anchor for Soj or for Spo0J in order to move the DNA along. Such an anchor protein remains to be identified.

From Leonard and Lowe 2005 (121)

A non-*par* mediated model for chromosome segregation

One of the difficulties of assessing the contribution of chromosomal *par* loci to the segregation of their respective chromosomes is the glaring lack of a *par* locus homolog on the chromosome of a bacterium that is known to be fully capable of faithful chromosome segregation—*E. coli*. If there is no dedicated partitioning machinery, then how does *E. coli* ensure chromosomal inheritance? It may be a matter of entropy. In the entropic model of chromosome segregation, replication increases the amount of DNA that has to be compacted into a finite space. This compaction, in turn leads an unfavorable situation in terms of conformational entropy. Subsequently, each copy of the DNA is driven outward (100). Computer simulations adopting the cellular constraints of bacterial chromosome segregation (ie. replication, supercoiling, condensation, etc.) show that modeled chromosomes can segregate themselves in the organized pattern very similar to what is observed *in vivo*. The effectiveness of this strategy increases with DNA size; therefore, plasmids have evolved *par* loci to avoid random segregation while larger chromosomes are sufficient without additional mechanisms (101). This does not explain how high copy plasmids are able to cluster at specific sub-cellular positions without the aid of dedicated positioning systems (158). However, the point is that chromosomal *par* loci may only have a limited role in partitioning, such as aiding *ori* separation.

Vibrio cholerae chromosome biology

Vibrio cholerae, a small Gram-negative curved rod, is the etiological agent of the severe diarrheal disease cholera. Using *V. cholerae* to study chromosomal biology offers an unusual perspective into how a bacterium is able to coordinate the partitioning of

multiple chromosomes because the genome is divided between two circular replicons of unequal sizes—chromosome I (chrI, 2.96 Mbp) and chromosome II (chrII, 1.07 Mbp) (84). And, while both chromosomes reside within the same bacterial cell, each chromosome encodes its own *par* locus instead of sharing a common partitioning mechanism. Plasmid stability assays show each *par* system is capable of conferring stability on an otherwise unstable plasmid, suggesting both *par* loci encode fully functional partitioning systems (173, 219).

Genetic and microscopy studies revealed that ParABS1 of chrI and ParABS2 of chrII function in non-redundant and independent fashions to mediate the localization of their cognate chromosomal origin regions *in vivo.* ChrI and chrII have two distinct sub-cellular localization patterns during the course of cell growth as shown in **Fig. 1-10** (57, 59). The chrI *ori* (*oriCI*) follows a localization pattern similar to that found in *C. crescentus*, and is unidirectional and asymmetric. The chrII *ori* (*oriCII*) follows a localization pattern similar to *B. subtilis* and low copy plasmids, and is bidirectional and symmetric. Deleting ParA1 resulted in mis-localization of *oriCI*, but chrI segregation as not detectably reduced and chrII was virtually unaffected (60, 173). In contrast, deletion of the entire *parAB2* locus resulted in gross defects in chrII localization and segregation. The severity of the phenotype was such that loss of the entire chromosome can be observed. Partitioning of chrI was unaffected (219).

Phylogenetically, only ParA1 shares sequence homology to other Type Ib chromosomal partitioning systems identified. ParA2 clusters with the Type Ia plasmid *par* systems, such as those found on F and P1 (220). Accordingly, ParA1 is the smaller

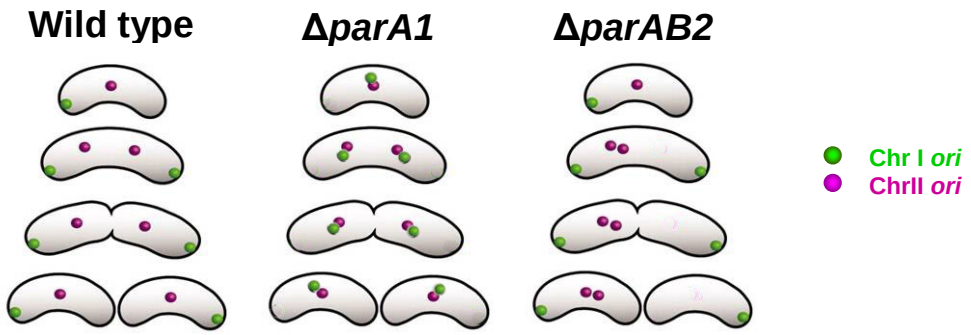

Fig. 1-10. Chromosome localization in wild type and *par* mutant backgrounds. Using FROS, the origins of chrI and chrII were visualized over the course of the *V. cholerae* cell cycle. Left**:** Localization of chrI and chrII origins in wild type cells. Middle: Localization of chrI and chrII origins in a Δ*parA1* background. Right: Localization of chrI and chrII origins in a Δ*parAB2* background.

Adapted from Yamaichi, et al. 2007 (219).

of the two partitioning proteins and lacks the additional N-terminal domain found in ParA2 and shown to be important for promoter binding in other Type Ia ParA proteins.

ParABS1 of* V. cholerae *chrI. As shown in **Fig. 1-11**, the *parAB1* operon and three *parS1* sites are located in the origin-proximal region of *oriCI* (218). Using fluorescent protein fusions, ParB1 movement was observed to be similar to movement of *oriCI*, suggestive of ParB1 binding to the *parS1* sites. ParA1 localizes between the cell pole and the chrI origins instead of between the two segregating copies of chrI as would be predicted based on the "pushing" model of plasmid segregation. This led to the proposal in **Fig. 1-12** of a pulling model of chromosomal segregation where polymerization of ParA1 outward from one pole captures a copy of the chrI *ori* at the opposite pole. De-polymerization of ParA1 retracts the polymer to pull chrI across the cell (60).

This model is based on the prediction that ParA1 behaves as a filament forming protein like its plasmid counterparts and hints of an intracellular helical ParA1 filament can be seen by de-convolution studies using fluorescence microscopy (60). However, the existence of ParA1 filaments—a critical component to a mitotic-like partitioning system proposed—remains to be shown.

ParABS2 of* V. cholerae *chrII. The molecular mechanisms behind ParABS2-mediated partitioning of chrII is even more obscure. The *parAB2* locus is located in the origin-proximal region of its cognate chromosome (**See Fig. 1-11**). Unlike chrI, there are more *parS* sites associated with the chrII partitioning system. A total of ten *parS2* sites have been identified: nine *parS2* sites scattered on chrII and one *parS2* site located on the

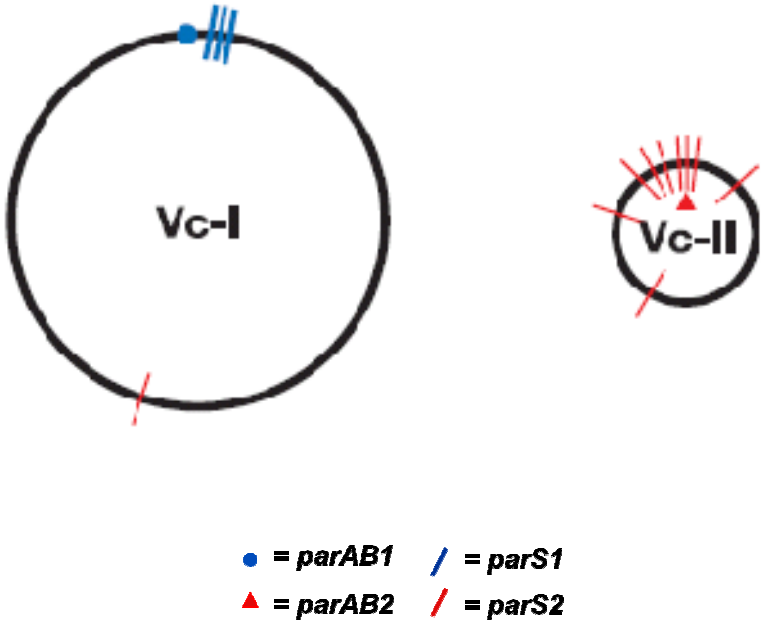

Fig. 1-11. Locations of the *V. cholerae parAB* operons and their respective *parS* sites. Left: The *parAB1* operon is located in the chrI origin-proximal region along with the three identified *parS1* sites. Right: The *parAB2* operon is located in the chrII origin-proximal region. Nine *parS2* sites have been identified on chrII and one *parS2* site has been identified near the chrI *ter*.

Adapted from Yamaichi et al. *(218).*

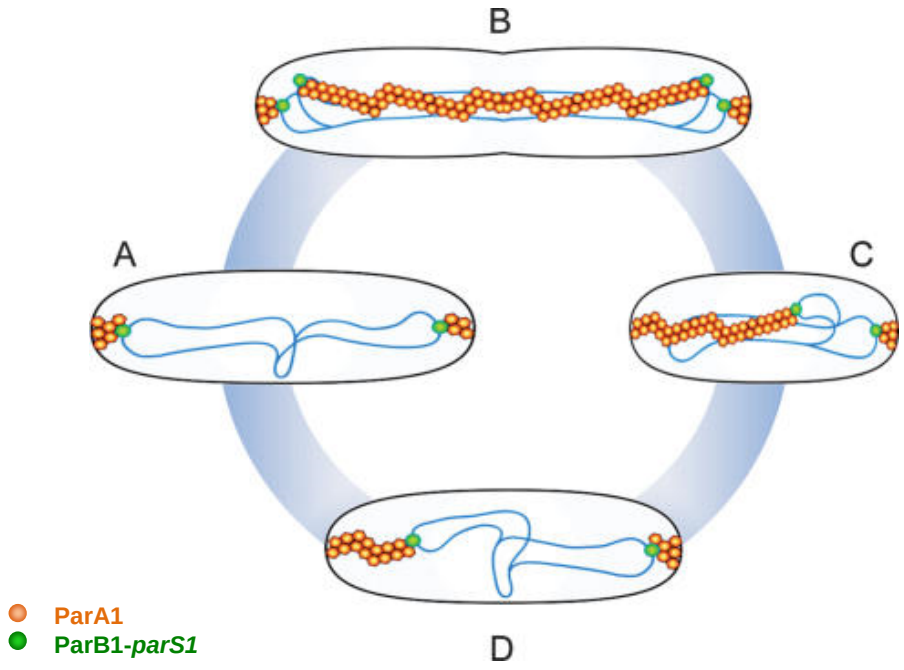

Fig. 1-12. Model for ParA1 mediated partitioning of chrI in *V. cholerae*. (A) Prior to cell division, the chrI *ori* localizes to the cell poles with the aid of ParA1; **(B)** As the division process initiates, ParA1 polymerizes outwards tom the division plane towards the chromosomal origins; **(C)** The polymerizing ParA1 interacts with one ParB-*parS* complex located at the poles; and **(D)** The ParA1 filaments depolymerize, pulling one chrI *ori* across the length of the cell to the opposite pole of the newly divided cell. At this point, a full cycle has been completed, and the process repeats.

Adapted from Fogel and Waldor 2006 (60).

ter of chrI (218). The biological significance of the one *parS2* site located at the chrI *ter* is unknown.

The fluorescence microscopy of ParABS2 has not been done to the same level of depth as for ParABS1, but preliminary studies tracking the localization of ParA2 show that it oscillates from pole to pole with a period of two minutes (60). Separate studies tracking ParB2 movement show it recapitulates movement of *oriCII*, suggestive of ParB2 binding to the origin-proximal *parS2* sites (60, 219). How ParA2, ParB2, and *parS2* interact to bring about partitioning of chrII is unclear.

Thesis goals

The roles these *par* loci play in *V. cholerae* chromosome segregation are poorly understood, and the goal of my thesis is to elucidate the potential mechanism(s) mediating chrII segregation, where it has been clearly shown that ParA2, ParB2, and the *parS2* sites are essential for chromosome inheritance. To achieve this end, I have focused on the *in vitro* and *in vivo* behaviors of ParA2, the protein hypothesized to provide the motive force for partitioning. Chapter Two details the nature of the filaments ParA2 forms *in vitro*. Chapter Three details the intracellular localization of ParA2 with respect to the nucleoid and ParB2. The implications of these studies are discussed in Chapter Four.

CHAPTER TWO

ParA2 forms left-handed helical filaments on DNA

Adapted from:

Hui, M. P.[1], Galkin, V. E.[2], Xiong Y.[2], Stasiak, A. Z.[3], Stasiak A.[3], Waldor M. K., and E. H. Egelman[2]. 2010. ParA2, a *Vibrio cholerae* chromosome partitioning protein, forms left-handed helical filaments on DNA. Proc. Natl. Acad. Sci. USA. **107:**4590-4595.

1. Performed all experiments except for the EM reconstruction and topology assays.
2. Performed the EM reconstructions and contour length mapping.
3. Performed the Topoisomerase I assay.

ABSTRACT

Most bacterial chromosomes contain homologs of plasmid partitioning (*par*) loci. These loci encode ATPases called ParA that are thought to contribute to the mechanical force required for chromosome and plasmid segregation. In *Vibrio cholerae*, the chromosome II (chrII) *par* locus is essential for chrII segregation. Here, we found that purified ParA2 had ATPase activities comparable to other ParA homologs, but, unlike many other ParA homologs, did not form high molecular weight complexes in the presence of ATP alone. Instead, formation of high molecular weight ParA2 polymers required DNA. Electron microscopy and three-dimensional reconstruction revealed that ParA2 formed bipolar helical filaments on double-stranded DNA in a sequence-independent manner. These filaments had a distinct change in pitch when ParA2 was polymerized in the presence of ATP versus in the absence of a nucleotide cofactor. Fitting a crystal structure of a ParA protein into our filament reconstruction showed how a dimer of ParA2 binds the DNA. The filaments formed with ATP are left-handed, but surprisingly these filaments exert no topological changes on the right-handed B-DNA to which they are bound. The stoichiometry of binding is one dimer for every eight base pairs, and this determines the geometry of the ParA2 filaments with 4.4 dimers per 120 Å pitch left-handed turn. Our findings will be critical for understanding how ParA proteins function in plasmid and chromosome segregation.

INTRODUCTION

Bacteria partition their chromosomes with remarkable accuracy. In *Bacillus subtilis,* for example, chromosome loss occurs in less than one in 10^4 cell divisions (120). The mechanisms mediating such high fidelity chromosome partitioning remain poorly understood. However, most bacterial chromosomes contain homologs of plasmid partitioning (*par*) loci, leading to speculation that chromosomal *par* loci contribute to the segregation of replicated chromosomes to daughter cells (70, 131, 220).

In low copy plasmids, *par* loci encode three components required for plasmid maintenance: a *cis*-acting (centromere-like) DNA site, a *trans*-acting protein that binds its cognate *cis*-acting site to form a nucleoprotein complex, and an ATPase that is thought to serve as the motor component for separating the nucleoprotein complexes (reviewed in (178)). Based on the ATPase structure, *par* systems are divided into two categories (70). Type I systems have ATPases that share a deviant Walker box ATP-binding motif, and are further classified into two subgroups based on the presence (Type Ia) or absence (Type Ib) of an additional N-terminal domain (70, 82). Type II systems have ATPases that are structurally homologous to eukaryotic actin (155, 200). With some exceptions, chromosomal *par* systems encode ATPases similar to the plasmid Type Ib ATPases, but form their own subgroup based on amino acid sequence similarities (70, 220).

The ATPase of *par* systems is thought to be critical for generating the force needed to physically separate and segregate replicated plasmids. Several of these proteins have been shown to form dynamic filamentous structures *in vivo* and/or ATP-dependent filaments *in vitro* (2, 11, 20, 45, 52, 81, 95, 120, 126, 138, 139, 161). The best

example of how a Par ATPase can drive the partitioning process is provided by studies of ParM, the Type II ATPase of plasmid R1. ParM polymerizes in an ATP-dependent manner to form inherently unstable filaments. Interactions of these filaments with ParR-*parC* nucleoprotein complexes enhances their stability, which enables additional polymerization that pushes sister plasmids apart (66, 67, 138).

In contrast, our understanding of how Type I ATPases (often referred to as ParA) function in partitioning is limited. Unlike ParM, which forms a filamentous structure *in vivo* extending between two segregating plasmids, many ParA proteins oscillate from one end of the cell to the other with periods that do not correspond to the dynamics of plasmid or chromosome segregation (52, 60, 81, 126, 134, 163). Furthermore, the structures of ParA filaments differ from their Type II counterparts, suggesting that Type I *par* systems rely on distinct mechanisms to mediate segregation. Several ParA homologs—including SopA of F (Ia), ParF of pTP228 (Ib), and ParA of pB171 (Ib)—form bundled filaments with one frayed end when incubated with ATP, leading to speculation that filament polarity is important for function (11, 20, 52).

Recent studies have revealed that the oligomeric state of certain ParA proteins is controlled by ParA interactions with DNA. For example, Soj of *Thermus thermophilus* and δ of *Streptococcus pyogenes* pSM19035 only form filaments on DNA (120, 161). In contrast, SopA filament formation has been proposed to be antagonized by its interaction with DNA (20, 31). While DNA appears to have different effects on the polymerization of Soj/δ and SopA, interactions of ParA proteins with DNA appear critical for function. Substitutions in Soj or SopA residues implicated in their respective interactions with non-specific DNA led to their mislocalization and abrogated their ability to stabilize an

unstable plasmid (31, 86). How iParA interactions with DNA translate into molecular mechanism(s) mediating partitioning remains unknown.

The genome of *Vibrio cholerae*, the gram-negative rod that causes cholera, is divided between two chromosomes, each of which contains its own *par* locus. The two *par* systems appear to work in a chromosome-specific fashion, and the chromosomes have distinct partitioning dynamics (59, 60, 219). Genetic and cytological analyses have revealed that the chromosome II (chrII) *par* locus, *parAB2*, is essential for chrII localization and segregation, as deletions in *parAB2* result in chrII mislocalization and loss (219). Unlike the majority of the chromosomal ParA proteins, ParA2 is most similar to plasmid Type Ia ParA proteins (220). ChrII segregates symmetrically to the quarter positions in the cell prior to cell division while ParA2 localization is oscillatory (59, 60). Here, we purified and characterized the activities of ParA2 to further our understanding of how this protein promotes chrII segregation. We found that ParA2 binds to and coats DNA independently of its sequence, forming regular left-handed helical structures. Fitting a known crystal structure of a Type Ia ParA protein into our reconstruction of the ParA2 nucleoprotein filaments enabled us to model how ParA2 binds and coats DNA without changing DNA twist. Our findings—the first characterization of the structure of a ParA nucleoprotein filament—will be essential for understanding how these filaments function in plasmid and chromosome segregation.

RESULTS

ParA2 does not form higher molecular weight structures in the presence of nucleotide alone. *V. cholerae* ParA2 was purified on a heparin column followed by gel filtration chromatography. We expected that, similar to several other Type I ParA proteins, purified ParA2 would form high molecular weight polymers in the presence of ATP, which can be detected using a pelleting assay (52). Surprisingly, we found that no protein was recovered in the pellet fraction after ParA2 was incubated with ATP (**Fig. 2-1A**). Reactions containing the slowly hydrolyzable ATP analog, ATPγS, also did not promote ParA2 pelleting, thus excluding the possibility that ATP hydrolysis may have led to polymer destabilization. Our failure to detect ParA2 pelleting suggested that either the purified ParA2 was inactive or that there was a missing component required for ParA2 polymerization.

The ATPase properties of ParA2 resemble those of other ParA homologs. To differentiate between these two possibilities, we tested whether ParA2 bound and hydrolyzed ATP—properties common to ParA homologs. Using a photoaffinity cross-linking assay (52), we found that ParA2 bound ATP (**Fig. 2-2A**). ParA2 also bound ADP and ATPγS, since the addition of either cold nucleotide in excess competed with [α^{32}P]-ATP for binding. A second ATP analog, the non-hydrolyzable AMPPNP, did not appear to interact with ParA2, so this analog was not used in subsequent assays. ParA2 also did not bind CTP or GTP (**Fig. 2-2A**). Therefore, ParA2 appears to selectively bind adenosine derivatives.

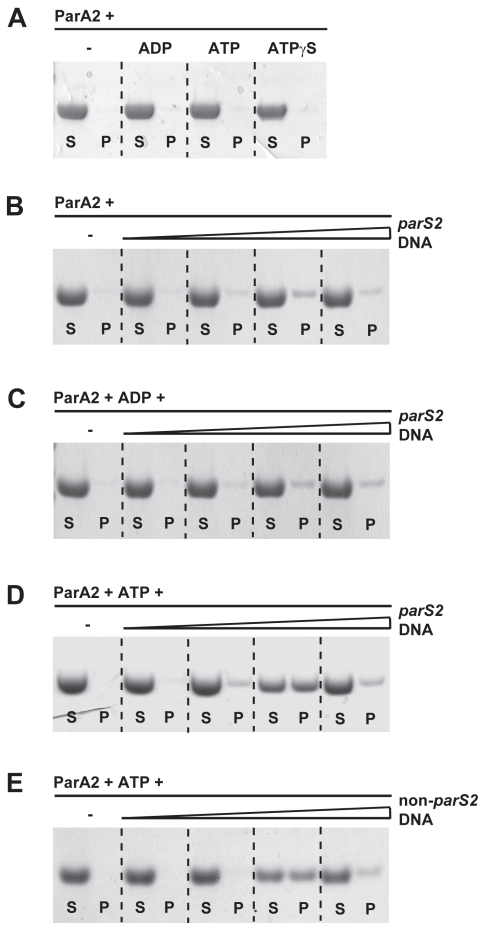

Fig. 2-1. Detection of higher molecular weight ParA2 structures with a pelleting assay. In each case, ParA2 was 10 μM and nucleotides were used at 1 mM. For the DNA titrations, 1.5 fmol – 1.5 pmol of pSM829 (B-D) or pSM833 (E), corresponding to ParA2:DNA molar ratios varying from 200,000:1 to 200:1 were used. (S) and (P) denote the supernatant and pellet fractions, respectively.

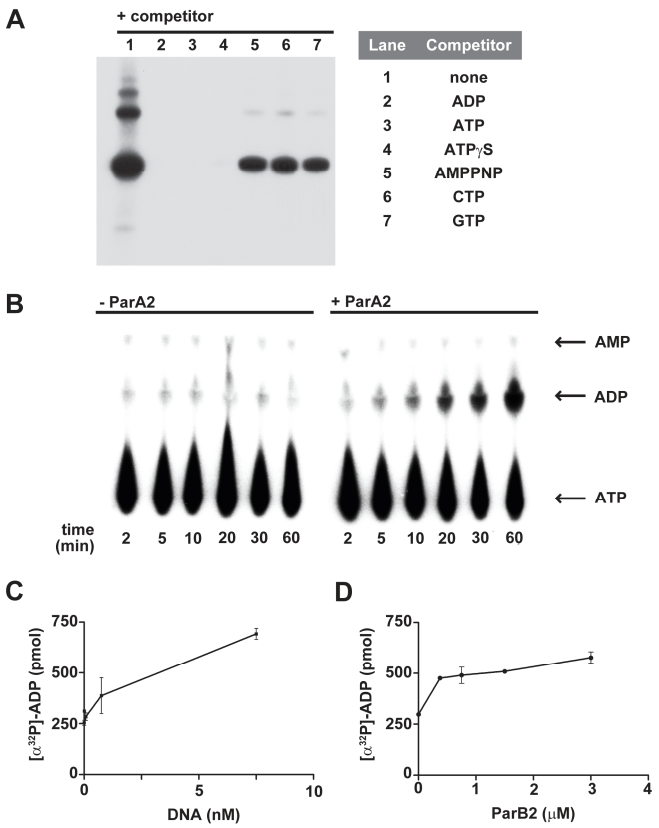

Fig. 2-2. ParA2 binding and hydrolysis of ATP. (A) ParA2 nucleotide binding as assessed by photoaffinity cross-linking. Reactions contained 5 μM ParA2 and 167 μM [α^{32}P]-ATP; excess cold nucleotide competitors were added to a final concentration of 2 mM. (B-D) ParA2 ATP hydrolysis detected by TLC. In (C), ParA2 was incubated with 7.5 pM – 7.5 nM pSM829, corresponding to a ParA2:DNA molar ratio range from 200,000:1 to 200:1. In (D) ParA2 was incubated with 0.38 -3.0 μM ParB2, corresponding to a ParA2:ParB2 molar ratio range from 4:1 to 1:2. Values in (C) and (D) were averaged from two independent experiments.

We carried out competitive binding experiments using ParA2, [α^{32}P]-ATP, and varying concentrations of cold ADP or ATP to compare the binding affinity of ParA2 for these two nucleotides, which have been shown to differentially regulate the activity of other ParA homologs (38). Although there was some variability in the absolute values obtained, competitive binding curves revealed that ParA2 had a 1.5- to 2-fold higher affinity for binding ATP than for binding ADP (**Fig. 2-3**). The significance of this small difference is not known, but similar values have been reported for ParA of P1 and SopA of F (20, 37, 208).

Thin layer chromatography (TLC) assays demonstrated that ParA2 was an active ATPase, with an apparent Km of 29 μM, a number within the range of values reported for other ParA homologs (**Fig. 2-2, 2-3**) (11, 20, 40, 47). The hydrolytic activity of ParA2 was enhanced in the presence of DNA and ParB2 (**Fig. 2-2C**). Taken together, these experiments demonstrated that the purified *V. cholerae* ParA2 was active and had ATP binding and hydrolytic activity similar to other Type I ParA proteins.

Formation of high molecular weight forms of ParA2 requires DNA. Since purified ParA2 had an ATPase activity *in vitro*, we suspected that additional factors or specific conditions might be required for ParA2 polymerization. The two most obvious candidates were the other components of the ParABS2 system, ParB2 and *parS2*. ParB2 did not appear to promote ParA2 pelleting under any condition tested (**Fig. 2-4**). Incubating ParA2 with DNA containing the *parS2* site, however, was sufficient for pelleting (**Fig. 2-1B**). Subsequent experiments revealed that the *parS2* DNA sequence was not required, as equivalent amounts of ParA2 were found in the pellet fraction using DNA that did not contain the *parS2* sequence (**Fig. 2-1D, E**). Thus, DNA, irrespective of

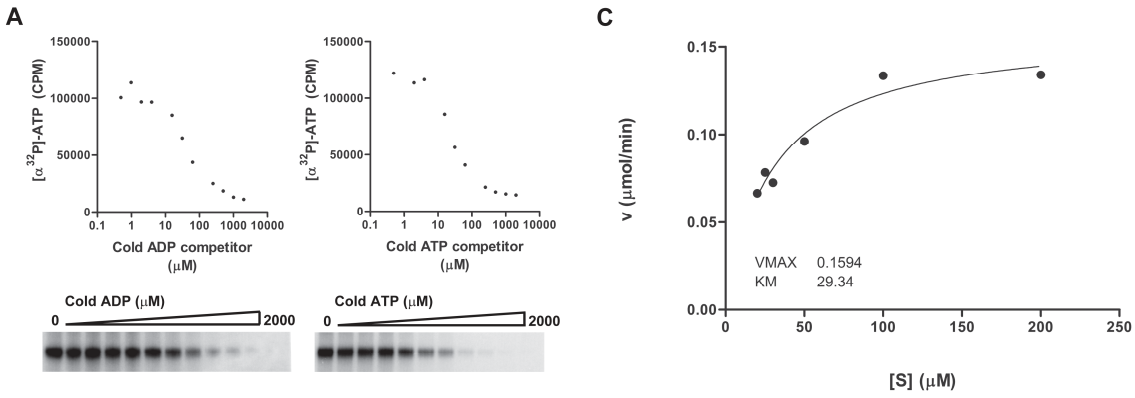

B

Experiment No.	ADP	ATP
1	42.17	32.08
2	41.39	23.71
3	19.74	10.26

Fig. 2-3. Kinetics of ParA2 binding and hydrolysis of ATP. (A) ParA2 preferentially binds ATP over ADP. Competitive binding curves for ADP and ATP are displayed along with the raw data from one representative experiment. In these experiments, a series of reactions with 0.5 μM to 2 mM ADP or ATP was incubated with 2.3 μM ParA2 and 0.1 μM [α^{32}P]-ATP in Buffer P. Bands corresponding to [α^{32}P]-ATP cross-linked ParA2 were quantified by phosphorimaging. Concentrations where 50% binding was observed were calculated using Prism software and non-linear regression curve fitting. (B) The values from three independent sets of ADP and ATP titrations at which 50% binding of [α^{32}P]-ATP was observed (units in μM). (C) Michaelis-Menten plot of ParA2 ATP hydrolysis kinetics. A series of reactions where 1.5 μM ParA2 was incubated with 20 μM to 200 μM ATP spiked with [α^{32}P]-ATP at 37ºC in 70 μl reaction volumes were carried out to produce the substrate versus time curves. Aliquots were removed and quenched at the time intervals indicated. Prism software was used to calculate the velocity of ATP hydrolysis, to plot the Michaelis-Menten graph, and to calculate Km using non-linear regression curve line fitting.

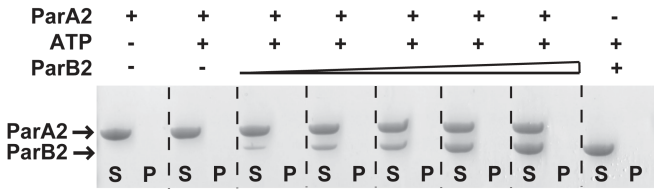

Fig. 2-4. **ParB2 does not promote ParA2 pelleting.** ParA2 (10 μM) is incubated with 2 – 10 μM ParB2 in the presence of ATP (1 mM), corresponding to a range of ParA2:ParB2 molar ratios from 5:1 to 1:1

its sequence, was necessary for formation of high molecular weight ParA2 species. Less protein was recovered in the pellet fractions at the highest DNA concentrations tested (**Fig. 2-1B, C, D, E**), most likely because formation of high molecular weight ParA2 species involves ParA2 polymerization on DNA (see below). At higher DNA concentrations, ParA2 may bind to a larger number of DNA molecules and the resulting molecular weights of such ParA2 polymers are insufficient for recovery by low speed centrifugation. Finally, pelleting of ParA2 and DNA was enhanced by the addition of ATP but not ADP (**Fig. 2-1C, D**). Most other ParA homologs do not pellet in the presence of ADP (11, 20, 120).

ParA2 binds and coats DNA in a non-sequence specific manner. Electrophoretic mobility shift assays (EMSA) and restriction enzyme protection assays were carried out to further characterize the interaction between ParA2 and DNA. In EMSAs, ParA2 shifted DNA probes that contained *parS2* (**Fig. 2-5A**) or a random DNA sequence (**Fig. 2-5B**) at similar points in the titration, demonstrating that ParA2 bound DNA in a non-specific fashion. Furthermore, under conditions where pelleting occurred, the interaction between ParA2 and DNA fully protected the DNA molecule from restriction by the endonuclease *Sau*3AI (**Fig. 2-5C**). Together, these observations suggest that ParA2 binds and coats DNA in a uniform fashion to form the higher molecular weight structures recovered in the pelleting assays.

ParA2 forms nucleoprotein filaments. Electron microscopy (EM) analyses of ParA2 prepared with calf thymus double-stranded DNA (dsDNA) yielded insight into the structure of the ParA2-DNA complexes. These images showed that ParA2 formed regular helical filaments in the presence of DNA but not in its absence (**Fig. 2-6**).

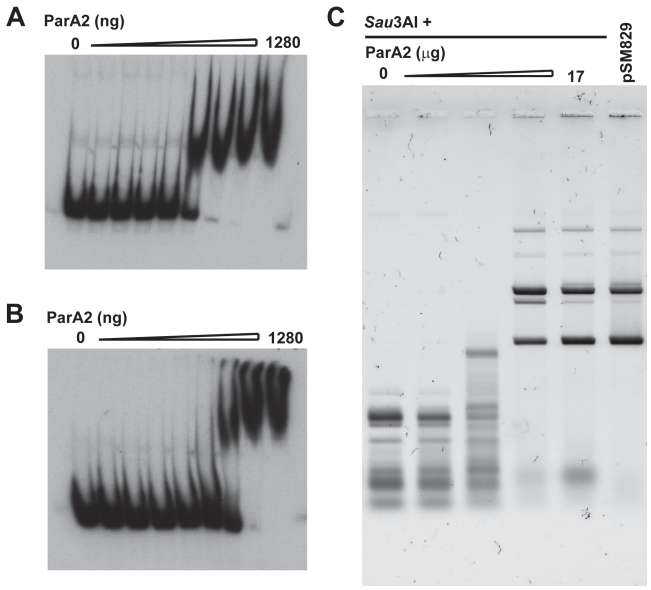

Fig. 2-5. ParA2 interacts with DNA in a non-sequence specific manner. EMSA of ParA2 binding to radio-labeled *parS2-A* DNA (A) or random DNA (B). ParA2 ranged from 0 – 1280 ng (0 - 1.4 μM). (C) ParA2 protection of pSM829 from restriction by *Sau*3AI. ParA2 ranged from 0.14 – 17 μg, corresponding to a molar ratio range of ParA2:DNA of 82:1 – 8237:1.

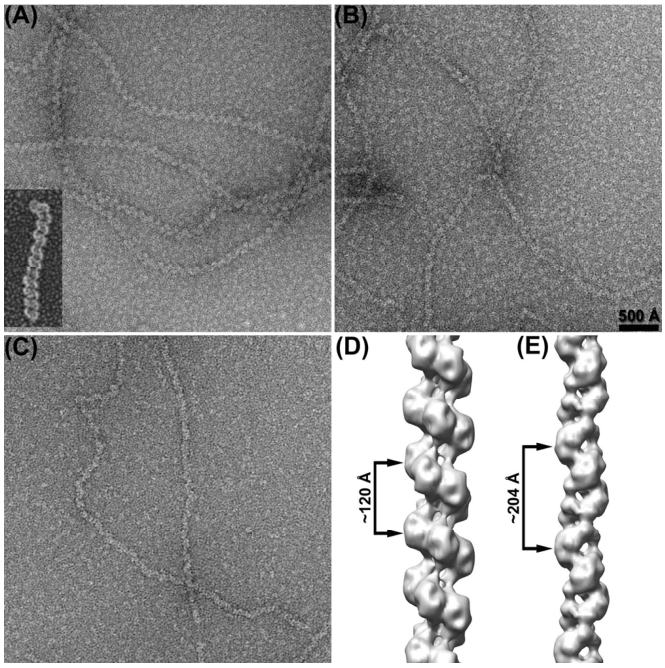

Fig. 2-6. Electron microscopy of ParA2-dsDNA filaments. Electron micrographs of negatively stained ParA2-dsDNA filaments formed in the presence of ATP (A), ParA2-dsDNA filaments formed in the presence of ADP (B), and ParA2-dsDNA filaments (C). The scale bar (B) is 500 Å, and applies to (A-C). The inset in (A) depicts a fast freeze/deep etch micrograph of a ParA2-DNA filament formed in the presence of ATP. Three-dimensional reconstructions of ParA2-dsDNA filaments formed with ATP (D) and ParA2-dsDNA filaments formed in the presence of ADP (E).

Coupled with the observations described above that ParA2 pellets in the presence of DNA, this strongly suggests that the observed ParA2 filaments are polymerized on DNA. ParA2 did not require a nucleotide cofactor for filament formation, as filaments were seen in the absence of a nucleotide cofactor (**Fig. 2-6C**) as well as in the presence of ADP (**Fig. 2-6B**) or ATP (**Fig. 2-6A**). However, the ParA2 filaments formed with ATP appeared more regular and thicker than those formed with ADP or in the absence of nucleotide cofactor. This impression was confirmed by three-dimensional reconstructions of these images. The filaments formed with ATP had ~ 4.4 subunits per turn of a ~ 120 Å pitch helix (**Fig. 2-6D**), whereas the filaments formed with either ADP or no nucleotide were very similar, and had ~ 4.1 subunits per turn of a ~ 204 Å pitch helix (**Fig. 2-6E**). Attempts were made to use cryo-EM of unstained samples to obtain higher resolution, but the filaments did not survive the specimen preparation procedures. Thus, negatively stained filaments were used for all analysis. Also, since the ParA2 filaments formed with ADP appeared more ordered than the filaments formed in the absence of nucleotide, ParA2 filaments polymerized in the presence of ADP were used for further studies.

ParA2 forms a bipolar, left-handed helix. Regardless of the nucleotide bound, ParA2 filaments were bipolar, so the asymmetric unit must contain a dimer of the ParA2 protein. However, helical reconstruction in the absence of any other information suffers from an enantiomorphic ambiguity, since projections of left-handed and a right-handed helices are indistinguishable (55). By fitting the P1 ParA crystal structure into the ParA2 filaments, several important features of the nucleoprotein filaments were revealed. The bipolar nature of the ParA2-dsDNA filaments formed with ATP could be easily explained

by fitting a crystal dimer of the P1 ParA protein bound to ADP (45) into the reconstruction (**Fig. 2-7**). Furthermore, the P1 ParA crystal structure only showed an excellent fit into the ParA2 filament if it was assumed to be left- and not right-handed. This was confirmed by using fast freeze/deep etch electron microscopy (87) (**Fig. 2-6A**, inset).

Our model predicts that the N-terminal helix-turn-helix (HTH) domain of ParA2 makes contact with the N-terminal domains from two other subunits in the filament (**Fig. 2-7A**), with one contact being longitudinal and the other lateral. This N-terminal domain is not present in other chromosome-encoded homologs of ParA2, such as Soj and ParA1. Residues that have been implicated in sequence-independent DNA-binding in two ParA2 homologs, Soj (86) and SopA (31), can be mapped onto the corresponding residues in the P1 ParA crystal structure (**Fig. 2-7B**, red and blue spheres, respectively). These residues would form part of the inner surface of the ParA2-dsDNA filament, and the residues in one ParA2 subunit would be near the corresponding residues in the other half of the dimer, forming a dsDNA binding surface as predicted (86). We were unable to definitively resolve the DNA in the EM reconstruction, likely because the staining of dsDNA can be quite variable in negative stain (DNA may either exclude stain or bind stain positively). However, there is a helical tube of negative density corresponding to a high concentration of stain that runs along the putative DNA-binding residues.

ParA2 does not alter DNA helicity. It seemed counterintuitive that a left-handed protein filament could form on right-handed DNA without altering its helicity. We measured the contour lengths of ϕX174 circular double-stranded DNA while complexed with ParA2 to explore the state of the DNA within the ParA2 filament. For

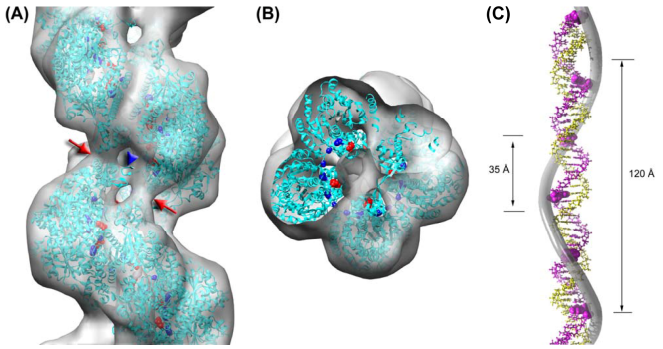

Fig. 2-7. Reconstructing ParA2-dsDNA filament formation. The three-dimensional reconstruction of ParA2-dsDNA filaments formed with ATP (transparent grey surface) can be fit by the unmodified crystal structure (45) of a P1 ParA-ADP dimer (PDB 3EZ2), shown as cyan ribbons. The side view (A) and the top view (B) show the good match between the density envelope and the high resolution protein structure. Atoms in P1 ParA residues 318 and 349 are represented as red spheres, and these correspond to residues 189 and 218 in Soj which have been shown to be crucial for sequence-independent DNA-binding (120). Atoms in P1 ParA residue 351 are shown as blue spheres, and this corresponds to residue 340 of SopA which has also been shown to be essential for sequence-independent DNA-binding (31). The HTH-domain is involved in both lateral (A, blue arrowhead), and longitudinal (B, red arrows) contacts within the ParA2-dsDNA-ATP filament. (C) The geometry of ParA2 binding to B-form DNA. One strand of the DNA is shown in magenta, and the other in yellow. The DNA has ~ 10.4 bp per turn, with a pitch of ~ 35 Å. Every eighth nucleotide along the magenta strand is indicated with the space-filling atoms. The helical path connecting these residues is shown by the grey transparent tube, which makes one left-handed turn every 120 Å, contacting 4.4 of the space-filling atoms per turn. These are the helical parameters of the ParA2 filament in (A).

these studies, the DNA molecules were nicked to eliminate any topological restrictions during covering by ParA2. Images of complexes formed in the presence of ATP (**Fig. 2-8A**) show nucleoprotein filaments without visible gaps. In B-form DNA, ϕX174 (5,386 base pairs) has a calculated contour length of 18,312 Å. The histogram showing the lengths of ParA2 complexes formed with ATP and ϕX174 DNA (**Fig. 2-8B**) suggests that completely covered DNA maintains the B-form length. Shorter contour lengths presumably arise from less than fully saturated binding. In these latter cases, interprotein interactions could close small gaps by folding them, leading to the relative shortening of filament lengths. In comparison, the contour lengths of ParA2 covered circles formed in the presence of ADP were consistently shorter than those observed for the ParA2 circles covered in the presence of ATP (**Fig. 2-8D**). The simplest explanation for the shorter contour lengths in the presence of ADP is that ParA2 binding is not saturating under this condition. Presumably ParA2 has lower affinity binding to DNA in the presence of ADP or in the absence of nucleotide than with ATP. The lower affinity is also reflected in the smaller quantity of ParA2 that pelleted with DNA when ATP is not present (**Fig. 2-1**).

The contour length measurements showed that the extension of the DNA is consistent with B-form, which has an axial rise per base pair of 3.4 Å. However, it is possible to have non-B-DNA structures with an average axial rise per base of 3.4 Å. We used a Topoisomerase I-based assay (104) to check whether ParA2 binding to DNA induces changes of DNA twist as compared to unbound DNA molecules. Despite the very high sensitivity of the assay, no shifts in the Gaussian distribution of topoisomers were seen (**Fig. 2-9**), either in the presence or absence of nucleotide. Control experiments using EM confirmed that under these conditions substantial coverage of the

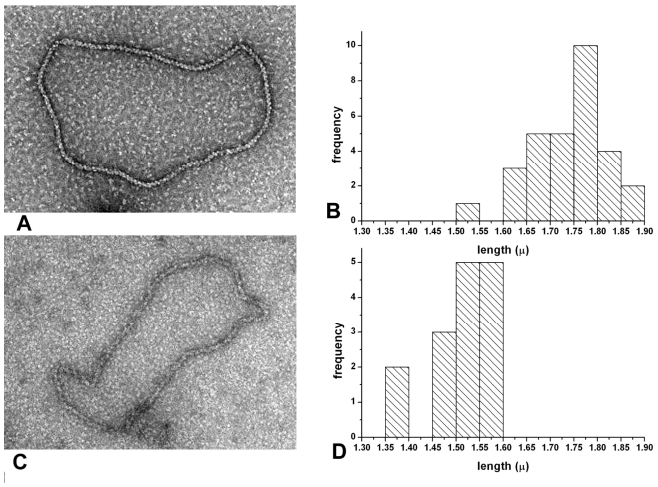

Fig. 2-8. Contour length mapping of ParA2-coated ϕX174 DNA. Nicked circular ϕX174 molecules were covered with ParA2 in the presence of ATP (A) or ADP (C). The histograms represent the contour lengths measured for ParA2 polymerized with ATP (B) or with ADP (D).

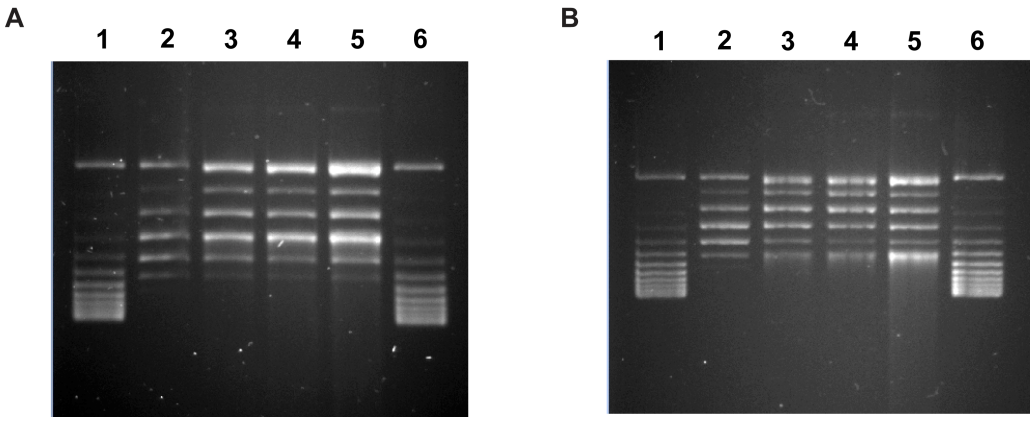

Fig. 2-9. Topoisomerase I assay assessing the topological effects of ParA2 binding on DNA. Reactions containing pUC18 supercoiled plasmid DNA were incubated with Topoisomerase I alone (2) or with Topoisomerase I and increasing amounts of ParA2 (3-5). Lane (5) represents a ParA2 concentration where 40% of the DNA molecule length were covered by ParA2. Lanes (1) and (6) show the topoisomers of pUC18 prior to treatment with Topoisomerase I. The assay was carried out in the presence (B) or absence (A) of ATP.

plasmid by ParA2 had been achieved, while still leaving some protein-free regions that would be needed for Topoisomerase I accessibility to DNA. Thus, the binding of ParA2 to the dsDNA does not involve any appreciable change in the twist of the DNA away from ~ 10.4 base pairs per turn.

DISCUSSION

ParA2 is essential for the partitioning of *V. cholerae* chrII, but the mechanism by which this Type Ia ParA protein promotes the segregation of the small *V. cholerae* chromosome is not known. Here, we purified native ParA2 and found that this protein bound and hydrolyzed ATP in a manner similar to other Type Ia ParA proteins. Unexpectedly, unlike ParA of P1 or SopA of F (two other Type Ia ParA proteins), formation of ParA2 filaments required DNA. We found that ParA2 polymerized on DNA independent of its sequence to form bipolar left-handed, helical filaments that maintained the axial spacing and the helical twist of B-DNA. The bipolar nature of ParA2-DNA filaments is in full agreement with a model presented for Soj (86), where it was suggested that a symmetrical dimer of Soj binds dsDNA in a sequence-independent manner. Filament formation did not require the presence of a nucleotide cofactor, but ParA2 nucleoprotein filaments formed with ATP were much more ordered and had a shorter pitch compared to filaments formed with ParA2 in the absence of nucleotide or in the presence of ADP. Our work does not address whether the ParA2-DNA filaments that we observed are functionally important for chromosome segregation directly, but mutagenesis of SopA (31) and Soj (86) revealed that their binding to non-specific DNA is essential for partitioning. Thus, the properties of ParA2-DNA filaments are likely to be essential for understanding how this protein promotes chrII partitioning.

While the DNA is not directly visible in our reconstruction, topological and contour length measurements define many of the parameters of the DNA in these complexes. When covered by ParA2 in the presence of ATP, the DNA is in a B-like

conformation. The absence of any change in twist in the DNA imposed by the left-handed ParA2 filament is explained by the binding stoichiometry of one ParA2 dimer for every eight base pairs. How can a left-handed ParA2 filament cover right-handed dsDNA so that each ParA2 dimer is making an equivalent interaction with the DNA? The observed stoichiometry in the ATP state—one ParA2 dimer per eight base pairs—provides a very simple explanation (**Fig. 2-7C**). The rotation per eight base pairs in B-DNA is ~ 278°, which is the same as a left-handed rotation of ~ -82°. The left-handed ParA2 helix, with ~ 4.4 dimers per turn, has a rotation per dimer of ~ -82°. Thus, the helical geometry of the ParA2-ATP filament appears to be dictated by making equivalent contacts every eight base pairs, which requires a left-handed protein helix with ~ 4.4 dimers per 120 Å pitch turn surrounding right-handed B-DNA. In the absence of nucleotide, the stoichiometry and mode of interaction between ParA2 and DNA is much less clear. One possibility is that the contacts between the ParA2 dimers and the DNA are not equivalent for every dimer, which could explain why these filaments are much more disordered than those formed with ATP.

The most intensively studied nucleoprotein filaments have been those formed by the RecA/Rad51 family of recombination filaments (170). These right-handed filaments have a pitch of ~ 95 Å, very different from the ~ 35 Å pitch of B-DNA. RecA/Rad51 impose their helical geometry on DNA by extending and untwisting the DNA (188). A detailed picture of how this is accomplished has only recently emerged (33), and involves the unstacking of triplets of base pairs along with a left-handed rotation between triplets, as opposed to the normal right-handed B-form rotation between adjacent bases. It is presumed, but not yet understood, that this is part of the mechanism for homologous

recognition that is catalyzed by these proteins. In striking contrast, we show here how left-handed filaments with a pitch of ~ 120 Å can bind to DNA without any detectable change in DNA helicity. Thus, ParA2 activities may not be linked to alterations in DNA topology.

The left-handed filament that we observed is similar to what has been proposed for a ParB homolog (ω from pSM19035) binding to multiple *parS* sites. These sites are spaced seven base pairs apart (211), and the periodicity of this heptad repeat led to the proposal that ω could generate a left-handed protein helix upon binding. This similarity could be coincidental. Alternatively, if ParB2 bound to multiple *parS2* sites forms a structure like that proposed for ω-*parS*, then the ParB2-*parS2* complex could act as a template for nucleation of ParA2-DNA filaments. Rad51, like ParA2, spontaneously self-nucleates and polymerizes on DNA in a sequence-independent manner *in vitro*. However, *in vivo*, its polymerization is thought to be tightly controlled by nucleating factors (221). A ParB2-*parS2* nucleation model would explain how ParA2 might bind to chrII and not chrI.

A number of models have been proposed to address how Type Ia ParA proteins promote partitioning of their respective replicons. Several of these models were developed for ParA proteins that only require ATP for their polymerization *in vitro* (20, 81, 126), so it is unlikely that they apply to ParA2. Treadmilling models are based upon the two ends of a filament being different, where one end is growing and the other depolymerizing. Such treadmilling of ParA2 could move the DNA to which the ParA2 filament is bound only if ParA2 were also bound to a fixed host factor (121). However, the bipolar nature of the ParA2-DNA filament that we observed suggests that such

models are unlikely, or that any polarity must be conferred by one end of the filament being in contact with ParB2 or some other as yet undetermined element.

Our work raises many questions regarding ParA2-mediated partitioning, and *par*-mediated partitioning in general. What is the link between ParA2-DNA filament formation *in vitro* and the oscillatory pattern of ParA2 localization seen *in vivo*? Second, how does ParA2 nucleoprotein filament formation fit into the larger scheme of ParA-mediated partitioning systems? Finally, do all ParA proteins form similar nucleoprotein complexes? Since both plasmid- and chromosome-encoded ParA homologs have been reported to interact with DNA in a sequence-independent manner, we propose that most, if not all, ParA proteins form filaments on DNA. Although the residues responsible for non-specific DNA interactions in SopA and Soj are not conserved, the positions of those residues map to the same region along the central core of our reconstructed filament, suggesting that the Type Ia and chromosomal ParA proteins might interact with DNA in a similar fashion. We observed that the N-terminal domains, present in Type Ia ParA proteins but absent in Type Ib ParA proteins, form important contacts that hold the nucleoprotein filament together. Since recent work indicates that δ, a Type Ib protein, also forms nucleoprotein filaments (161), there appears to be multiple means for ParA proteins to polymerize on DNA.

METHODS

Purification of ParA2. The *parA2* coding region was amplified from the *V. cholerae* N16961 chromosome using primers ParA2F (5'-CCATGGCAATGAAAAGAGAACA-3') and MHp031 (5'-GATCATCTC GAGTTACCCCTGATTCAGTGAAGACC-3'), cloned into pCR2.1-TOPO using the TOPO TA Cloning Kit (Invitrogen), and sub-cloned into pET28b via *Nco*I and *Xho*I (sites underlined), yielding pMH118. The construct was verified by sequencing. *E. coli* BL21(DE3)/pMH118 was grown in 400 ml LB containing 50 μg/ml kanamycin at 37°C shaking until $OD_{600} \approx 0.6$, when ParA2 expression was induced with 1 mM IPTG at 25°C for 2 h. Cells were harvested by centrifugation at 5,000 x *g* for 10 min at 4°C, and the pellet was stored overnight at -20°C. The pellet was resuspended in 10 ml Buffer B (30 mM Tris-HCl [pH 8.0], 100 mM NaCl, 1 mM $MgCl_2$, 2 mM DTT, 1 Complete Mini protease inhibitor tablet [Roche]). Cells were lysed using a French-pressure cell, and the lysate was clarified by centrifugation at 20,000 x *g* for 1 h at 4°C before loading onto a 1 ml HiTrap Heparin HP FPLC column (GE Healthcare) equilibrated with Buffer B at 4°C. ParA2 was eluted using a 20 ml NaCl gradient of 0.1-1.0 M in Buffer E (30 mM Tris-HCl [pH 8.0], 1 mM $MgCl_2$, 2 mM DTT). Fractions judged to be ≥95% pure on a Coomassie Brilliant Blue stained SDS-PAGE gel were pooled, concentrated using an Amicon Ultra-4 Centrifugal Filter Unit (Millipore), loaded onto a 24 ml Superdex200 10/300 GL FPLC column (GE Healthcare) equilibrated in Buffer B at 4°C, and eluted at a flow rate of 0.2 ml/min. Fractions judged to be ≥99% pure on a Coomassie Brilliant Blue stained SDS-PAGE gel were pooled, dialyzed overnight into Buffer D (30 mM Tris-

HCl [pH 8.0], 250 mM NaCl, 1 mM $MgCl_2$, 1 mM DTT, 50% glycerol [v/v]), and stored at -20°C.

Purification of ParB2-His_6. C-terminal His_6-tagged ParB2 was purified as previously described (218).

Other reagents. The *parS2-A* site was amplified from pYB086 (218) using primers YPR141 (5'-GTGTAGGCTGGAGCTGCTTCG-3') and YPR163 (5'-AGTAGCTGACATTCATCCGG-3'), and cloned into pCR2.1-TOPO to create pSM829. The empty vector control, pSM833, is equivalent to circularized pCR2.1-TOPO without the *parS2-A* insert.

Pelleting Assay. The pelleting assay was done according to (52) with modifications. Briefly, pre-spun 10 μM ParA2 was incubated at 30°C for 10 min in Buffer P (30 mM Tris-HCl [pH 8.0], 5 mM $MgCl_2$, 100 mM KCl, 2 mM DTT) with 1 mM nucleotide, DNA, and/or ParB2 added where indicated. Reactions were centrifuged at 20,000 x *g* for 20 min at 4°C. The supernatant was removed, the pellet was resuspended in 30 μl of Buffer P, and 30 μl of 2X SDS loading buffer was added to all fractions. Protein was visualized on SDS-PAGE gels stained with Coomassie Brilliant Blue.

Photoaffinity cross-linking. Photoaffinity cross-linking was performed as described in (52) with modifications. Binding reactions contained 10 mM Tris-HCl (pH 8.0), 100 mM KCl, 10 mM $MgCl_2$, 5 μM ParA2, and 10 μCi [α-^{32}P] ATP (167 μM) in a 20 μl volume. TCA-precipitated pellets were rinsed with 95% ethanol (v/v) before drying at 37°C. The pellet fractions were resuspended in 25 μl of 1X SDS loading buffer, of which 10 μl was loaded onto SDS-PAGE gels.

Thin layer chromatography. Standard 15 μl reactions consisting of 1.5 μM ParA2 in 30 mM Tris-HCl (pH 8.0), 5 mM $MgCl_2$, 1 mM DTT, 100 μM ATP, and 32 nM [α^{32}P]-ATP were incubated at 30°C for 2 h 15 min before quenching with 0.75 mM KH_2PO_4 (pH 3.3). A microliter from each reaction was spotted onto TLC PEI-Cellulose F plates (EMD Chemicals), and plates were developed using 1 M formic acid/0.5 M LiCl as the mobile phase. The dried plate was exposed to a phosphor screen for quantification.

Electrophoretic mobility shift assays. EMSAs were carried out according to (105) with minor modifications. Primers YPR141 and YPR163 were radio-labeled and used to PCR amplify a 200 bp probe containing *parS2-A* from pSM829 (218). For the random DNA probe, radio-labeled primers M13F and M13R were used with pSM833 as the PCR template. Binding reactions contained 20 mM Tris-HCl (pH 8.0), 1 mM EDTA, 0.1 mg/ml bovine serum albumin, and 80 mM NaCl, and were incubated at room temperature for 10 min before the addition of 10% glycerol [final (v/v)] and immediate loading onto a 6% acrylamide DNA retardation gel.

Restriction protection assay. ParA2 was incubated with DNA in 1X NEB *Sau*3AI buffer, 100 mg/ml BSA, 1 mM ATP, and 1 mM DTT for 1 h at 37°C before treatment with 28 mM EDTA and 17% SDS. The DNA was subsequently treated with proteinase K, phenol-chloroform extracted, and run on a 0.8% agarose gel in 1X TAE.

Filament formation and electron microscopy. ParA2-dsDNA filaments polymerized with ATP were prepared with 1.3 μM ParA2 in 25 mM Tris-HCl (pH 7.2), 1.3 mM ATP, and 2.5 mM magnesium acetate with a ParA2 to calf thymus linear dsDNA ratio of 40:1 (w/w). This mixture was incubated at 37°C for 10 min before application to glow-discharged carbon-covered 300-mesh copper grids. ParA2-dsDNA and ParA2-

dsDNA filaments formed in the presence of ADP were prepared the same way, except without nucleotide or with 1.3 mM ADP instead of ATP, respectively. The grids were negatively stained with 1% (w/v) uranyl acetate. Images were collected on film using a Tecnai 12 (80 kV and x 30,000 magnification). Films were scanned on a Nikon Coolscan 8000 with a sampling of 4.16 Å per pixel.

Segments of filaments (each 330 Å long) were used in the Iterative Helical Real Space Reconstruction procedure (54) to make overall three-dimensional reconstructions in the presence of ATP (5,425 segments) or ADP (4,041 segments). The two sets yielded symmetries of -81° rotation and 26.9 Å rise (ATP), and -88.6° rotation and 50.3 Å rise (ADP).

Topoisomerase I assay. Reactions containing pUC18 and 0 – 50 μM ParA2 were pre-incubated at 37°C for 20 min in 50 mM Tris-HCl (pH 7.9), 50 mM NaCl, 5 mM $MgCl_2$, 1mM EDTA, 1mM DTT, 1mM ATP, and 20% glycerol before the addition of Wheat Germ Topoisomerase I (Inspiralis). After an additional 20 min incubation, the DNA was extracted using phenol-chloroform and loaded onto a 1.2% agarose gel containing 0.3 μg/ml of chloroquine. The gel was run for 3 h at 60 V.

ACKNOWLEDGEMENTS

We thank Brigid Davis for helpful comments on the manuscript, and John Heuser for the fast freeze/deep etch EM. We also thank Maria Schumacher for providing us with the coordinates of her ParA crystal structure in advance of release. This work was supported by NIH R37 AI-42347 and HHMI (MKW) and NIH GM035269 (EHE).

CHAPTER THREE

The intracellular dynamics of ParA2

INTRODUCTION

Biochemistry is a powerful tool for dissecting the molecular mechanisms of biological processes. By studying proteins in controlled environments on an individual and on a combinatorial basis, one can try to extrapolate the proteins' activities *in vivo* and predict how the proteins will react when encountering their interacting partners. The previous chapter described such an approach to investigate the properties of *V. cholerae* ParA2. We learned that ParA2 is a non-specific binding protein that assembles along DNA in a regular manner to form filaments. These filaments do not appear to exert changes to the DNA on which they are bound and these filaments are not polarized since one end of the polymer is structurally identical to the opposite end of the polymer. Hence, any models for ParA2 function should take into account the symmetrical nature of this filament.

The work described in this chapter takes a complimentary approach and examines ParA2 in the context of the living cell. Very little is known about the chrII partitioning system *in vivo*. The chrII *ori* (*oriC*$_{II}$) undergoes a symmetrical segregation pattern from the mid-cell to the quarter-cell positions and ParB2 has been observed to undergo the same localization pattern, suggestive of ParB2 binding to the *parS2* sequences in the *oriC*$_{II}$ proximal region (57, 59, 219). The chrII *ter* localizes to the mid-cell (187). However, where ParA2 localizes with respect to ParB2 and with respect to certain sub-cellular locales—such as the cell poles—has not been investigated.

Two main questions are addressed in this chapter. First, how does ParA2 localize with respect to ParB2 *in vivo*? Second, is the non-specific DNA binding property of

ParA2, which was observed *in vitro,* detectable *in vivo*? My findings suggest that there is no chromosome specificity of ParA2 binding in the cell. ParA2 displays a highly dynamic localization pattern and its intracellular dynamics are dependent on ParB2 and its capacity to hydrolyze ATP and bind DNA. Furthermore, visualization of ParA2 and ParB2 simultaneously revealed that ParA2 routinely localizes between a ParB2 focus and the nearest cell pole towards which the chrII *ori* is moving in late dividing cells. Together, these data are consistent with a model in which ParA2 movement over the nucleoid mediates the pulling of sister copies of chrII to the quarter-positions prior to cell division.

RESULTS

The intracellular localization of ParA2 is dynamic. The reported intracellular dynamics of Type I Walker box ParA proteins—both plasmid- and chromosome-encoded—span a wide range of phenotypes. In *B. subtilis*, Soj (ParA) localizes as discrete foci near the septa and within the nucleoid region (143). In contrast, ParA of pB171 alternates localization from pole to pole (169). The ParA of the P1 prophage is simply found as a nucleoid-associated haze with a bright blinking focus, while SopA from the F plasmid forms a focus that oscillates along a helical path in the cell (80, 81). Therefore, there is no single localization pattern observed for all Type I ParA proteins.

In order to learn about the distribution of ParA2 in *V. cholerae*, a ParA2-YFP fusion protein was constructed, placed under the control of an arabinose inducible promoter on pBAD33, and expressed in wild type *V. cholerae* N16961 grown in M63 minimal medium (a meridiploid strain). Care was taken to ensure the induction did not last longer than 1 h since it was observed that gross over-expression of ParA2-YFP leads to a static high intensity signal that masks the intracellular dynamics of the protein (data not shown). Three distinct classes of ParA2 localization were observed by fluorescence microscopy (**Fig. 3-1A**). The first class was comprised of cells where ParA2 was found at the polar regions of the cell and absent in the mid-cell region (right panel). These cells were typically longer, older cells whose division septa have noticeably started to constrict. The second class consisted of cells where ParA2 localized as a general haze

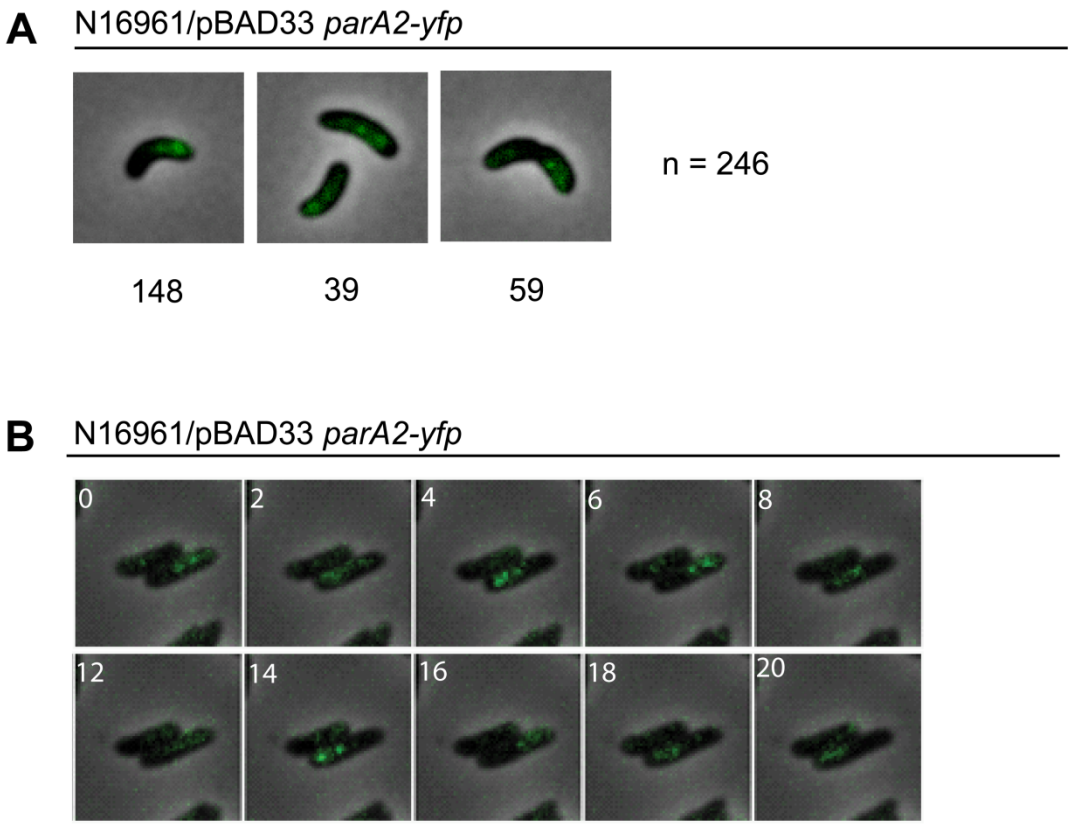

Fig. 3-1. Intracellular dynamics of ParA2. (A) Representative cells of the three different localization patterns observed in wild type *V. cholerae* cells expressing ParA2-YFP and the frequency at which these cells are found in the population. **(B)** Timelapse of ParA2-YFP movement in the cell. Images were taken at 2 min intervals over the course of 20 min.

throughout the cell without a clearly definable pattern (middle panel). The final class was the largest of the three classes by far. Approximately 60% of the cell population had ParA2 localization skewed towards one half of the cell (left panel). ParA2 formed a comet-shaped cloud or haze with one bright edge near the cell pole that decreased in fluorescence intensity towards the mid-cell. Members of this class included cells of a variety of lengths (ages).

Timelapse images revealed that ParA2 is an extremely dynamic protein in the cells of this last class (**Fig. 3-1B**). In full accordance with the preliminary observations by Fogel and Waldor (60), ParA2 oscillates from one cell half to the other cell half in a continuous fashion for the entire duration of the timelapse. This redistribution of ParA2-YFP from one cell pole to the other can occur within as little as two minutes. Furthermore, a closer look reveals that the period of oscillation is irregular. At the start of the timelapse, it takes four minutes for ParA2 to move from one pole to the other, while in the following frame at the six minute mark, ParA2 moves back to the starting pole within two minutes. The reason for this variability in ParA2 oscillation is unclear, but this variability has also been observed for F (81). It is possible that the irregular periodicity reflects ParA2 adjusting its movements accordingly in response to changes in cellular conditions. Alternatively, it may simply be that the period of oscillation is not as vital for ParA2-mediated partitioning as the actual pole to pole movements are.

ParA2 dynamics depend on ATP hydrolysis, DNA binding, and ParB2. For the plasmid ParA proteins, two key properties are essential to plasmid stability: ATP hydrolysis and non-specific DNA binding (31, 41). To determine how these properties affect ParA2 dynamics, three separate mutations were introduced into ParA2-YFP on

pBAD33 *parA2-yfp* and their intracellular dynamics were observed by timelapse microscopy in wild type cells (still expresses wild type *parA2*). ParA2 K124A and ParA2 D151A contain single amino acid substitutions in the Walker box ATP binding motif. Similar mutations in ParA2 homologs have resulted in mutants defective in ATP binding and ATP hydrolysis, respectively (143). ParA2 R352A carries a mutation at a residue predicted to be critical for non-specific DNA binding. This mutation was identified by building a homology model of ParA2 based on the crystallized structure of Soj_{Tth} using SWISS-MODEL (6, 103, 156). For Soj_{Tth}, residues R189 and R218 are both required to bind DNA non-specifically (86). The ParA2 residue R352 is found in a similar location as Soj R218.

In both Walker box mutants, ParA2 localization is altered and there is a complete loss of ParA2 dynamic movement. ParA2 K124A is found diffuse throughout the cell (**Fig. 3-2A**, top row). ParA2 D151A, on the other hand, is found as bright punctuate foci that appear to randomly drift in a subset of cells (**Fig. 3-2A**, middle row). This focus might represent a sustained ParA2 interaction with ParB2, as has been reported for Soj (143). Finally, in R352A, the DNA binding mutant, there is diffuse ParA2 localization and lack of dynamic motion (**Fig. 3-2A**, bottom row). Together, these observations suggest that ParA2 dynamics depend on its capacity to bind and hydrolyze ATP as well as its capacity to bind DNA.

In order to determine how ParB2 and *parS2* affects ParA2 oscillations, pBAD33 *parA2-yfp* was introduced into a Δ*parB2* mutant where the *parB2* gene was replaced with the spectinomycin cassette. The Δ*parB2* background shares the same phenotype as the Δ*parAB2* cells as diagrammed in **Fig. 1-10** (219). Roughly one-third of the cells loses

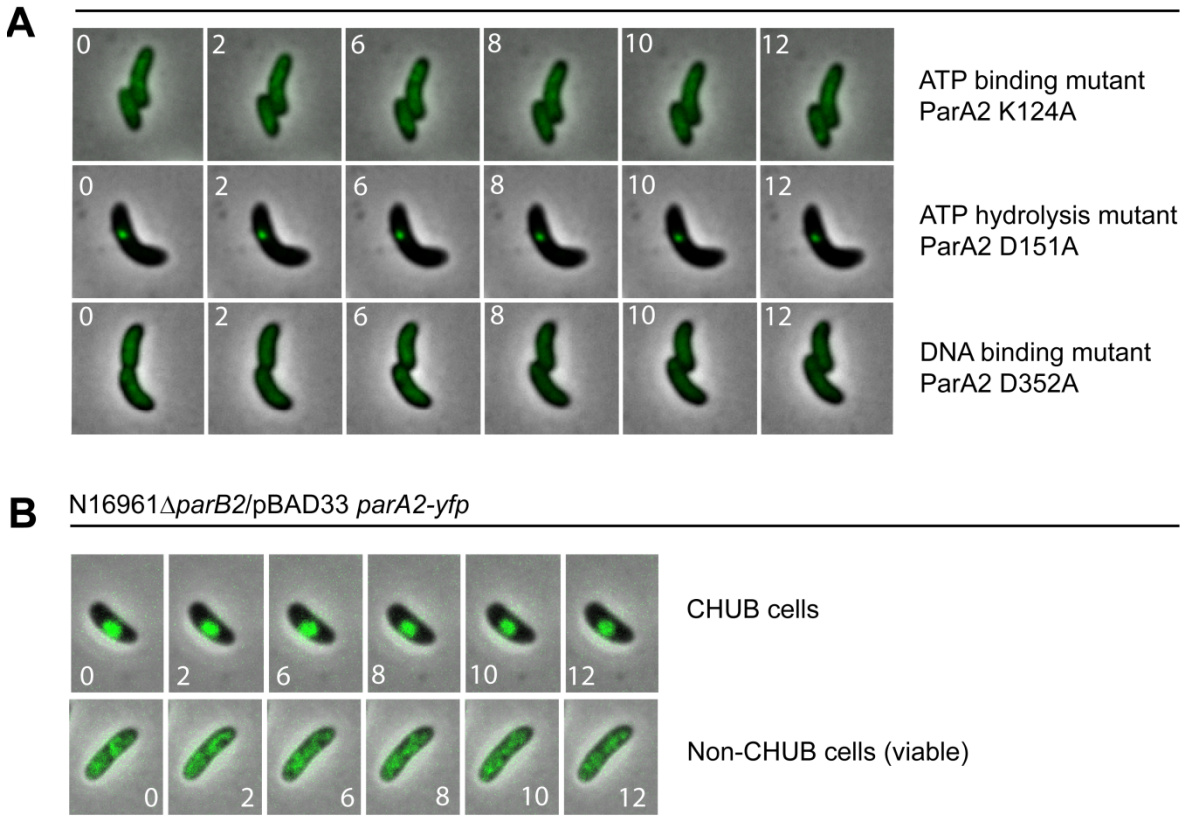

Fig. 3-2. ParA2 dynamics depend on ATP hydrolysis, DNA binding, and ParB2. Timelapse images of: **(A)** ParA2-YFP K124A, a ATP binding mutant (top row), ParA2-YFP D151A, a ATP binding mutant (middle row), and ParA2-YFP R352A, a DNA-binding mutant (bottom row); **(B)** ParA2-YFP in the non-dividing CHUB cells in the Δ*parB2* background (top row), and ParA2-YFP in the viable cells found in the Δ*parB2* background (bottom row). Images were taken at every 2 min intervals over the course of the timelapse.

chrII and become CHUB cells, which are named for their altered cytological phenotypes (condensed nucleoid, hypertrophic, undividing bacteria) and cell shape. Cells lacking chrII are unable to proceed past one round of cell division before they die. The rest of the population of cells appear as wild type in shape and continue to carry out cell division.

The localization of ParA2-YFP was visualized in both CHUB and normal appearing Δ*parB2* cells. In the CHUB cells where there is neither chrII *parS2* nor ParB2, ParA2-YFP was observed to remain in the centroid region of the cell as a condensed bright patch (**Fig. 3-2B**, top row). Likely ParA2 is simply binding to the chrI nucleoid, which is condensed in CHUB cells. In the wild type appearing cells where there are chrII *parS2* sites but no ParB2 and the nucleoid is not condensed, ParA2 occupies the same sub-cellular regions as the found in wild type strains. However, the dynamics are distinctly altered as the oscillations are no longer easily seen (**Fig. 3-2B**, bottom row). Instead, ParA2 localizes throughout the cell. Together, these observations indicate that ParB2 and/or the *parS2* sites on chrII are required for dynamic ParA2 intracellular movement, and suggests that stimulation of ParA2 ATPase activity via ParB2-*parS2* interaction is required for ParA2 dynamics. As discussed in Chapter 2, ParB2 and *parS2* can stimulate ParA2 ATP hydrolysis (92).

Co-visualizing ParA2 and ParB2 in the cell. How does ParA2 oscillation translate into successful partitioning of chrII? The first step to addressing this question is to examine the intracellular localization of ParA2 with respect to ParB2. ParA2-YFP and ParB2-CFP were co-visualized in *V. cholerae* by electroporating pBAD33 *parA2-yfp* into wild type *V. cholerae* where *parB2* was replaced with *parB2-cfp* at the *parAB2* chromosomal locus. ParB2-CFP chosen to serve as a marker for $oriC_{II}$ movement in the

cell since it has been shown that movement of ParB2 bound to the *parS2* sites recapitulates the movements of $oriC_{II}$ (219). Due to the low expression of ParB2-CFP, it was not technically feasible to carry out a full scale timelapse before photobleaching of the CFP fluorophore. However, the static images of ParA2 localization with respect to ParB2 in the cell yielded important hints concerning the mechanism of ParA2-mediated localization of ParB2-*parS2*—and by extension, the $oriC_{II}$ region.

The seven different observed localization patterns of ParA2 and ParB2, along with representative images, are listed in **Fig. 3-3**. Three classes were predominant: Class Three, where ParA2 localized between the ParB2 focus and the farthest cell pole; Class Six, where ParA2 localized between the cell pole and the closest ParB2 focus; and Class Seven, where ParA2 localized between the cell poles and the two ParB2 foci. One striking observation was the lack of cells in which ParA2 was only found between two separated ParB2 foci. Instead, ParA2 was always located between ParB2 and the pole towards which ParB2 was traveling while ParB2 was located at the trailing edge of the ParA2 cloud. This strongly hints at a pulling mechanism at work for chrII segregation.

Since timelapse studies could not be carried out, cell cycle progression was inferred using cell length measurements and ParB2 focus separation. The different classes of ParA2-ParB2 localization were plotted as a function of cell length to look for specific patterns associated with different stages of the cell cycle (**Fig. 3-4**). From this scatter plot, a general trend emerges. The smaller cells typically contain one ParB2 focus with ParA2 located to one side (Class Three, solid red triangles). The mid-sized cells contain either one ParB2 focus or two closely spaced ParB2 foci (Class Four and Five, solid and hollow black circles) with ParA2 located throughout the cell. The largest cells

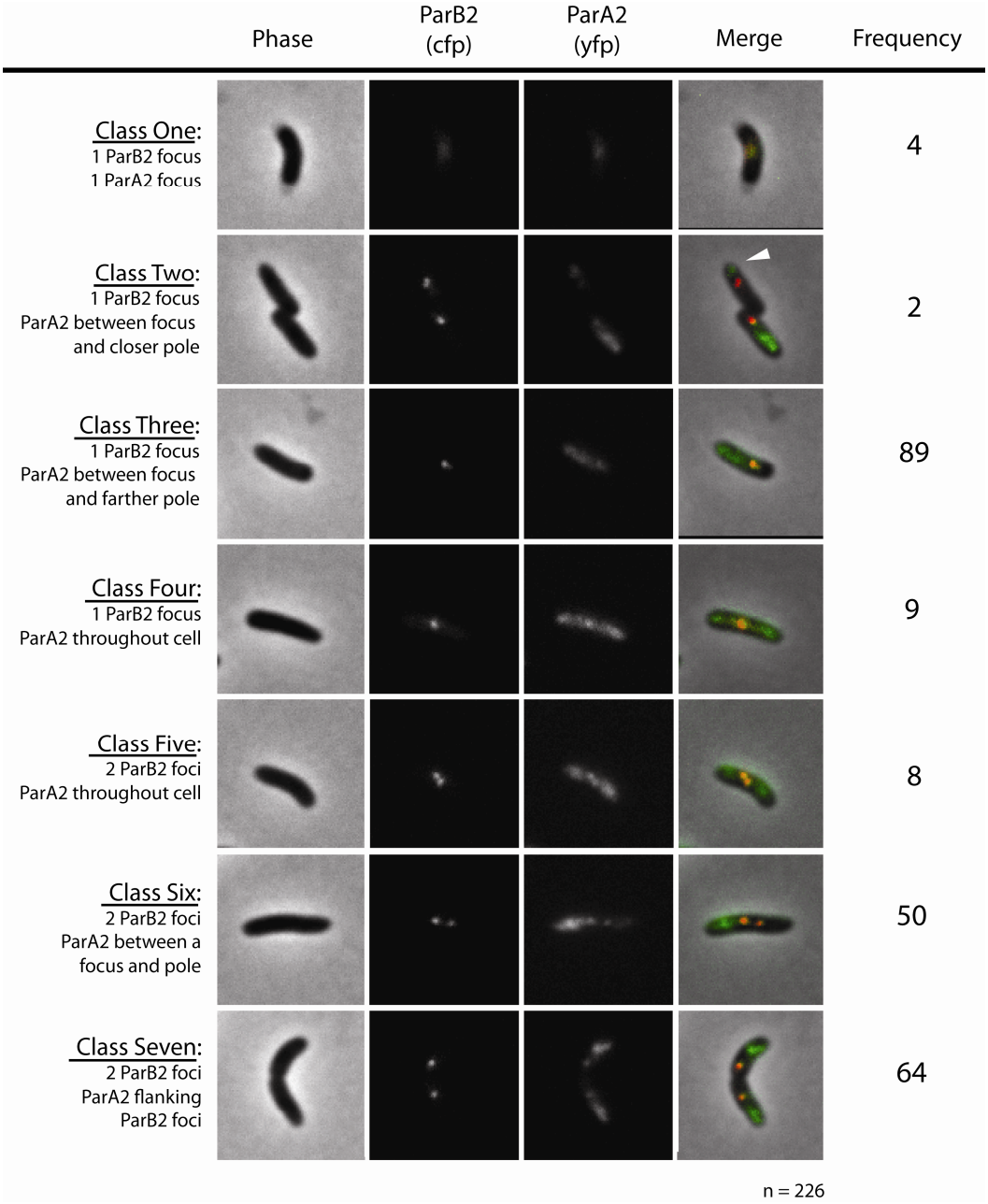

Fig. 3-3. Classification of ParA2/ParB2 co-visualization patterns. Images of ParA2-YFP and ParB2-CFP were acquired and processed as described in the Methods section. The white arrowhead marks one of two representatives found to fit the Class Two localization pattern. In 226 cells analyzed, no cells were found to have ParA2 located only between the two separated ParB2 foci.

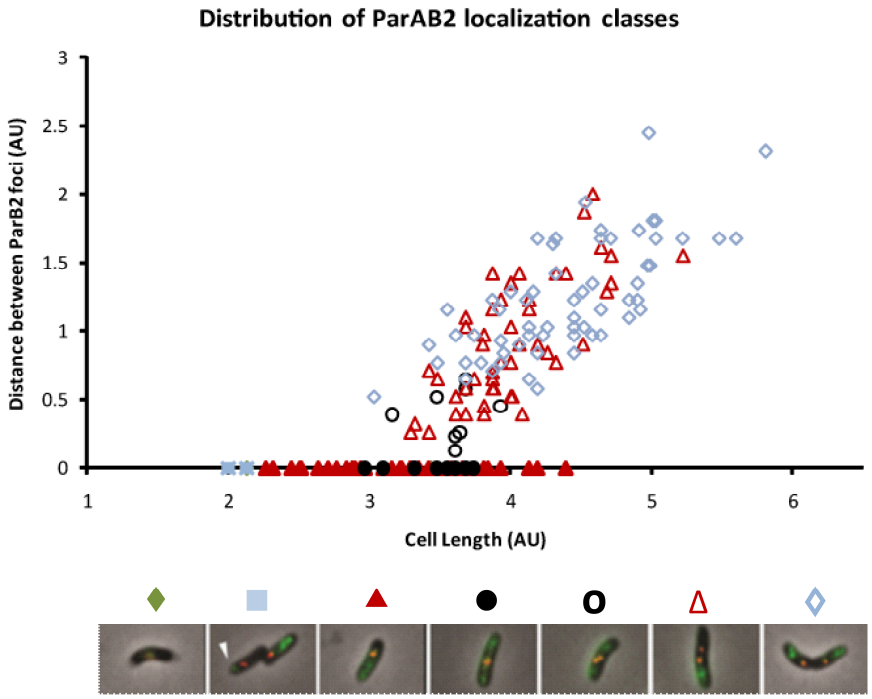

Fig. 3-4. Distribution of the ParAB2 localization classes with respect to cell length.

Measurements were taken as detailed in the Methods section. AU = arbitrary units.

contain two ParB2 foci, with either ParA2 localized to one side of the cell (Class Six, hollow red triangles) or with ParA2 flanking the two ParB2 focus (Class Seven, hollow blue diamonds). The division septum was clearly visible for cells in the latter category. Together with the ParA2 timelapse, these data suggest that ParA2 oscillates during the course of the cell cycle to separate and pull sister copies of chrII towards opposite directions.

ParA2 binding displays no chromosome specificity *in vivo*. The microscopy studies hint at a pulling model of ParA2 function. Since ParA2 is a non-specific DNA binding protein and *V. cholerae* has two chromosomes, there are three scenarios in which ParA2 could be binding to DNA to mediate partitioning. First, ParA2 could be binding to chrI and utilizing chrI DNA as track to pull chrII towards opposite sides of the cell. Second, ParA2 could be binding to chrII and mediate chrII partitioning through a treadmilling effect. This would be similar to the model proposed for Soj in *B. subtilis* and would require the existence of a host anchor (121). Third, ParA2 could be binding to the nucleoid region in general to mediate ParB2 separation and chrII partitioning. This scenario would be similar to the models proposed by Vecchiarelli *et al*. for the plasmid P1 and Ringgaard *et al*. for pB171 (169, 202). In the first two scenarios, chromosome specificity can be dictated by the absence (scenario one) or presence (scenario two) of ParB2-*parS2* complexes.

To determine whether ParA2 DNA binding displays chromosome specificity *in vivo*, chromatin immunoprecipitation (ChIP) was carried out on formaldehyde cross-linked wild type N16961 *V. cholerae* cells using a polyclonal rabbit α-ParA2 antisera (Genscript). DNA samples were saved at the start of the procedure to assess the percent

chromosome composition of the starting total DNA. The total DNA and the immunoprecipitated (IP) DNA were subsequently cloned and sequenced. As a control, a parallel experiment was carried out using N16961 Δ*parA2*, where the IP step should yield little to no DNA. Some DNA was recovered from this strain after the IP procedure, as five colonies were isolated after the TOPO-cloning step (versus >1000 for N16961). However, subsequent sequencing of the plasmids isolated from these colonies showed them all to carry the same 16 bp fragment from chrII. Therefore, this fragment was omitted from the final tallies for the N16961 IP samples by pre-screening for plasmids for inserts >50 bp.

Comparing the total starting N16961 DNA and the IP N1961 DNA, there does not appear to be any significant bias or enrichment towards the recovery of chrI over chrII or vice versa (**Fig. 3-5A**). The starting total DNA consisted of 73% DNA from chrI and 27% DNA from chrII. This approximate ratio of 3:1 of chrI to chrII DNA is precisely what would be expected given that the size of chrI is roughly three times that of chrII. Since the proportions of DNA sequenced from the pool of IP N1691 DNA are similar, ParA2 does not seem to bind solely chrI or chrII *in vivo*. Rather, it binds to both chromosomes with no apparent specificity.

This approach also allowed for visualizing whether ParA2 has any regional binding preferences on the two chromosomes. Mapping the sequenced IP DNA fragments showed no apparent bias in terms of where ParA2 binds on the chromosomes with respect to the *ori*, *ter*, or various *parS* sites on chrI or chrII (**Fig. 3-5B**). A caveat is that if localization is cell cycle dependent, it would not be seen since the ChIP was performed on unsynchronized cell cultures. However, given the rapid nature of ParA2

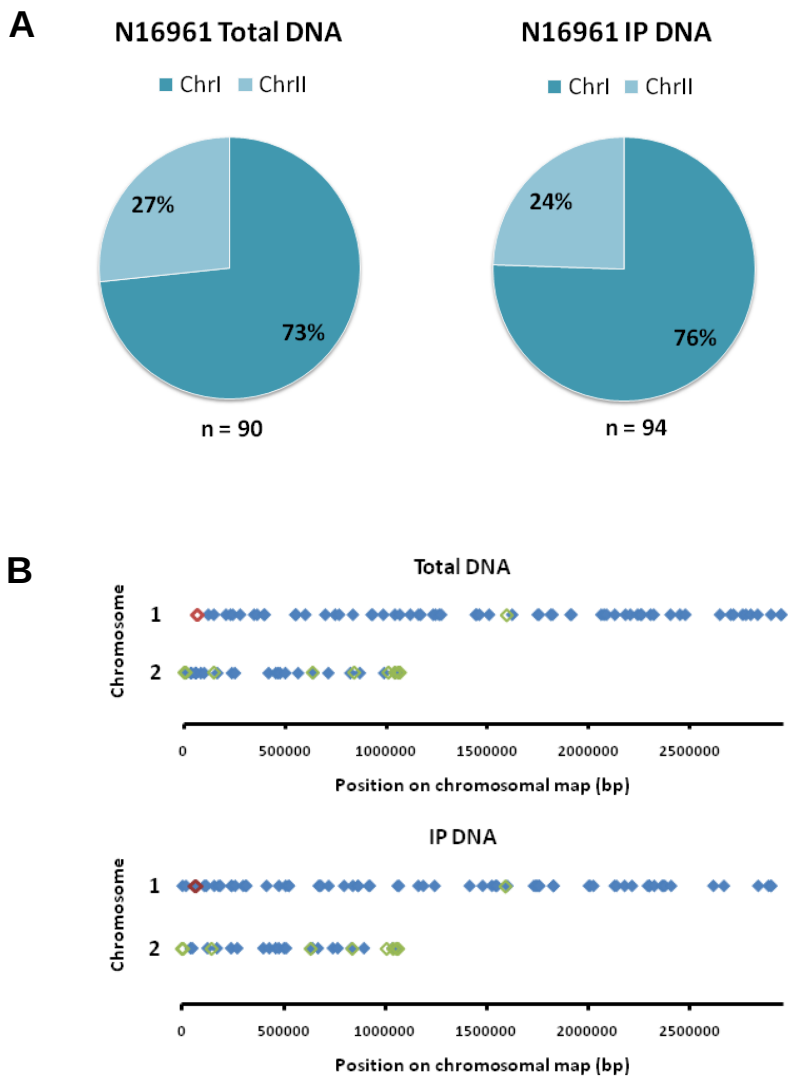

Fig. 3-5. Distribution of ParA2 binding on DNA *in vivo*. (A) Pie charts displaying the contribution of each chromosome to the final pool of sequenced DNA from ChIP using α-ParA2 antisera. **(B)** Chromosome map of the sequenced ChIP DNA. The red diamonds indicate the location of the three *parS1* sites on chrI. The green diamonds indicate the location of the nine *parS2* sites on chrII and the one *parS2* site on chrI.

oscillation, it is unlikely there is a cell cycle dependent localization of ParA2 over the nucleoid.

DISCUSSION

The purpose of the work described in this chapter is to begin to address several gaps in our knowledge regarding the relationship of ParA2 intracellular localization with the localization of other components of the partitioning system, ParB2-*parS2* and DNA. I observed that ParA2 redistributes from pole to pole in an apparent oscillatory-like fashion. This behavior was dependent on the capacity of ParA2 to hydrolyze ATP and bind DNA, as well as the presence of ParB2. Strikingly, co-visualization studies of ParA2 and ParB2 showed that ParB2 is always associated with the retreating edge of the ParA2 cloud while ParA2 is generally located between a ParB2 focus and the pole, but importantly never only between two ParB2 foci.

Taken together, my data suggests that ParA2 mediates chrII partitioning through a pulling mechanism of action by assembling on the nucleoid (**Fig. 3-6A**). The process can be divided into the following 4 steps: 1. In newborn cells with one ParB2 focus (which co-localizes with $oriC_{II}$), ParA2 redistributes from pole to pole. 2. As the cell cycle progresses and the $oriC_{II}$ region of chrII is replicated, the duplicated ParB2-*parS2* complexes are separated by repeated interactions with the end(s) of ParA2 filament(s) near the mid-cell, resulting in bidirectional ParB2-*parS2* movement. 3. The separation of the two ParB2-*parS2* complexes towards the cell poles continues due to the action of ParA2, which polymerizes outwards from the cell poles towards the ParB2-*parS2* complexes and de-polymerizes to pull each complex towards the closer pole. 4. As the cell enters the late stages of the cell cycle, ParA2 can be seen simultaneously at opposite

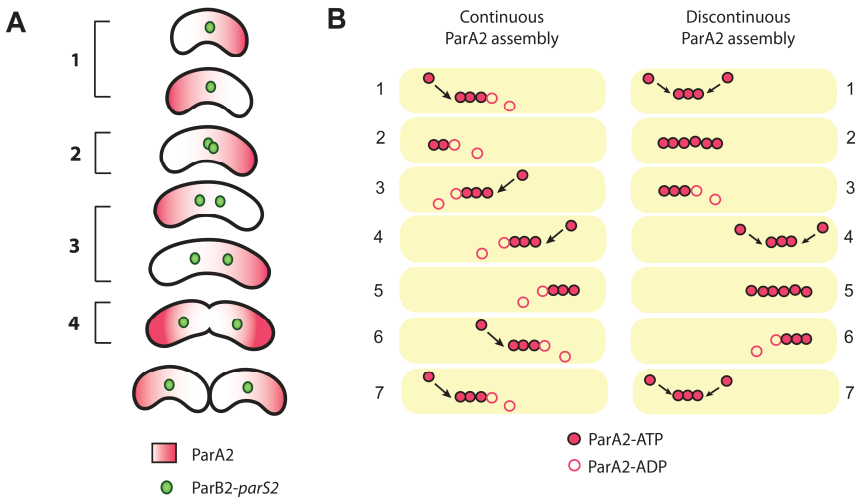

Fig. 3-6. Model for ParA2 function. (A) Model for ParA2 oscillation mediated partitioning of the ParB2-*parS2* complexes. For description, see text. **(B)** Schematic of two filament assembly mechanisms that explains the oscillatory phenotype observed for ParA2.

ends of the cell, positioning ParB2-*parS2* at the quarter-cell positions. 5. After cell division, the cycle continues and ParA2 redistributes from pole to pole.

One potentially confusing issue in this model and in the ParA literature in general is the use of the word 'oscillation'. At face value 'oscillation' implies that ParA2 polymerization occurs in a unidirectional fashion with addition of subunits to one end and concomitant de-polymerization at the opposite end (**Fig. 3-6B,** left side). However, generation of ParA2 polymers from alternating cell poles could also give the appearance of oscillation (**Fig. 3-6B,** right side). My microscopy data does not distinguish between these two scenarios of ParA2 assembly *in vivo*. In both schematics of intracellular ParA2 polymerization, timelapse images for frames 1, 4, and 7 would look virtually identical. However, since our biochemical studies revealed that the structure of the ParA2 filament is symmetrical (92), it is likely that polymerization occurs in a bipolar fashion as outlined in **Fig. 3-6B**, right panel.

This model is nearly identical to the model presented by Ringgaard *et al*. for pB171, where repeated continuous cycles of ParA polymerization and de-polymerization result in equipositioning of pB171 along the length of the nucleoid (169). The localization patterns of pB171 ParA and ParB are very similar to that seen for ParA2 and ParB2. However, with pB171, ParA was also capable of polymerizing between ParB foci to mediate positioning of multiple plasmids along the length of the bacteria. This does not appear to be the case for ParA2, where ParA2 localization is predominantly found between a pole and a ParB2 focus regardless of the distance between separated ParB2 foci. One explanation for this discrepancy is that pB171 is present in higher copy, and thus, supports filament growth between plasmids in order to separate a larger number of

plasmids. Therefore, in rapidly growing *V. cholerae* cells when multiple rounds of replication have initiated or in cephalexin treated cells, it would be predicted that ParA2 would also be able to polymerize between $oriC_{II}$ to mediate proper partitioning.

If ParA2 does utilize the same partitioning mechanism of pB171, then it raises one intriguing issue regarding the positioning of the chrII $oriC_{II}$ region. The localization pattern of ParB2-*parS2* has been reported to match those of plasmid partitioning systems and follow a symmetrical, mid-cell to quarter-cell localization pattern. However, in many of the plasmid systems studied, such as P1, F, and pB171, the nucleoid region is known to occupy the space between the quarter-cell positions, which can be considered a natural stopping point for ParA mediated plasmid movement along the nucleoid. In *V. cholerae* the space occupied by the nucleoid may be greater due to the presence of chrI, which is known to have the *ori* anchored at one cell pole and the *ter* extending towards the opposite pole. How, then, does *V. cholerae* position $oriC_{II}$ at the quarter positions? DAPI stained *V. cholerae* cells suggest that the $oriC_{I}$ region extends out from the bulk of the nucleoid (59). It is possible that this extended area is (for a yet unknown reason) not suitable as a track for ParA2 polymerization.

Finally, the contrast between the two partitioning systems *V. cholerae* uses to position chrI and chrII in the cell is particularly striking. While ParA2 oscillations appear to be rapid and initiate from both poles, ParA1 oscillates only once per cell cycle in an asymmetrical fashion by extending outwards from one pole to capture a ParB1-*parS1* complex and retracting to pull the complex across the length of the cell (60). Interestingly even though the two ParA proteins share only 25% similarity and 14% identity, my results suggest that the mechanisms by which these ATPases move their

respective replicon may rely on a similar pulling mechanism where ParB stimulated disassembly of ParA filaments yields movement of the centromeric complexes. Despite this underlying similarity, the distinct dynamics of the two *V. cholerae* ParA proteins suggests that two different mechanisms are likely at work in *V. cholerae* chromosome segregation. Evolution may have taken the same fundamental molecular mechanism and adapted it to suit the partitioning of each chromosome in *V. cholerae*.

METHODS

Strains and growth conditions. All strains (**Table 3-1**) in this study are derivatives of the sequenced El Tor clinical isolate N16961 (84). Unless otherwise stated, *V. cholerae* was grown in M63 medium supplemented with 0.1% casamino acids and 0.2% glucose as the carbon source. Strains with the N16961Δ*parB2* background were grown in LB as M63 minimal medium did not support growth of the cells during timelapse microscopy. Parallel timelapses of N16961/pBAD33 *parA2-yfp* grown in LB were done to ensure that ParA2 localization was the same regardless of growth medium. For strains containing plasmids derived from pBAD33, chloramphenicol was added to a final concentration of 5 μg/ml.

Microscopy. Overnight cultures were diluted 1:100 into fresh media and grown until OD_{600} = 0.4, when *parA2-yfp* expression was induced by the addition of 0.08% L-arabinose for 1 h at 37°C. Approximately 20 μl were adsorbed onto a thin 1.5% M63 agarose pad on a microscopy slide. Images were collected at 35°C using a Zeiss Axioplan 2 microscope equipped with a 100x Alpha Plan lens fitted with filter sets for YFP and CFP fluorescence and a cooled CCD Hamamatsu Orca. The brightness and contrast of images were adjusted using Metamorph and ImageJ.

Measuring fluorescence localization and cell length. For measuring ParB2 foci separation distance, the CFP fluorescence intensity values along the longitudinal axis of each cell were plotted and the distance between the two peak intensity values were recorded in arbitrary units (AU) using the 'Linescan' feature in Metamorph. The same

Table 3-1. Strains used in this study

Strain	Genotype	Relevant information & references
N16961	-	(84)
MH170	N16961 / pBAD33 *parA2-yfp*	The *parA2* coding region was amplified from the *V. cholerae* N16961 chromosome using primers MFp132 (5'-CCACCGAGCTCA**AGGAGG**TGTGAATTGGCAATGAAAAGAGAAC-3') and MFp133 (5'-CACTGGATCCTGCCCCTGATTCAGTGA-3'), and cloned via *Sac*I and *BamH*I (sites underlined) into p4414, a plasmid containing the monomeric version of *yfp* (gift of S. Bunnell, Tufts Medical School). The *parA2-yfp* fusion was subsequently sub-cloned into pBAD33 via *Sac*I and *Xba*I. A Shine-Delgarno sequence (in bold) was added to allow for expression of the fusion protein. (60)
MH423	N16961 / pBAD33 *parA2K124A-yfp*	D151A was introduced into pBAD33 *parA2-yfp* using the primers MHp161 (5'-GGGTGGTACGGGGGCGTCAATGACCGCGG-3') and MHp162 (5'-CCGCGGTCATTGACGCCCCGTACCACCC-3') using Quikchange (Stratagene). The altered bases are underlined.
MH232	N16961 / pBAD33 *parA2D151A-yfp*	D151A was introduced into pBAD33 *parA2-cfp* using the primers MHp053 (5'-CGCATCTGCTTGATTGACTTAGCGCCACAAGGTTCATTACGCC-3') and MHp054 (5'-GGCGTAATGAACCTTGTGGCGCTAAGTCAATCAAGCAGATGCG-3') using Quikchange (Stratagene). The altered bases are underlined.
MH424	N16961 / pBAD33 *parAR352A-yfp*	R352A was introduced into pBAD33 *parA2-yfp* using the primers MHp165 (5'-CACCATCCCACGCAGCGCGGCGTTTGAAACCTGTG-3') and MHp166 (5'-CACAGGTTTCAAACGCCGCGCTGCGTGGGATGGTG-3') using Quikchange (Stratagene). The altered bases are underlined.
YBB324	N16961 *parB2::spc*	Y. Yamaichi
MH439	N16961 *parB2::spc* / pBAD33 *parA2-yfp*	This study
YBB171	N16961 *VCA1114::parB2-cfp*	Y. Yamaichi
MH435	N16961 *VCA1114::parB2-cfp* / pBAD33 *parA2-yfp*	This study

longitudinal axis was used to measure cell length and to classify ParA2 localization in relation to the cell poles and/or ParB2 foci.

Chromatin immunoprecipitation studies. The ChIP studies were carried out according to the protocol of Ben-Yehuda *et al*. (14) with modifications. Cultures were grown in LB to OD_{600} = 0.6 before cross-linking. For the immunoprecipitation step, 4µl of rabbit polyclonal antibodies raised to ParA2 (Genscript) were used. The antiserum was cleaned twice by adsorbing cross-reactive antibodies with acetone precipitated proteins from N16961Δ*parAB2*. Recovered DNA from the total DNA and the IP samples were cloned using the Zero Blunt TOPO PCR Cloning Kit (Invitrogen). Clones were patched and colony PCR was carried out using M13F and M13R primers to select for clones harboring plasmids with inserts >50 bp. Plasmids were then mini-prepped using the Qiaprep Spin Miniprep kit (Qiagen) and sequenced using the M13F primer (Genewiz).

ACKNOWLEDGEMENTS

I would like to thank Yoshiharu Yamaichi for strains and technical advice.

CHAPTER FOUR

Discussion and future considerations

Each *V. cholerae* chromosome encodes a *par* locus that has been genetically shown to be important for the localization and/or segregation of its respective replicon. In the case of chrII, the *par* locus is essential. The aim of this thesis was to examine how ParABS2 mediates chrII partitioning by studying the properties of the ParA homolog, ParA2, *in vitro* and *in vivo*.

In vitro analysis of ParA2 activity detailed in Chapter Two revealed that ParA2 shares the common biochemical characteristics that define members of the ParA family of partitioning proteins. It binds and hydrolyzes ATP with similar kinetics as reported for other ParA proteins. Surprisingly, ParA2 was not able to polymerize into filaments unless DNA was present. Previously, such nucleoprotein filaments had only been described for the Type Ib ParA proteins, Soj of *B. subtilis* and δ of pSM19035. ParA2 is the first example of a Type Ia ParA protein polymerizing on DNA.

Our collaboration with the Egelman Lab (U. of Virginia) revealed the unique structure of the ParA2 DNA filament: ParA2 wraps itself around the right-handed DNA helix by generating a left-handed helix without exerting any topological changes to the DNA. Furthermore, the polymer is bipolar and symmetrical, so one end is not distinguishable from the other. There has been no evidence, thus far, of ParB2 nucleating ParB2 assembly (See **Appendix A**, **Fig. 5-1**). This suggests that ParA2 can form filaments by spontaneous nucleating and polymerizing outward from both ends.

In Chapter Three, microscopy localization studies of ParA2 show it to be a highly dynamic protein, whose apparent oscillations rely on its ATPase and DNA binding motifs. Consistent with the non-specific DNA binding observed *in vitro*, ParA2 did not display a preference in chromosome binding *in vivo*. Most revealing, however, was the

observation that ParA2 consistently localized between a ParB2-*parS2* complex and the pole towards which that complex was moving.

A model for ParA2 mediated chrII partitioning

Together, these observations are consistent with the model originally proposed by Ringgaard *et al*. for the partitioning of the low copy plasmid, pB171 (See **Fig. 1-4**) (169). According to this model, ParA polymerizes outward on DNA in a bidirectional manner beginning from one polar region of the cell. Contact with a ParB-*parS* complex at one end of the polymer causes de-polymerization of the filament. A second polymer assembles at the opposite end of the cell, until contact with a ParB-*parS* complex results in de-polymerization of that filament. Continued rounds of polymerization and de-polymerization at alternating nucleation sites from one cell half to the cell half results in the oscillatory pattern observed for ParA2. Transient contacts between the de-polymerizing ("retracting") edge of the ParA filament and the ParB-*parS* complex yield net movement of the plasmid DNA and the gradual separation of ParB2-*parS2* to the quarter-cell positions. This model takes into account the bipolar structure of the ParA2 filament, as well as the dynamic localization pattern observed for ParA2 in relation to ParB2-*parS2*. Timelapse studies tracking the localization of ParA2 and ParB2-*parS2* over the course of the cell cycle would be very useful to validate or refute this model. I was unable to carry out such experiments due to technical issues with CFP photobleaching. Engineering a ParB2 protein fused to a more stable fluorophore, such as mCherry, could circumvent this issue.

Are the mechanisms for chromosome and plasmid partitioning conserved?

The similarities between ParA-ParB localization in pB171 and ParA2-ParB2 of *V. cholerae* chrII leads one to wonder if the mechanisms for plasmid and chromosome partitioning are conserved, particularly since a number of Walker box ParA homologs are hypothesized to use a pulling mechanism of action. The chrII *parAB2* locus is unusual among the chromosomally encoded *par* loci, as seen in **Fig. 1-7**. Perhaps as a reflection of having possibly evolved from a megaplasmid, chrII carries a *par* locus whose ParA clusters with the plasmid Type Ia homologs, rather than with the tightly clustered chromosomally encoded ParA homologs. Furthermore, in a number of cases, chromosomal partitioning systems have been adapted by the host cell to provide a number of accessory functions not found (or not yet described) in most plasmid partitioning systems. In *B. subtilis* and *V. cholerae* chrI, ParA proteins link chromosome replication and segregation, and in *C. crescentus* ParA provides a link between cell division and segregation (102, 143, 196). It is likely that some of the fundamental molecular interactions are retained in plasmid and chromosome encoded Par systems, while each partitioning system has adapted to fit its host and replicon requirements. For example, the prediction for bipolar Soj polymerization coincides nicely with the structure of the ParA2 polymer, but the localization patterns and the intracellular roles of the two proteins are clearly different. While there may be some degree of mechanistic conservation between plasmid/chrII and most chromosome partitioning systems, the biological importance of these systems differ: plasmid/chrII partitioning systems are essential whereas most chromosome partitioning systems are not.

Positioning of the nucleoid during the cell cycle

Having a common mechanism of partitioning raises a conundrum in bacteria that only have one chromosome that needs to be partitioned. For bacteria with multipartite genomes (such as *V. cholerae*), the nucleoid region is not solely defined by the replicon being segregated. Secondary replicons (in the case of *V. cholerae*, chrII can use chrI) can rely on the other replicon to provides cues for partitioning. However, things become complicated if Soj during vegetative growth, for example, were to use the pB171 mechanism to partition itself. The nucleoid must expand in order to maintain its location between the quarter positions of the cell as the cell grows. If the nucleoid remains static in two-dimensional space, how can Soj position the chromosome origin at the quarter-position at a sub-cellular location where there is no DNA? This argues that there must be biophysical aspects to chromosome segregation as well, as proposed by Jun and Mulder, and Jun and Wright (100, 101).

If ParA1 and ParA2 both bind DNA, then the nucleoid must be a very crowded place

Quantitative westerns show that there are ~750 ParA2 molecules in the cell, roughly enough to cover a small fraction of the total intracellular DNA (See **Appendix A**, **Fig. 5-2**). If, hypothetically, ParA1 is in similar quantities and also binds to non-specifically to DNA as reported for ParA2, then only a small fraction of the chromosome will be occupied by a ParA protein at the any given point in time. What happens if/when ParA1 encounters ParA2? If both proteins utilize the nucleoid DNA to polymerize, the consequences of ParA polymer collisions could be catastrophic.

Unresolved questions and future considerations

The intracellular dynamics of chrII and the products of the *parAB2* locus remain fertile ground for continued study. One potential avenue of research lies in the plasticity and movement of chrII during the partitioning progress. For chrI, it was observed that origin proximal loci separated by as little as 50 kbp on the chromosome can be stretched far apart during partitioning, apparently due to action of ParA1 pulling the ParB1/parS1 complex away from other origin proximal regions (60). Do chrII loci, especially those near the origin, also exhibit similar stretching resulting from the action of ParA2 pulling the ParB2/parS2 complex? A related avenue of research is fine scale analysis of in vivo ParA2 polymerization dynamics through the use of photo-ablation/FRAP studies. This could enable measuring the polymerization and de-polymerization dynamics of the ParA2 filaments *in vivo*. Incidentally, this approach can also be used to analyze ParA1 polymerization parameters. I have created some of the vectors that will be useful for such studies and my preliminary images look encouraging.

On the biochemical side, the determinants for ParA2, ParB2, and *parS2* interactions can be probed. How does ParA2 distinguish ParB2 from ParB1? One approach to address this issue is domain swapping experiments between the components of the ParAB2 and the ParAB1 systems; this approach enabled the Austin Lab (NIH/NCI-Frederick) to dissect the ParB and *parS* specificity determinants for the P1 and P7 partitioning systems. Another area worthy of further study is the analysis of ParA2-ParA2 interactions. Based on our reconstruction studies, ParA2 appears to use its N-terminal domain—previously thought to be only important for ParA mediated repression of the *par* operon—for maintaining polymer structure. Yet, ParA homologs lacking this

N-terminal domain are still able to polymerize on DNA and residues important for non-specific DNA binding are located at the C-terminal region of the protein. Is the N-terminal domain needed for filament formation? Mutations in this domain should answer this question.

Another key unanswered question is what cues does chrII use to localize at the mid-cell and quarter-cell positions? This issue also applies to other chromosomes and plasmids. The edge of the nucleoid is often invoked to explain the quarter-cell positioning of chromosome origins, but the *V. cholerae* chrI nucleoid extends all the way to cell pole, arguing that the nucleoid per se does not determine positioning. Furthermore, chrII positioning does not appear to be affected by the positioning of $oriC_I$ DNA, as Δ*parA1* mutants do not alter chrII partitioning and localization. Also, what is the purpose of the chrI encoded *parS2* site? Finally, ParA2 is observed as a polymerizing cloud—is there an underlying structure or cohesiveness to the ParA2 polymers? In cells where the chrII *ori* is present at one to two copies, it is hard to imagine that one ParB2-*parS2* complex would be able to stimulate de-polymerization of a relatively much larger mass of ParA2 filaments formed over the nucleoid. Clearly, much more needs to be done before chromosome partitioning is fully understood.

APPENDIX A

Additional observations on ParA2

Nucleation of ParA2 filaments

In Chapter 2, structure modeling and reconstruction revealed that ParA2 forms nucleoprotein filaments with an unusual geometry. ParA2-ATP assembles into a left-handed helix wrapped around a dsDNA core, with each ParA2 dimer occupying 8 bp of the DNA helix.

The observed geometry of ParA2 binding to DNA is remarkably similar to models of ω (ParB) from pSM19035 binding to its cognate *parS* sites. In pSM19035, the *parS* sites are comprised of a series of 7 bp repeats and a ω dimer is predicted to bind to each of the 7 bp repeats to form a left handed helix (161). Comparing the helical assembly of the two proteins has led to speculation that one role of ParB2 may be to nucleate ParA2 filament formation *in vivo* since ParA2 has been observed to form its filaments on DNA irrespective of DNA sequence *in vitro*. This nucleation, in turn, would allow the chrII segregation machinery to distinguish chrII from chrI in the cell.

To test this hypothesis, DNaseI footprinting was carried out to determine whether there were conditions in which ParA2 formed nucleoprotein filaments in the presence of ParB2 but not in its absence. As seen in **Fig. 5-1**, the presence of ParB2 binding to *parS2* did not trigger ParA2 assembly along the DNA to give protection to the non-ParB2 occupied regions of the strand from DNaseI cleavage. These results were confirmed by EM studies of our collaborators at the Egelman lab (U. of Virginia, personal communication). Therefore, ParB2 does not nucleate ParA2 filament assembly *in vitro*, and likely *in vivo*.

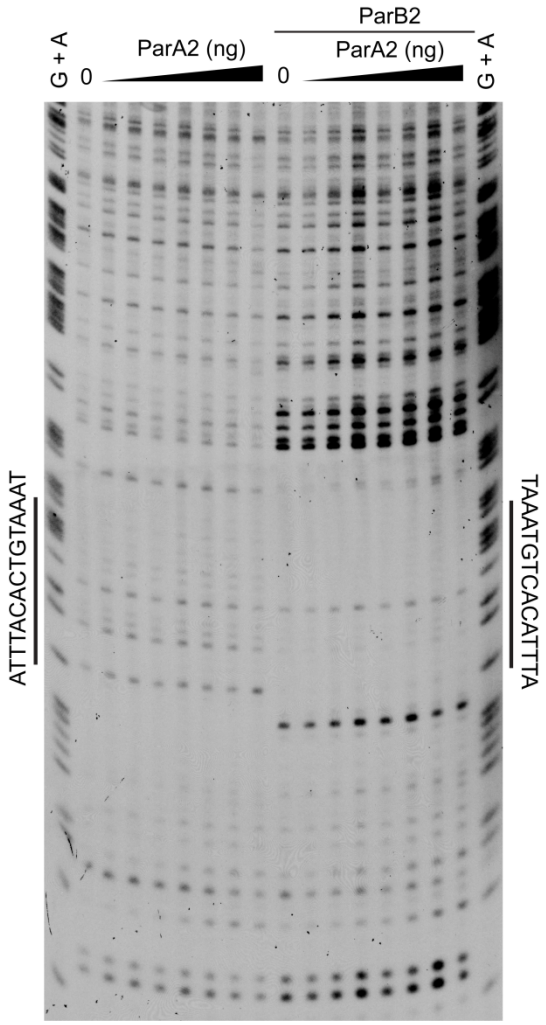

Fig. 5-1. DNaseI footprint of ParA2 and ParB2 at the *parS2-A* site. ParA2, with amounts ranging from 0 ng to 1280 ng, was added to either labeled probe containing the *parS2-A* sequence (left) or labeled probe pre-incubated for 10 min with 80 ng ParB2 (right). Footprint reactions were done according to (218). The *parS2-A* site, flanked by the characteristic hypersensitive spots as observed previously, is marked on either side of the footprint. G + A = G + A sequencing ladder.

Intracellular levels of ParA2 in *V. cholerae*

The finding that ParA2 binds to DNA led to the question: what is the maximum percentage of the *V. cholerae* chromosome can be occupied by ParA2 at any given time? To answer this, the intracellular levels of ParA2 were determined by quantitative western blot (**Fig. 5-2**). A serial dilution of purified ParA2 was run alongside a sample taken from N16961. Simultaneously, the N16961 sample was plated for CFUs to allow for calculating the number of ParA2 molecules per cell, and a N16961Δ*parA2* sample was included as a control.

As it turns out, the amount of ParA2 molecules in the cell is low—roughly about 750-850 molecules, corresponding to approximately 400 dimers. Given the knowledge gleaned from the ParA2 structural studies that each dimer occupies 8 bp along the DNA helix, this means that ParA2 is capable of binding to 0.3% of chrII, 0.1% of chrI, or 0.08% of the total DNA in the cell. Interestingly, 400 ParA2 dimers are able to assemble into a physical filament of 1 μm in length, which is the average length of *V. cholerae*. However, such a long filament is never observed *in vivo*. This suggests that the ParA2 cloud is likely comprised of a series of shorter ParA2 filaments that mediate partitioning of chrII en masse.

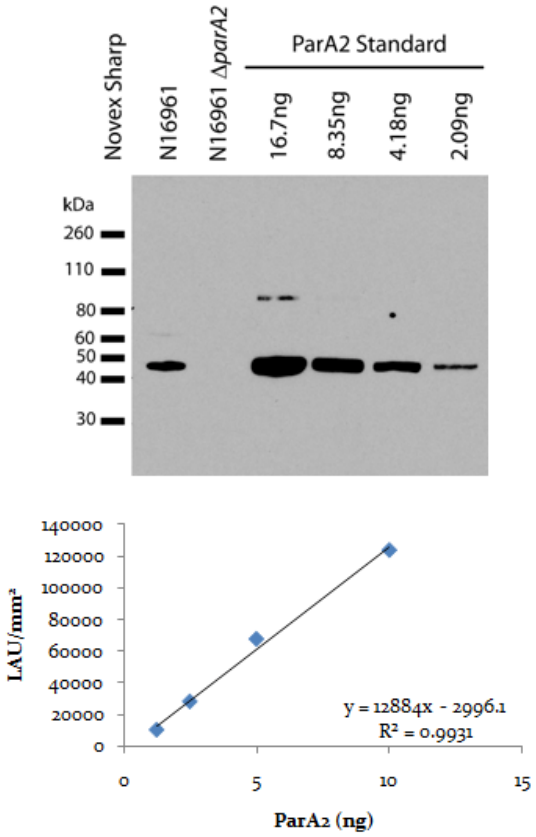

Fig. 5-2. Western blot quantitating the intracellular levels of ParA2. N16961 and N16961Δ*parA2* were grown to mid-exponential phase when samples were plated for CFUs and taken for western blot analysis using polyclonal rabbit α-ParA2 antiserum (Genscript). These samples were run alongside a protein standard of ParA2 purified protein. Blots were visualized on film by chemiluminescence using HRP-conjugated goat α-rabbit antibodies (Pierce) and the SuperSignal West Pico Chemiluminescent Substrate kit (Pierce). The bands were scanned for densitometric analysis. This experiment was repeated at least three independent times, and one representative experiment is shown.

APPENDIX B

Observations on ParA1 biochemistry

The bulk of this thesis has revolved around the biochemical and intracellular properties of ParA2 in *V. cholerae.* This appendix addresses the biochemical properties of the other ParA protein in the cell, ParA1. When Fogel and Waldor looked at the intracellular localization of ParA1 in relation to $oriC_I$, they found visual evidence suggesting that ParA1 may effect chrI segregation by employing a pulling, mitotic-like mechanism as outlined in **Fig. 1-12**. ParA1 was always located between the cell pole and the $oriC_I$ region, rather than between the newly replicated $oriC_I$ regions as would be expected for a pushing model of segregation (60).

The *parABS1* locus of chrI is not essential, as single and double mutants of ParA1 and ParB1 cause a minor chrI mis-localization phenotype observable by fluorescence microscopy (60, 102, 173). However, *parABS1* is able to confer stability to an otherwise unstable F plasmid deleted for *sopABC* in a heterologous host, suggesting that the locus does encode a functional partitioning system (173). How does this locus mediate partitioning of chrI? And does it utilize a molecular mechanism akin to what has been hypothesized based on the microscopy studies? To address these questions, a biochemical approach was utilized to determine: 1. whether ParA1 can polymerize as would be predicted based on its homology to the plasmid ParA proteins; and 2. what factors influence ParA1 polymerization.

ParA1 forms high molecular weight species in the presence of ATP and Mg^{2+}. Previous biochemical studies on other ParA orthologs show that these proteins are capable of polymerization in the presence of ATP or ATP non-hydrolyzable analogs, leading to the hypothesis that ATP binding aids polymer formation while ATP hydrolysis

results in de-polymerization. To determine whether ParA1 of *V. cholerae* also behaves in this fashion, a C-terminal his_6-tagged version of ParA1 was purified using Ni^{2+} affinity chromatography. This protein was used subsequently in a pelleting assay devised by Barillá et al. to assess its ability to form higher molecular weight species (11). Recovery of ParA in the pellet fraction has often correlated with ParA filament formation visualized by EM (11, 20, 52, 120). ParA1 was found to pellet in the presence of ATP, but not when ADP was present or when there was an absence of nucleotide (**Fig. 5-1A**). Pelleting also required the presence of Mg^{2+}. Surprisingly, no ParA1 was recovered in the pellet fractions of reactions that included the slowly hydrolyzable ATP analog, ATPγS. However, a nucleotide binding assay shows that ParA1 does bind ATPγS under these conditions (**Fig. 5-1B**, done by S. McLeod). Together, these results suggest that ParA1 requires ATP binding and hydrolysis in order to polymerize.

ParA1 pellets in the presence of ATP and dATP. To ensure that ParA1 recovery in the pellet fraction was not due to an artifact of the assay, ParA1 pelleting was assessed with a range of nucleotides to determine nucleotide specificity. Consistent with being a deviant Walker Box ATPase, comparatively little ParA1 was recovered in the pellet fractions for all nucleotides tested save two: the reactions containing ATP and dATP (**Fig. 5-1C**). The ability of ParA1 to respond to dATP and ATP may not be surprising given the structural similarity between the two nucleotides. A number of enzymes in prokaryotic and eukaryotic cells have been reported to bind to both the deoxyribose and ribose form of their preferred nucleotide cofactor (77, 79, 135, 157).

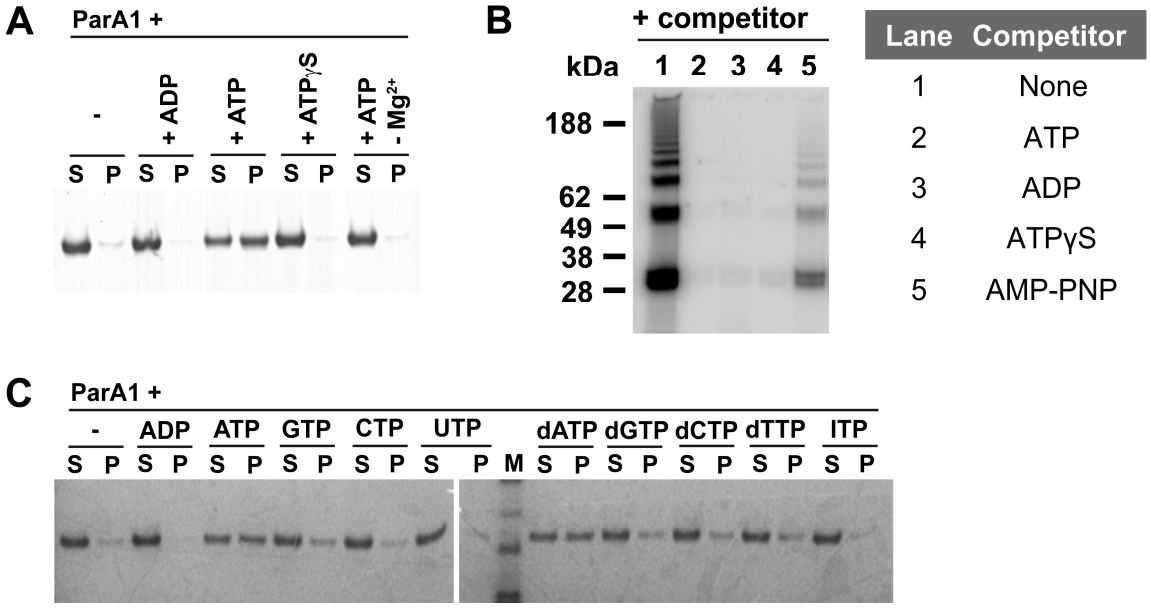

Fig. 6-1. ParA1 polymerization requires ATP and Mg^{2+}. (A) Detecting high molecular weight ParA1 species with a pelleting assay as described in the Methods. **(B)** Photo-affinity cross-linking of ParA1 nucleotide binding. Reactions contain 5 μM ParA2 and 167 μM [α-^{32}P]-ATP; excess cold nucleotide competitors were added to a final concentration of 2 mM. Done by S. McLeod. **(C)** Determining the specificity of ParA1 pelleting. In the pelleting assays, (S) and (P) denote the supernatant and pellet fractions, respectively.

However, given the knowledge that the intracellular concentration of ATP is much higher than that of dATP, ATP is most likely the preferred nucleotide.

Stability of the ParA1 species is affected by ParBS1. In some plasmid systems, ParA filament stability has been observed to be sensitive to the presence of other components of the partitioning system, such as ParB and DNA (11, 20). In order to assess the stability of ParA1 filaments, several order of addition pelleting experiments were done. ParA1 was incubated with ATP and Mg^{2+} for 10 min to allow for polymer formation. After 10 min, the reactions were treated with one of the following components and incubated for an additional 10 min: water, ParB1, or ParB1 pre-incubated for 10 min with *parS1* containing DNA (to simulate the nucleoprotein complex). As a control to ensure ParA1 polymerized prior to the second incubation step, one reaction was placed on ice at the end of the first 10 min incubation.

Under the initial conditions tested, the addition of ParB1 appears to have little effect on the pre-polymerized ParA1 (**Fig. 5-2A**). However, the addition of ParB1-*parS1* is sufficient to cause de-polymerization of ParA1. A titration of ParB1 with respect to pre-polymerized ParA1 showed that ParB1 had no destabilizing effect on ParA1 polymers (**Fig. 5-2B**). It is still possible that ParB1 may have stabilizing effect on ParA1 polymers or no effect at all. In contrast, a titration of *parS1* containing DNA showed a decrease in pelleting with increasing amounts of DNA (**Fig. 5-2C**). This strongly suggests that DNA is primarily responsible for triggering ParA1 de-polymerization, not ParB1.

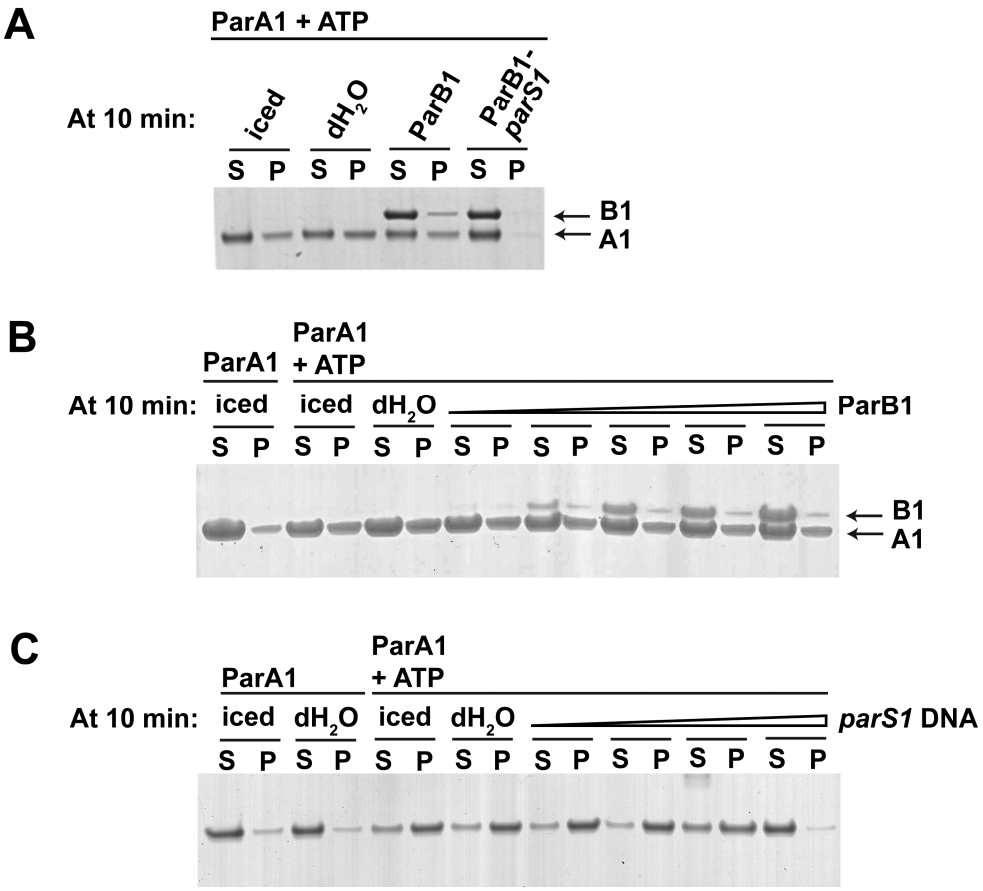

Fig. 6-2. The effect of ParB1 and *parS1* DNA on ParA1 filaments. (A) Initial observations of the effects of ParB1 or ParB1-*parS1* on ParA1 polymers. ParB1 was added to a final concentration of 2 μM where indicated. The *parS1* site was supplied on a plasmid at 1.5 pmol. **(B)** Titration of ParB1 from 2 μM to 10 μM incubated with pre-polymerized ParA1. **(C)** Titration of *parS1* containing plasmid from 1.5 fmol to 1.5 pmol incubated with pre-polymerized ParA1. (S) and (P) denote the supernatant and pellet fractions, respectively.

Visualizing ParA1 by electron microscopy. Visualizing ParA1 by electron microscopy, however, showed that the pellet fractions predominantly consisted of large protein clusters rather than the filaments as expected (**Fig. 5-3**). In these clusters, some hint of a filamentous structure can be observed, but the most likely explanation is that ParA1 is aggregating, resulting in recovery of the protein in the pellet fractions of the sedimentation assays.

A curious point is that the formation of these aggregates is ATP dependent since no protein is recovered in the pellet in the presence of ADP. Futhermore, based on the pelleting studies using 'pre-polymerized' ParA1, the aggregation is clearly reversible, since there is a reduction in protein recovered in the pellet fraction with an increase in DNA. While I cannot provide a reasonable explanation for the first observation, it is possible that the addition of ParA1 allows redistribution of ParA1 from the aggregate onto the DNA to form complexes unable to be captured by low speed centrifugation. A simple gel-shift experiment of ParA1 and DNA or electron microscopy of ParA1 incubated with ATP and DNA should shed light on the matter. An alternative explanation is that ParA1 does form filaments in an ATP dependent manner that does not require DNA, but requires another factor to direct the conformation of the assembled polymer (ie. not let it aggregate).

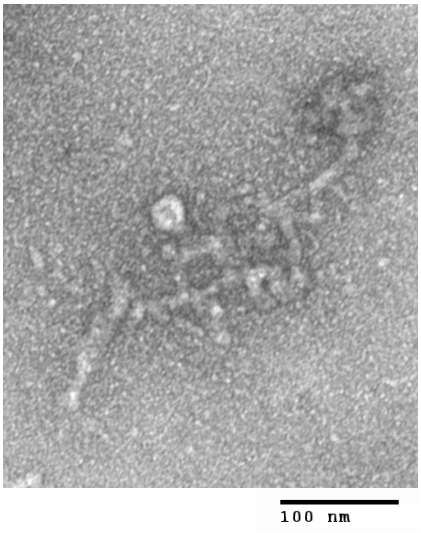

Fig. 6-3. Negative stain EM of ParA1 'polymers'. Samples were prepared by incubating ParA1 with ATP under the same conditions examined for the pelleting assays as described in the Methods. Working magnification: 49,000X.

METHODS

Purification of ParA1-his$_6$. The *parA1* coding region was amplified from the *V. cholerae* N16961 chromosome using primers MFp130 (5'-CCACCGAGCTCAAGGAGGTGTGAGGTGGGTAAAATCGTAGC-3') and MFp153 (5'-CACTGCATGCTGCGGGAATCTCTTCGC-3'), triple ligated into pBAD33 using the enzymes *Sac*I, *Sph*I, and *Hind*III (sites underlined) along with a fragment produced by annealing oligos MFp151 (5' - CGGATCAGCAGGTTCTGCTCATCACCATCACCATCACTAGA-3') and MFp152 (5'-AGCTTCTAGTGATGGTGATGGTGATGAGCAGAACCTGCTGATCCGCATG-3') containing *Sph*I and *Hind*III overhangs, and sub-cloned into pET11a via *Nhe*I and *BamH*I, yielding pSM808. The construct was verified by sequencing. *E. coli* BL21(DE3)/pSM808 was grown in 1 L LB containing 100 μg/ml ampicillin at 37°C shaking until $OD_{600} \approx 0.6$, when ParA1 expression was induced with 1 mM IPTG at 25°C for 1 h. Cells were harvested by centrifugation at 5,000 x *g* for 10 min at 4°C, and the pellet was stored overnight at -20°C. The pellet was resuspended in 10 ml Buffer B (50 mM sodium phosphate [pH 8.0], 500 mM NaCl, 10% glycerol [v/v], 3 mM DTT, 1 mM EDTA, 20 mM imidiazole [EMD], 1X HALT protease inhibitor cocktail [Pierce]). Cells were lysed using a French-pressure cell, and the lysate was clarified by centrifugation at 10,000 x *g* for 1 hr at 4°C before loading onto a 1 ml HisTrap FF Crude FPLC column (GE Healthcare) equilibrated with Buffer B at 4°C. ParA1 was eluted using a 20 ml imidazole gradient of 20 - 500 mM in Buffer E (50 mM sodium phosphate buffer [pH 8.0], 500 mM NaCl, 10% glycerol [v/v], 3 mM DTT, 1 mM EDTA). Fractions judged to

be ≥99% pure on an SDS-PAGE gel stained with Invitrogen Simply Blue Safestain were pooled, dialyzed overnight into Buffer D (20 mM Tris-HCl [pH 8.0], 500 mM NaCl, 0.1 mM EDTA, 5 mM DTT, 50% glycerol [v/v]), and stored at -20°C.

Purification of ParB1-his$_6$. The ParB1 coding region was amplified from the *V. cholerae* N16961 chromosome using primers Bfnde (5'-CATATGACTAAACGTGGTTTAGG- 3') and Brxho (5'-CTCGAGTTAGTTTTGCAGCTTGGCAA-3'), cloned into pCR2.1-TOPO using the TOPO TA Cloning Kit (Invitrogen), and sub-cloned into pET28b via *Nde*I and *Xho*I (sites underlined), yielding pSM823. Purification was carried out as for ParA1-his$_6$.

Pelleting Assay. The pelleting assay was done according to (92). Protein was visualized on SDS-PAGE gels stained with Invitrogen Simply Blue Safestain.

Photoaffinity cross-linking assay. Photoaffinity cross-linking was performed as described in (92).

Negative stain electron microscopy. 10 μM ParA1 was incubated in Buffer P and 1 mM nucleotide in a 30 μl reaction at 25°C for 10 min on parafilm. Samples were fixed by inverting freshly glow discharged carbon coated copper grids (EMS) onto the reaction droplet for 30 sec before removing the excess by blotting with Whatman filter paper. The grids were then inverted onto a solution of 2% uranyl formate for 30 sec. Excess stain was removed by blotting. Visualization was done using a **Tecnai™ G² Spirit BioTWIN electron microscope equipped with an** AMT 2k CCD camera at the indicated working magnification.

WORKS CITED

1. **Abeles, A. L., S. A. Friedman, and S. J. Austin.** 1985. Partition of unit-copy miniplasmids to daughter cells. III. The DNA sequence and functional organization of the P1 partition region. J Mol Biol **185:**261-72.
2. **Adachi, S., K. Hori, and S. Hiraga.** 2006. Subcellular positioning of F plasmid mediated by dynamic localization of SopA and SopB. J Mol Biol **356:**850-63.
3. **Ah-Seng, Y., F. Lopez, F. Pasta, D. Lane, and J. Y. Bouet.** 2009. Dual role of DNA in regulating ATP hydrolysis by the SopA partition protein. J Biol Chem **284:**30067-75.
4. **Akhtar, P., S. P. Anand, S. C. Watkins, and S. A. Khan.** 2009. The tubulin-like RepX protein encoded by the pXO1 plasmid forms polymers in vivo in Bacillus anthracis. J Bacteriol **191:**2493-500.
5. **Anand, S. P., P. Akhtar, E. Tinsley, S. C. Watkins, and S. A. Khan.** 2008. GTP-dependent polymerization of the tubulin-like RepX replication protein encoded by the pXO1 plasmid of Bacillus anthracis. Mol Microbiol **67:**881-90.
6. **Arnold, K., L. Bordoli, J. Kopp, and T. Schwede.** 2006. The SWISS-MODEL workspace: a web-based environment for protein structure homology modelling. Bioinformatics **22:**195-201.
7. **Austin, S., and A. Abeles.** 1983. Partition of unit-copy miniplasmids to daughter cells. I. P1 and F miniplasmids contain discrete, interchangeable sequences sufficient to promote equipartition. J Mol Biol **169:**353-72.
8. **Austin, S., and A. Abeles.** 1983. Partition of unit-copy miniplasmids to daughter cells. II. The partition region of miniplasmid P1 encodes an essential protein and a centromere-like site at which it acts. J Mol Biol **169:**373-87.
9. **Aylett, C. H., Q. Wang, K. A. Michie, L. A. Amos, and J. Lowe.** 2010. Filament structure of bacterial tubulin homologue TubZ. Proc Natl Acad Sci U S A **107:**19766-71.
10. **Barilla, D., and F. Hayes.** 2003. Architecture of the ParF*ParG protein complex involved in prokaryotic DNA segregation. Mol Microbiol **49:**487-99.
11. **Barilla, D., M. F. Rosenberg, U. Nobbmann, and F. Hayes.** 2005. Bacterial DNA segregation dynamics mediated by the polymerizing protein ParF. EMBO J **24:**1453-64.
12. **Bartosik, A. A., K. Lasocki, J. Mierzejewska, C. M. Thomas, and G. Jagura-Burdzy.** 2004. ParB of Pseudomonas aeruginosa: interactions with its partner ParA and its target parS and specific effects on bacterial growth. J Bacteriol **186:**6983-98.
13. **Becker, E., N. C. Herrera, F. Q. Gunderson, A. I. Derman, A. L. Dance, J. Sims, R. A. Larsen, and J. Pogliano.** 2006. DNA segregation by the bacterial actin AlfA during Bacillus subtilis growth and development. Embo J **25:**5919-31.
14. **Ben-Yehuda, S., D. Z. Rudner, and R. Losick.** 2003. RacA, a bacterial protein that anchors chromosomes to the cell poles. Science **299:**532-6.
15. **Berkmen, M. B., and A. D. Grossman.** 2007. Subcellular positioning of the origin region of the Bacillus subtilis chromosome is independent of sequences within oriC, the site of replication initiation, and the replication initiator DnaA. Mol Microbiol **63:**150-65.

16. **Bernhardt, T. G., and P. A. de Boer.** 2005. SlmA, a nucleoid-associated, FtsZ binding protein required for blocking septal ring assembly over Chromosomes in E. coli. Mol Cell **18:**555-64.
17. **Berry, C., S. O'Neil, E. Ben-Dov, A. F. Jones, L. Murphy, M. A. Quail, M. T. Holden, D. Harris, A. Zaritsky, and J. Parkhill.** 2002. Complete sequence and organization of pBtoxis, the toxin-coding plasmid of Bacillus thuringiensis subsp. israelensis. Appl Environ Microbiol **68:**5082-95.
18. **Biek, D. P., and J. Strings.** 1995. Partition functions of mini-F affect plasmid DNA topology in Escherichia coli. J Mol Biol **246:**388-400.
19. **Bork, P., C. Sander, and A. Valencia.** 1992. An ATPase domain common to prokaryotic cell cycle proteins, sugar kinases, actin, and hsp70 heat shock proteins. Proc Natl Acad Sci U S A **89:**7290-4.
20. **Bouet, J. Y., Y. Ah-Seng, N. Benmeradi, and D. Lane.** 2007. Polymerization of SopA partition ATPase: regulation by DNA binding and SopB. Mol Microbiol **63:**468-81.
21. **Bouet, J. Y., and B. E. Funnell.** 1999. P1 ParA interacts with the P1 partition complex at parS and an ATP-ADP switch controls ParA activities. EMBO J **18:**1415-24.
22. **Bouet, J. Y., and D. Lane.** 2009. Molecular basis of the supercoil deficit induced by the mini-F plasmid partition complex. J Biol Chem **284:**165-73.
23. **Bouet, J. Y., J. Rech, S. Egloff, D. P. Biek, and D. Lane.** 2005. Probing plasmid partition with centromere-based incompatibility. Mol Microbiol **55:**511-25.
24. **Bouet, J. Y., J. A. Surtees, and B. E. Funnell.** 2000. Stoichiometry of P1 plasmid partition complexes. J Biol Chem **275:**8213-9.
25. **Bowman, G. R., L. R. Comolli, J. Zhu, M. Eckart, M. Koenig, K. H. Downing, W. E. Moerner, T. Earnest, and L. Shapiro.** 2008. A polymeric protein anchors the chromosomal origin/ParB complex at a bacterial cell pole. Cell **134:**945-55.
26. **Breier, A. M., and A. D. Grossman.** 2007. Whole-genome analysis of the chromosome partitioning and sporulation protein Spo0J (ParB) reveals spreading and origin-distal sites on the Bacillus subtilis chromosome. Mol Microbiol **64:**703-18.
27. **Bylund, J. E., M. A. Haines, P. J. Piggot, and M. L. Higgins.** 1993. Axial filament formation in Bacillus subtilis: induction of nucleoids of increasing length after addition of chloramphenicol to exponential-phase cultures approaching stationary phase. J Bacteriol **175:**1886-90.
28. **Cabrera, J. E., C. Cagliero, S. Quan, C. L. Squires, and D. J. Jin.** 2009. Active transcription of rRNA operons condenses the nucleoid in Escherichia coli: examining the effect of transcription on nucleoid structure in the absence of transertion. J Bacteriol **191:**4180-5.
29. **Cabrera, J. E., and D. J. Jin.** 2003. The distribution of RNA polymerase in Escherichia coli is dynamic and sensitive to environmental cues. Mol Microbiol **50:**1493-505.
30. **Campbell, C. S., and R. D. Mullins.** 2007. In vivo visualization of type II plasmid segregation: bacterial actin filaments pushing plasmids. J Cell Biol **179:**1059-66.

31. **Castaing, J. P., J. Y. Bouet, and D. Lane.** 2008. F plasmid partition depends on interaction of SopA with non-specific DNA. Mol Microbiol **70:**1000-11.
32. **Chen, Y., and H. P. Erickson.** 2008. In vitro assembly studies of FtsZ/tubulin-like proteins (TubZ) from Bacillus plasmids: evidence for a capping mechanism. J Biol Chem **283:**8102-9.
33. **Chen, Z., H. Yang, and N. P. Pavletich.** 2008. Mechanism of homologous recombination from the RecA-ssDNA/dsDNA structures. Nature **453:**489-4.
34. **Choi, C. L., S. A. Claridge, E. C. Garner, A. P. Alivisatos, and R. D. Mullins.** 2008. Protein-nanocrystal conjugates support a single filament polymerization model in R1 plasmid segregation. J Biol Chem **283:**28081-6.
35. **Dam, M., and K. Gerdes.** 1994. Partitioning of plasmid R1. Ten direct repeats flanking the parA promoter constitute a centromere-like partition site parC, that expresses incompatibility. J Mol Biol **236:**1289-98.
36. **Dame, R. T., C. Wyman, and N. Goosen.** 2000. H-NS mediated compaction of DNA visualised by atomic force microscopy. Nucleic Acids Res **28:**3504-10.
37. **Davey, M. J., and B. E. Funnell.** 1997. Modulation of the P1 plasmid partition protein ParA by ATP, ADP, and P1 ParB. J Biol Chem **272:**15286-92.
38. **Davey, M. J., and B. E. Funnell.** 1994. The P1 plasmid partition protein ParA. A role for ATP in site-specific DNA binding. J Biol Chem **269:**29908-13.
39. **Davis, M. A., and S. J. Austin.** 1988. Recognition of the P1 plasmid centromere analog involves binding of the ParB protein and is modified by a specific host factor. EMBO J **7:**1881-8.
40. **Davis, M. A., K. A. Martin, and S. J. Austin.** 1992. Biochemical activities of the parA partition protein of the P1 plasmid. Mol Microbiol **6:**1141-7.
41. **Davis, M. A., L. Radnedge, K. A. Martin, F. Hayes, B. Youngren, and S. J. Austin.** 1996. The P1 ParA protein and its ATPase activity play a direct role in the segregation of plasmid copies to daughter cells. Mol Microbiol **21:**1029-36.
42. **de la Hoz, A. B., F. Pratto, R. Misselwitz, C. Speck, W. Weihofen, K. Welfle, W. Saenger, H. Welfle, and J. C. Alonso.** 2004. Recognition of DNA by omega protein from the broad-host range Streptococcus pyogenes plasmid pSM19035: analysis of binding to operator DNA with one to four heptad repeats. Nucleic Acids Res **32:**3136-47.
43. **Derman, A. I., E. C. Becker, B. D. Truong, A. Fujioka, T. M. Tucey, M. L. Erb, P. C. Patterson, and J. Pogliano.** 2009. Phylogenetic analysis identifies many uncharacterized actin-like proteins (Alps) in bacteria: regulated polymerization, dynamic instability and treadmilling in Alp7A. Mol Microbiol **73:**534-52.
44. **Dmowski, M., I. Sitkiewicz, and P. Ceglowski.** 2006. Characterization of a novel partition system encoded by the delta and omega genes from the streptococcal plasmid pSM19035. J Bacteriol **188:**4362-72.
45. **Dunham, T. D., W. Xu, B. E. Funnell, and M. A. Schumacher.** 2009. Structural basis for ADP-mediated transcriptional regulation by P1 and P7 ParA. EMBO J **28:**1792-802.
46. **Dworkin, J., and R. Losick.** 2002. Does RNA polymerase help drive chromosome segregation in bacteria? Proc Natl Acad Sci U S A **99:**14089-94.

47. **Easter, J., Jr., and J. W. Gober.** 2002. ParB-stimulated nucleotide exchange regulates a switch in functionally distinct ParA activities. Mol Cell **10:**427-34.
48. **Ebersbach, G., A. Briegel, G. J. Jensen, and C. Jacobs-Wagner.** 2008. A self-associating protein critical for chromosome attachment, division, and polar organization in caulobacter. Cell **134:**956-68.
49. **Ebersbach, G., and K. Gerdes.** 2004. Bacterial mitosis: partitioning protein ParA oscillates in spiral-shaped structures and positions plasmids at mid-cell. Mol Microbiol **52:**385-98.
50. **Ebersbach, G., and K. Gerdes.** 2001. The double par locus of virulence factor pB171: DNA segregation is correlated with oscillation of ParA. Proc Natl Acad Sci U S A **98:**15078-83.
51. **Ebersbach, G., and K. Gerdes.** 2005. Plasmid segregation mechanisms. Annu Rev Genet **39:**453-79.
52. **Ebersbach, G., S. Ringgaard, J. Moller-Jensen, Q. Wang, D. J. Sherratt, and K. Gerdes.** 2006. Regular cellular distribution of plasmids by oscillating and filament-forming ParA ATPase of plasmid pB171. Mol Microbiol **61:**1428-42.
53. **Edgar, R., D. K. Chattoraj, and M. Yarmolinsky.** 2001. Pairing of P1 plasmid partition sites by ParB. Mol Microbiol **42:**1363-70.
54. **Egelman, E. H.** 2000. A robust algorithm for the reconstruction of helical filaments using single-particle methods. Ultramicroscopy **85:**225-34.
55. **Egelman, E. H., and L. A. Amos.** 2009. Electron microscopy of helical filaments: rediscovering buried treasures in negative stain. Bioessays **31:**909-11.
56. **Erdmann, N., T. Petroff, and B. E. Funnell.** 1999. Intracellular localization of P1 ParB protein depends on ParA and parS. Proc Natl Acad Sci U S A **96:**14905-10.
57. **Fiebig, A., K. Keren, and J. A. Theriot.** 2006. Fine-scale time-lapse analysis of the biphasic, dynamic behaviour of the two Vibrio cholerae chromosomes. Mol Microbiol **60:**1164-78.
58. **Figge, R. M., J. Easter, and J. W. Gober.** 2003. Productive interaction between the chromosome partitioning proteins, ParA and ParB, is required for the progression of the cell cycle in Caulobacter crescentus. Mol Microbiol **47:**1225-37.
59. **Fogel, M. A., and M. K. Waldor.** 2005. Distinct segregation dynamics of the two *Vibrio cholerae* chromosomes. Mol Microbiol **55:**125-36.
60. **Fogel, M. A., and M. K. Waldor.** 2006. A dynamic, mitotic-like mechanism for bacterial chromosome segregation. Genes Dev **20:**3269-82.
61. **Fung, E., J. Y. Bouet, and B. E. Funnell.** 2001. Probing the ATP-binding site of P1 ParA: partition and repression have different requirements for ATP binding and hydrolysis. EMBO J **20:**4901-11.
62. **Funnell, B. E.** 1988. Mini-P1 plasmid partitioning: excess ParB protein destabilizes plasmids containing the centromere parS. J Bacteriol **170:**954-60.
63. **Funnell, B. E.** 1991. The P1 plasmid partition complex at parS. The influence of Escherichia coli integration host factor and of substrate topology. J Biol Chem **266:**14328-37.
64. **Funnell, B. E.** 1988. Participation of Escherichia coli integration host factor in the P1 plasmid partition system. Proc Natl Acad Sci U S A **85:**6657-61.

65. **Funnell, B. E., and L. Gagnier.** 1993. The P1 plasmid partition complex at parS. II. Analysis of ParB protein binding activity and specificity. J Biol Chem **268:**3616-24.
66. **Garner, E. C., C. S. Campbell, and R. D. Mullins.** 2004. Dynamic instability in a DNA-segregating prokaryotic actin homolog. Science **306:**1021-5.
67. **Garner, E. C., C. S. Campbell, D. B. Weibel, and R. D. Mullins.** 2007. Reconstitution of DNA segregation driven by assembly of a prokaryotic actin homolog. Science **315:**1270-4.
68. **Gelles, J., and R. Landick.** 1998. RNA polymerase as a molecular motor. Cell **93:**13-6.
69. **Gerdes, K., J. E. Larsen, and S. Molin.** 1985. Stable inheritance of plasmid R1 requires two different loci. J Bacteriol **161:**292-8.
70. **Gerdes, K., J. Moller-Jensen, and R. Bugge Jensen.** 2000. Plasmid and chromosome partitioning: surprises from phylogeny. Mol Microbiol **37:**455-66.
71. **Glaser, P., M. E. Sharpe, B. Raether, M. Perego, K. Ohlsen, and J. Errington.** 1997. Dynamic, mitotic-like behavior of a bacterial protein required for accurate chromosome partitioning. Genes Dev **11:**1160-8.
72. **Gordon, G. S., R. P. Shivers, and A. Wright.** 2002. Polar localization of the Escherichia coli oriC region is independent of the site of replication initiation. Mol Microbiol **44:**501-7.
73. **Gordon, G. S., D. Sitnikov, C. D. Webb, A. Teleman, A. Straight, R. Losick, A. W. Murray, and A. Wright.** 1997. Chromosome and low copy plasmid segregation in E. coli: visual evidence for distinct mechanisms. Cell **90:**1113-21.
74. **Gordon, S., J. Rech, D. Lane, and A. Wright.** 2004. Kinetics of plasmid segregation in Escherichia coli. Mol Microbiol **51:**461-9.
75. **Green, E. W., and M. Schaechter.** 1972. The mode of segregation of the bacterial cell membrane. Proc Natl Acad Sci U S A **69:**2312-6.
76. **Gruber, S., and J. Errington.** 2009. Recruitment of condensin to replication origin regions by ParB/SpoOJ promotes chromosome segregation in B. subtilis. Cell **137:**685-96.
77. **Hamel, E., and C. M. Lin.** 1981. Interaction of tubulin with ribose-modified analogs of GTP and GDP: evidence for two mutually exclusive exchangeable nucleotide binding sites. Proc Natl Acad Sci U S A **78:**3368-72.
78. **Hanai, R., R. Liu, P. Benedetti, P. R. Caron, A. S. Lynch, and J. C. Wang.** 1996. Molecular dissection of a protein SopB essential for Escherichia coli F plasmid partition. J Biol Chem **271:**17469-75.
79. **Handke, L. D., R. P. Shivers, and A. L. Sonenshein.** 2008. Interaction of Bacillus subtilis CodY with GTP. J Bacteriol **190:**798-806.
80. **Hatano, T., and H. Niki.** 2010. Partitioning of P1 plasmids by gradual distribution of the ATPase ParA. Mol Microbiol **78:**1182-98.
81. **Hatano, T., Y. Yamaichi, and H. Niki.** 2007. Oscillating focus of SopA associated with filamentous structure guides partitioning of F plasmid. Mol Microbiol **64:**1198-213.
82. **Hayes, F.** 2000. The partition system of multidrug resistance plasmid TP228 includes a novel protein that epitomizes an evolutionarily distinct subgroup of the ParA superfamily. Mol Microbiol **37:**528-41.

83. **Hayes, F., and S. Austin.** 1994. Topological scanning of the P1 plasmid partition site. J Mol Biol **243:**190-8.
84. **Heidelberg, J. F., J. A. Eisen, W. C. Nelson, R. A. Clayton, M. L. Gwinn, R. J. Dodson, D. H. Haft, E. K. Hickey, J. D. Peterson, L. Umayam, S. R. Gill, K. E. Nelson, T. D. Read, H. Tettelin, D. Richardson, M. D. Ermolaeva, J. Vamathevan, S. Bass, H. Qin, I. Dragoi, P. Sellers, L. McDonald, T. Utterback, R. D. Fleishmann, W. C. Nierman, O. White, S. L. Salzberg, H. O. Smith, R. R. Colwell, J. J. Mekalanos, J. C. Venter, and C. M. Fraser.** 2000. DNA sequence of both chromosomes of the cholera pathogen Vibrio cholerae. Nature **406:**477-83.
85. **Helsberg, M., and R. Eichenlaub.** 1986. Twelve 43-base-pair repeats map in a cis-acting region essential for partition of plasmid mini-F. J Bacteriol **165:**1043-5.
86. **Hester, C. M., and J. Lutkenhaus.** 2007. Soj (ParA) DNA binding is mediated by conserved arginines and is essential for plasmid segregation. Proc Natl Acad Sci U S A **104:**20326-31.
87. **Heuser, J.** 1981. Preparing biological samples for stereomicroscopy by the quick-freeze, deep-etch, rotary-replication technique. Methods Cell Biol **22:**97-122.
88. **Hiraga, S., H. Niki, T. Ogura, C. Ichinose, H. Mori, B. Ezaki, and A. Jaffe.** 1989. Chromosome partitioning in Escherichia coli: novel mutants producing anucleate cells. J Bacteriol **171:**1496-505.
89. **Hirano, M., H. Mori, T. Onogi, M. Yamazoe, H. Niki, T. Ogura, and S. Hiraga.** 1998. Autoregulation of the partition genes of the mini-F plasmid and the intracellular localization of their products in Escherichia coli. Mol Gen Genet **257:**392-403.
90. **Hoischen, C., M. Bussiek, J. Langowski, and S. Diekmann.** 2008. Escherichia coli low-copy-number plasmid R1 centromere parC forms a U-shaped complex with its binding protein ParR. Nucleic Acids Res **36:**607-15.
91. **Howard, M., and K. Gerdes.** 2010. What is the mechanism of ParA-mediated DNA movement? Mol Microbiol **78:**9-12.
92. **Hui, M. P., V. E. Galkin, X. Yu, A. Z. Stasiak, A. Stasiak, M. K. Waldor, and E. H. Egelman.** 2010. ParA2, a Vibrio cholerae chromosome partitioning protein, forms left-handed helical filaments on DNA. Proc Natl Acad Sci U S A **107:**4590-5.
93. **Ireton, K., N. W. t. Gunther, and A. D. Grossman.** 1994. spo0J is required for normal chromosome segregation as well as the initiation of sporulation in *Bacillus subtilis*. J Bacteriol **176:**5320-9.
94. **Jacob, F., S. Brenner, and F. Cuzin.** 1963. On the regulation of DNA replication in bactera. Cold Spring Harbor Symp. Quant. Biol. **28:**329-347.
95. **Jakimowicz, D., P. Zydek, A. Kois, J. Zakrzewska-Czerwinska, and K. F. Chater.** 2007. Alignment of multiple chromosomes along helical ParA scaffolding in sporulating *Streptomyces* hyphae. Mol Microbiol **65:**625-41.
96. **Jensen, R. B., and K. Gerdes.** 1997. Partitioning of plasmid R1. The ParM protein exhibits ATPase activity and interacts with the centromere-like ParR-parC complex. J Mol Biol **269:**505-13.

97. **Jensen, R. B., R. Lurz, and K. Gerdes.** 1998. Mechanism of DNA segregation in prokaryotes: replicon pairing by parC of plasmid R1. Proc Natl Acad Sci U S A **95:**8550-5.
98. **Jensen, R. B., and L. Shapiro.** 1999. The Caulobacter crescentus smc gene is required for cell cycle progression and chromosome segregation. Proc Natl Acad Sci U S A **96:**10661-6.
99. **Jensen, R. B., S. C. Wang, and L. Shapiro.** 2001. A moving DNA replication factory in Caulobacter crescentus. Embo J **20:**4952-63.
100. **Jun, S., and B. Mulder.** 2006. Entropy-driven spatial organization of highly confined polymers: lessons for the bacterial chromosome. Proc Natl Acad Sci U S A **103:**12388-93.
101. **Jun, S., and A. Wright.** 2010. Entropy as the driver of chromosome segregation. Nat Rev Microbiol **8:**600-7.
102. **Kadoya, R., J. H. Baek, A. Sarker, and D. K. Chattoraj.** 2011. Participation of a Chromosome Segregation Protein ParAI of Vibrio cholerae in Chromosome Replication. J Bacteriol.
103. **Kiefer, F., K. Arnold, M. Kunzli, L. Bordoli, and T. Schwede.** 2009. The SWISS-MODEL Repository and associated resources. Nucleic Acids Res **37:**D387-92.
104. **Kiianitsa, K., and A. Stasiak.** 1997. Helical repeat of DNA in the region of homologous pairing. Proc Natl Acad Sci U S A **94:**7837-40.
105. **Kimsey, H. H., and M. K. Waldor.** 2004. The CTXphi repressor RstR binds DNA cooperatively to form tetrameric repressor-operator complexes. J Biol Chem **279:**2640-7.
106. **Koonin, E. V.** 1993. A superfamily of ATPases with diverse functions containing either classical or deviant ATP-binding motif. J Mol Biol **229:**1165-74.
107. **Koppes, L. J., C. L. Woldringh, and N. Nanninga.** 1999. Escherichia coli contains a DNA replication compartment in the cell center. Biochimie **81:**803-10.
108. **Kubitschek, H. E.** 1990. Cell volume increase in Escherichia coli after shifts to richer media. J Bacteriol **172:**94-101.
109. **Kusukawa, N., H. Mori, A. Kondo, and S. Hiraga.** 1987. Partitioning of the F plasmid: overproduction of an essential protein for partition inhibits plasmid maintenance. Mol Gen Genet **208:**365-72.
110. **Lane, D., R. Rothenbuehler, A. M. Merrillat, and C. Aiken.** 1987. Analysis of the F plasmid centromere. Mol Gen Genet **207:**406-12.
111. **Larsen, R. A., C. Cusumano, A. Fujioka, G. Lim-Fong, P. Patterson, and J. Pogliano.** 2007. Treadmilling of a prokaryotic tubulin-like protein, TubZ, required for plasmid stability in Bacillus thuringiensis. Genes Dev **21:**1340-52.
112. **Lau, I. F., S. R. Filipe, B. Soballe, O. A. Okstad, F. X. Barre, and D. J. Sherratt.** 2003. Spatial and temporal organization of replicating Escherichia coli chromosomes. Mol Microbiol **49:**731-43.
113. **Lee, M. J., C. H. Liu, S. Y. Wang, C. T. Huang, and H. Huang.** 2006. Characterization of the Soj/Spo0J chromosome segregation proteins and identification of putative parS sequences in Helicobacter pylori. Biochem Biophys Res Commun **342:**744-50.

114. **Lee, P. S., and A. D. Grossman.** 2006. The chromosome partitioning proteins Soj (ParA) and Spo0J (ParB) contribute to accurate chromosome partitioning, separation of replicated sister origins, and regulation of replication initiation in Bacillus subtilis. Mol Microbiol **60:**853-69.
115. **Lee, P. S., D. C. Lin, S. Moriya, and A. D. Grossman.** 2003. Effects of the chromosome partitioning protein Spo0J (ParB) on oriC positioning and replication initiation in Bacillus subtilis. J Bacteriol **185:**1326-37.
116. **Lemon, K. P., and A. D. Grossman.** 2001. The extrusion-capture model for chromosome partitioning in bacteria. Genes Dev **15:**2031-41.
117. **Lemon, K. P., and A. D. Grossman.** 1998. Localization of bacterial DNA polymerase: evidence for a factory model of replication. Science **282:**1516-9.
118. **Lemon, K. P., and A. D. Grossman.** 2000. Movement of replicating DNA through a stationary replisome. Mol Cell **6:**1321-30.
119. **Lemonnier, M., J. Y. Bouet, V. Libante, and D. Lane.** 2000. Disruption of the F plasmid partition complex in vivo by partition protein SopA. Mol Microbiol **38:**493-505.
120. **Leonard, T. A., P. J. Butler, and J. Lowe.** 2005. Bacterial chromosome segregation: structure and DNA binding of the Soj dimer--a conserved biological switch. EMBO J **24:**270-82.
121. **Leonard, T. A., J. Moller-Jensen, and J. Lowe.** 2005. Towards understanding the molecular basis of bacterial DNA segregation. Philos Trans R Soc Lond B Biol Sci **360:**523-35.
122. **Lewis, P. J., and J. Errington.** 1997. Direct evidence for active segregation of oriC regions of the Bacillus subtilis chromosome and co-localization with the SpoOJ partitioning protein. Mol Microbiol **25:**945-54.
123. **Li, Y., and S. Austin.** 2002. The P1 plasmid is segregated to daughter cells by a 'capture and ejection' mechanism coordinated with Escherichia coli cell division. Mol Microbiol **46:**63-74.
124. **Li, Y., K. Sergueev, and S. Austin.** 2002. The segregation of the Escherichia coli origin and terminus of replication. Mol Microbiol **46:**985-96.
125. **Libante, V., L. Thion, and D. Lane.** 2001. Role of the ATP-binding site of SopA protein in partition of the F plasmid. J Mol Biol **314:**387-99.
126. **Lim, G. E., A. I. Derman, and J. Pogliano.** 2005. Bacterial DNA segregation by dynamic SopA polymers. Proc Natl Acad Sci U S A **102:**17658-63.
127. **Lin, D. C., and A. D. Grossman.** 1998. Identification and characterization of a bacterial chromosome partitioning site. Cell **92:**675-85.
128. **Lin, D. C., P. A. Levin, and A. D. Grossman.** 1997. Bipolar localization of a chromosome partition protein in Bacillus subtilis. Proc Natl Acad Sci U S A **94:**4721-6.
129. **Lindow, J. C., R. A. Britton, and A. D. Grossman.** 2002. Structural maintenance of chromosomes protein of Bacillus subtilis affects supercoiling in vivo. J Bacteriol **184:**5317-22.
130. **Liu, G., G. C. Draper, and W. D. Donachie.** 1998. FtsK is a bifunctional protein involved in cell division and chromosome localization in Escherichia coli. Mol Microbiol **29:**893-903.

131. **Livny, J., Y. Yamaichi, and M. K. Waldor.** 2007. Distribution of centromere-like *parS* sites in bacteria: insights from comparative genomics. J Bacteriol **189:**8693-703.
132. **Lutkenhaus, J.** 2007. Assembly dynamics of the bacterial MinCDE system and spatial regulation of the Z ring. Annu Rev Biochem **76:**539-62.
133. **Lynch, A. S., and J. C. Wang.** 1995. SopB protein-mediated silencing of genes linked to the sopC locus of Escherichia coli F plasmid. Proc Natl Acad Sci U S A **92:**1896-900.
134. **Marston, A. L., and J. Errington.** 1999. Dynamic movement of the ParA-like Soj protein of *B. subtilis* and its dual role in nucleoid organization and developmental regulation. Mol Cell **4:**673-82.
135. **Matson, S. W., and J. W. George.** 1987. DNA helicase II of Escherichia coli. Characterization of the single-stranded DNA-dependent NTPase and helicase activities. J Biol Chem **262:**2066-76.
136. **Mohl, D. A., J. Easter, Jr., and J. W. Gober.** 2001. The chromosome partitioning protein, ParB, is required for cytokinesis in Caulobacter crescentus. Mol Microbiol **42:**741-55.
137. **Mohl, D. A., and J. W. Gober.** 1997. Cell cycle-dependent polar localization of chromosome partitioning proteins in Caulobacter crescentus. Cell **88:**675-84.
138. **Moller-Jensen, J., J. Borch, M. Dam, R. B. Jensen, P. Roepstorff, and K. Gerdes.** 2003. Bacterial mitosis: ParM of plasmid R1 moves plasmid DNA by an actin-like insertional polymerization mechanism. Mol Cell **12:**1477-87.
139. **Moller-Jensen, J., R. B. Jensen, J. Lowe, and K. Gerdes.** 2002. Prokaryotic DNA segregation by an actin-like filament. EMBO J **21:**3119-27.
140. **Moller-Jensen, J., S. Ringgaard, C. P. Mercogliano, K. Gerdes, and J. Lowe.** 2007. Structural analysis of the ParR/parC plasmid partition complex. EMBO J **26:**4413-22.
141. **Mori, H., A. Kondo, A. Ohshima, T. Ogura, and S. Hiraga.** 1986. Structure and function of the F plasmid genes essential for partitioning. J Mol Biol **192:**1-15.
142. **Mori, H., Y. Mori, C. Ichinose, H. Niki, T. Ogura, A. Kato, and S. Hiraga.** 1989. Purification and characterization of SopA and SopB proteins essential for F plasmid partitioning. J Biol Chem **264:**15535-41.
143. **Murray, H., and J. Errington.** 2008. Dynamic control of the DNA replication initiation protein DnaA by Soj/ParA. Cell **135:**74-84.
144. **Murray, H., H. Ferreira, and J. Errington.** 2006. The bacterial chromosome segregation protein Spo0J spreads along DNA from parS nucleation sites. Mol Microbiol **61:**1352-61.
145. **Ni, L., W. Xu, M. Kumaraswami, and M. A. Schumacher.** 2010. Plasmid protein TubR uses a distinct mode of HTH-DNA binding and recruits the prokaryotic tubulin homolog TubZ to effect DNA partition. Proc Natl Acad Sci U S A **107:**11763-8.
146. **Nielsen, H. J., Y. Li, B. Youngren, F. G. Hansen, and S. Austin.** 2006. Progressive segregation of the Escherichia coli chromosome. Mol Microbiol **61:**383-93.

147. **Nielsen, H. J., J. R. Ottesen, B. Youngren, S. J. Austin, and F. G. Hansen.** 2006. The Escherichia coli chromosome is organized with the left and right chromosome arms in separate cell halves. Mol Microbiol **62:**331-8.
148. **Niki, H., and S. Hiraga.** 1998. Polar localization of the replication origin and terminus in Escherichia coli nucleoids during chromosome partitioning. Genes Dev **12:**1036-45.
149. **Niki, H., and S. Hiraga.** 1997. Subcellular distribution of actively partitioning F plasmid during the cell division cycle in E. coli. Cell **90:**951-7.
150. **Niki, H., Y. Yamaichi, and S. Hiraga.** 2000. Dynamic organization of chromosomal DNA in Escherichia coli. Genes Dev **14:**212-23.
151. **Nordstrom, K., S. Molin, and H. Aagaard-Hansen.** 1980. Partitioning of plasmid R1 in Escherichia coli. I. Kinetics of loss of plasmid derivatives deleted of the par region. Plasmid **4:**215-27.
152. **Ogura, T., and S. Hiraga.** 1983. Partition mechanism of F plasmid: two plasmid gene-encoded products and a cis-acting region are involved in partition. Cell **32:**351-60.
153. **Ogura, T., H. Niki, H. Mori, M. Morita, M. Hasegawa, C. Ichinose, and S. Hiraga.** 1990. Identification and characterization of gyrB mutants of Escherichia coli that are defective in partitioning of mini-F plasmids. J Bacteriol **172:**1562-8.
154. **Ogura, Y., N. Ogasawara, E. J. Harry, and S. Moriya.** 2003. Increasing the ratio of Soj to Spo0J promotes replication initiation in Bacillus subtilis. J Bacteriol **185:**6316-24.
155. **Orlova, A., E. C. Garner, V. E. Galkin, J. Heuser, R. D. Mullins, and E. H. Egelman.** 2007. The structure of bacterial ParM filaments. Nat Struct Mol Biol **14:**921-6.
156. **Peitsch, M. C.** 1995. Protein modeling E-mail Bio/Technology **13:**658-660.
157. **Phizicky, E. M., and J. W. Roberts.** 1981. Induction of SOS functions: regulation of proteolytic activity of E. coli RecA protein by interaction with DNA and nucleoside triphosphate. Cell **25:**259-67.
158. **Pogliano, J., T. Q. Ho, Z. Zhong, and D. R. Helinski.** 2001. Multicopy plasmids are clustered and localized in Escherichia coli. Proc Natl Acad Sci U S A **98:**4486-91.
159. **Polka, J. K., J. M. Kollman, D. A. Agard, and R. D. Mullins.** 2009. The structure and assembly dynamics of plasmid actin AlfA imply a novel mechanism of DNA segregation. J Bacteriol **191:**6219-30.
160. **Popp, D., A. Narita, U. Ghoshdastider, K. Maeda, Y. Maeda, T. Oda, T. Fujisawa, H. Onishi, K. Ito, and R. C. Robinson.** 2010. Polymeric structures and dynamic properties of the bacterial actin AlfA. J Mol Biol **397:**1031-41.
161. **Pratto, F., A. Cicek, W. A. Weihofen, R. Lurz, W. Saenger, and J. C. Alonso.** 2008. *Streptococcus pyogenes* pSM19035 requires dynamic assembly of ATP-bound ParA and ParB on *parS* DNA during plasmid segregation. Nucleic Acids Res **36:**3676-89.
162. **Ptacin, J. L., S. F. Lee, E. C. Garner, E. Toro, M. Eckart, L. R. Comolli, W. E. Moerner, and L. Shapiro.** 2010. A spindle-like apparatus guides bacterial chromosome segregation. Nat Cell Biol **12:**791-8.

163. **Quisel, J. D., D. C. Lin, and A. D. Grossman.** 1999. Control of development by altered localization of a transcription factor in *B. subtilis*. Mol Cell **4:**665-72.
164. **Ramamurthi, K. S., and R. Losick.** 2009. Negative membrane curvature as a cue for subcellular localization of a bacterial protein. Proc Natl Acad Sci U S A **106:**13541-5.
165. **Ravin, N. V., J. Rech, and D. Lane.** 2003. Mapping of functional domains in F plasmid partition proteins reveals a bipartite SopB-recognition domain in SopA. J Mol Biol **329:**875-89.
166. **Reyes-Lamothe, R., C. Possoz, O. Danilova, and D. J. Sherratt.** 2008. Independent positioning and action of Escherichia coli replisomes in live cells. Cell **133:**90-102.
167. **Ringgaard, S., G. Ebersbach, J. Borch, and K. Gerdes.** 2007. Regulatory cross-talk in the double par locus of plasmid pB171. J Biol Chem **282:**3134-45.
168. **Ringgaard, S., J. Lowe, and K. Gerdes.** 2007. Centromere pairing by a plasmid-encoded type I ParB protein. J Biol Chem **282:**28216-25.
169. **Ringgaard, S., J. van Zon, M. Howard, and K. Gerdes.** 2009. Movement and equipositioning of plasmids by ParA filament disassembly. Proc Natl Acad Sci U S A **106:**19369-74.
170. **Roca, A. I., and M. M. Cox.** 1997. RecA protein: structure, function, and role in recombinational DNA repair. Prog Nucleic Acid Res Mol Biol **56:**129-223.
171. **Rodionov, O., M. Lobocka, and M. Yarmolinsky.** 1999. Silencing of genes flanking the P1 plasmid centromere. Science **283:**546-9.
172. **Rodionov, O., and M. Yarmolinsky.** 2004. Plasmid partitioning and the spreading of P1 partition protein ParB. Mol Microbiol **52:**1215-23.
173. **Saint-Dic, D., B. P. Frushour, J. H. Kehrl, and L. S. Kahng.** 2006. A parA homolog selectively influences positioning of the large chromosome origin in Vibrio cholerae. J Bacteriol **188:**5626-31.
174. **Salje, J., and J. Lowe.** 2008. Bacterial actin: architecture of the ParMRC plasmid DNA partitioning complex. EMBO J **27:**2230-8.
175. **Sawitzke, J. A., and S. Austin.** 2000. Suppression of chromosome segregation defects of Escherichia coli muk mutants by mutations in topoisomerase I. Proc Natl Acad Sci U S A **97:**1671-6.
176. **Sawitzke, J. A., Y. Li, K. Sergueev, B. Youngren, T. Brendler, K. Jones, and S. Austin.** 2002. Transcriptional interference by a complex formed at the centromere-like partition site of plasmid P1. J Bacteriol **184:**2447-54.
177. **Schofield, W. B., H. C. Lim, and C. Jacobs-Wagner.** 2010. Cell cycle coordination and regulation of bacterial chromosome segregation dynamics by polarly localized proteins. Embo J **29:**3068-81.
178. **Schumacher, M. A.** 2008. Structural biology of plasmid partition: uncovering the molecular mechanisms of DNA segregation. Biochem J **412:**1-18.
179. **Schumacher, M. A., T. C. Glover, A. J. Brzoska, S. O. Jensen, T. D. Dunham, R. A. Skurray, and N. Firth.** 2007. Segrosome structure revealed by a complex of ParR with centromere DNA. Nature **450:**1268-71.
180. **Schumacher, M. A., K. M. Piro, and W. Xu.** 2010. Insight into F plasmid DNA segregation revealed by structures of SopB and SopB-DNA complexes. Nucleic Acids Res **38:**4514-26.

181. **Sengupta, M., H. J. Nielsen, B. Youngren, and S. Austin.** 2010. P1 plasmid segregation: accurate redistribution by dynamic plasmid pairing and separation. J Bacteriol **192:**1175-83.
182. **Sharpe, M. E., and J. Errington.** 1996. The Bacillus subtilis soj-spo0J locus is required for a centromere-like function involved in prespore chromosome partitioning. Mol Microbiol **21:**501-9.
183. **Sharpe, M. E., and J. Errington.** 1995. Postseptational chromosome partitioning in bacteria. Proc Natl Acad Sci U S A **92:**8630-4.
184. **Shebelut, C. W., J. M. Guberman, S. van Teeffelen, A. A. Yakhnina, and Z. Gitai.** 2010. Caulobacter chromosome segregation is an ordered multistep process. Proc Natl Acad Sci U S A **107:**14194-8.
185. **Soberon, N. E., V. S. Lioy, F. Pratto, A. Volante, and J. C. Alonso.** 2010. Molecular anatomy of the Streptococcus pyogenes pSM19035 partition and segrosome complexes. Nucleic Acids Res.
186. **Spurio, R., M. Durrenberger, M. Falconi, A. La Teana, C. L. Pon, and C. O. Gualerzi.** 1992. Lethal overproduction of the Escherichia coli nucleoid protein H-NS: ultramicroscopic and molecular autopsy. Mol Gen Genet **231:**201-11.
187. **Srivastava, P., R. A. Fekete, and D. K. Chattoraj.** 2006. Segregation of the replication terminus of the two Vibrio cholerae chromosomes. J Bacteriol **188:**1060-70.
188. **Stasiak, A., and E. Di Capua.** 1982. The helicity of DNA in complexes with recA protein. Nature **299:**185-6.
189. **Straight, A. F., A. S. Belmont, C. C. Robinett, and A. W. Murray.** 1996. GFP tagging of budding yeast chromosomes reveals that protein-protein interactions can mediate sister chromatid cohesion. Curr Biol **6:**1599-608.
190. **Sullivan, N. L., K. A. Marquis, and D. Z. Rudner.** 2009. Recruitment of SMC by ParB-parS organizes the origin region and promotes efficient chromosome segregation. Cell **137:**697-707.
191. **Tanaka, T.** 2010. Functional analysis of the stability determinant AlfB of pBET131, a miniplasmid derivative of bacillus subtilis (natto) plasmid pLS32. J Bacteriol **192:**1221-30.
192. **Tang, M., D. K. Bideshi, H. W. Park, and B. A. Federici.** 2007. Iteron-binding ORF157 and FtsZ-like ORF156 proteins encoded by pBtoxis play a role in its replication in Bacillus thuringiensis subsp. israelensis. J Bacteriol **189:**8053-8.
193. **Tang, M., D. K. Bideshi, H. W. Park, and B. A. Federici.** 2006. Minireplicon from pBtoxis of Bacillus thuringiensis subsp. israelensis. Appl Environ Microbiol **72:**6948-54.
194. **Teleman, A. A., P. L. Graumann, D. C. Lin, A. D. Grossman, and R. Losick.** 1998. Chromosome arrangement within a bacterium. Curr Biol **8:**1102-9.
195. **Thanbichler, M., and L. Shapiro.** 2006. Chromosome organization and segregation in bacteria. J Struct Biol **156:**292-303.
196. **Thanbichler, M., and L. Shapiro.** 2006. MipZ, a spatial regulator coordinating chromosome segregation with cell division in Caulobacter. Cell **126:**147-62.
197. **Thomaides, H. B., M. Freeman, M. El Karoui, and J. Errington.** 2001. Division site selection protein DivIVA of Bacillus subtilis has a second distinct function in chromosome segregation during sporulation. Genes Dev **15:**1662-73.

198. **Tinsley, E., and S. A. Khan.** 2006. A novel FtsZ-like protein is involved in replication of the anthrax toxin-encoding pXO1 plasmid in Bacillus anthracis. J Bacteriol **188:**2829-35.
199. **Toro, E., S. H. Hong, H. H. McAdams, and L. Shapiro.** 2008. Caulobacter requires a dedicated mechanism to initiate chromosome segregation. Proc Natl Acad Sci U S A **105:**15435-40.
200. **van den Ent, F., J. Moller-Jensen, L. A. Amos, K. Gerdes, and J. Lowe.** 2002. F-actin-like filaments formed by plasmid segregation protein ParM. EMBO J **21:**6935-43.
201. **van Noort, J., S. Verbrugge, N. Goosen, C. Dekker, and R. T. Dame.** 2004. Dual architectural roles of HU: formation of flexible hinges and rigid filaments. Proc Natl Acad Sci U S A **101:**6969-74.
202. **Vecchiarelli, A. G., Y. W. Han, X. Tan, M. Mizuuchi, R. Ghirlando, C. Biertumpfel, B. E. Funnell, and K. Mizuuchi.** 2010. ATP control of dynamic P1 ParA-DNA interactions: a key role for the nucleoid in plasmid partition. Mol Microbiol **78:**78-91.
203. **Viollier, P. H., M. Thanbichler, P. T. McGrath, L. West, M. Meewan, H. H. McAdams, and L. Shapiro.** 2004. Rapid and sequential movement of individual chromosomal loci to specific subcellular locations during bacterial DNA replication. Proc Natl Acad Sci U S A **101:**9257-62.
204. **Volkov, A., J. Mascarenhas, C. Andrei-Selmer, H. D. Ulrich, and P. L. Graumann.** 2003. A prokaryotic condensin/cohesin-like complex can actively compact chromosomes from a single position on the nucleoid and binds to DNA as a ring-like structure. Mol Cell Biol **23:**5638-50.
205. **Wang, X., X. Liu, C. Possoz, and D. J. Sherratt.** 2006. The two Escherichia coli chromosome arms locate to separate cell halves. Genes Dev **20:**1727-31.
206. **Wang, X., C. Possoz, and D. J. Sherratt.** 2005. Dancing around the divisome: asymmetric chromosome segregation in Escherichia coli. Genes Dev **19:**2367-77.
207. **Watanabe, E., S. Inamoto, M. H. Lee, S. U. Kim, T. Ogua, H. Mori, S. Hiraga, M. Yamasaki, and K. Nagai.** 1989. Purification and characterization of the sopB gene product which is responsible for stable maintenance of mini-F plasmid. Mol Gen Genet **218:**431-6.
208. **Watanabe, E., M. Wachi, M. Yamasaki, and K. Nagai.** 1992. ATPase activity of SopA, a protein essential for active partitioning of F plasmid. Mol Gen Genet **234:**346-52.
209. **Webb, C. D., P. L. Graumann, J. A. Kahana, A. A. Teleman, P. A. Silver, and R. Losick.** 1998. Use of time-lapse microscopy to visualize rapid movement of the replication origin region of the chromosome during the cell cycle in Bacillus subtilis. Mol Microbiol **28:**883-92.
210. **Webb, C. D., A. Teleman, S. Gordon, A. Straight, A. Belmont, D. C. Lin, A. D. Grossman, A. Wright, and R. Losick.** 1997. Bipolar localization of the replication origin regions of chromosomes in vegetative and sporulating cells of B. subtilis. Cell **88:**667-74.
211. **Weihofen, W. A., A. Cicek, F. Pratto, J. C. Alonso, and W. Saenger.** 2006. Structures of omega repressors bound to direct and inverted DNA repeats explain modulation of transcription. Nucleic Acids Res **34:**1450-8.

212. **Weitao, T., S. Dasgupta, and K. Nordstrom.** 2000. Plasmid R1 is present as clusters in the cells of Escherichia coli. Plasmid **43:**200-4.
213. **Wu, L. J., and J. Errington.** 1994. Bacillus subtilis SpoIIIE protein required for DNA segregation during asymmetric cell division. Science **264:**572-5.
214. **Wu, L. J., and J. Errington.** 2004. Coordination of cell division and chromosome segregation by a nucleoid occlusion protein in Bacillus subtilis. Cell **117:**915-25.
215. **Wu, L. J., and J. Errington.** 2002. A large dispersed chromosomal region required for chromosome segregation in sporulating cells of Bacillus subtilis. Embo J **21:**4001-11.
216. **Wu, L. J., and J. Errington.** 2003. RacA and the Soj-Spo0J system combine to effect polar chromosome segregation in sporulating Bacillus subtilis. Mol Microbiol **49:**1463-75.
217. **Wu, L. J., S. Ishikawa, Y. Kawai, T. Oshima, N. Ogasawara, and J. Errington.** 2009. Noc protein binds to specific DNA sequences to coordinate cell division with chromosome segregation. Embo J **28:**1940-52.
218. **Yamaichi, Y., M. A. Fogel, S. M. McLeod, M. P. Hui, and M. K. Waldor.** 2007. Distinct centromere-like *parS* sites on the two chromosomes of *Vibrio* spp. J Bacteriol **189:**5314-24.
219. **Yamaichi, Y., M. A. Fogel, and M. K. Waldor.** 2007. *par* genes and the pathology of chromosome loss in *Vibrio cholerae*. Proc Natl Acad Sci U S A **104:**630-5.
220. **Yamaichi, Y., and H. Niki.** 2000. Active segregation by the *Bacillus subtilis* partitioning system in *Escherichia coli*. Proc Natl Acad Sci U S A **97:**14656-61.
221. **Yang, H., Q. Li, J. Fan, W. K. Holloman, and N. P. Pavletich.** 2005. The BRCA2 homologue Brh2 nucleates RAD51 filament formation at a dsDNA-ssDNA junction. Nature **433:**653-7.